Hydroxyl regioisomerization of anthracycline catalyzed by a four-enzyme cascade

Zhuan Zhang[a,1], Yu-Kang Gong[a,1], Qiang Zhou[a], Yu Hu[a], Hong-Min Ma[a], Yong-Sheng Chen[a], Yasuhiro Igarashi[b], Lifeng Pan[a,2], and Gong-Li Tang[a,2]

[a]State Key Laboratory of Bio-organic and Natural Products Chemistry, Shanghai Institute of Organic Chemistry, Chinese Academy of Sciences, Shanghai 200032, China; and [b]Biotechnology Research Center, Toyama Prefectural University, Toyama 939-0398, Japan

Edited by Jerrold Meinwald, Cornell University, Ithaca, NY, and approved January 4, 2017 (received for review June 21, 2016)

Ranking among the most effective anticancer drugs, anthracyclines represent an important family of aromatic polyketides generated by type II polyketide synthases (PKSs). After formation of polyketide cores, the post-PKS tailoring modifications endow the scaffold with various structural diversities and biological activities. Here we demonstrate an unprecedented four-enzyme-participated hydroxyl regioisomerization process involved in the biosynthesis of kosinostatin. First, KstA15 and KstA16 function together to catalyze a cryptic hydroxylation of the 4-hydroxyl-anthraquinone core, yielding a 1,4-dihydroxyl product, which undergoes a chemically challenging asymmetric reduction-dearomatization subsequently acted by KstA11; then, KstA10 catalyzes a region-specific reduction concomitant with dehydration to afford the 1-hydroxyl anthraquinone. Remarkably, the shunt product identifications of both hydroxylation and reduction-dehydration reactions, the crystal structure of KstA11 with bound substrate and cofactor, and isotope incorporation experiments reveal mechanistic insights into the redox dearomatization and rearomatization steps. These findings provide a distinguished tailoring paradigm for type II PKS engineering.

biosynthesis | C-4 deoxyanthracycline | two-component hydroxylase | NmrA-like short-chain dehydrogenase | dehydroxylation

Anthracycline antibiotics, including doxorubicin, daunorubicin, idarubicin, epirubicin, and aclacinomycin (Fig. 1*A*), rank among the most effective anticancer drugs. However, large-scale clinical application of them is often hampered by the risk of inducing cardiomyopathy (1). Hence, there have been intensive attempts to develop analogs with an improved therapeutic index. In the last 50 y, most modifications have been focused on the sugar moiety, providing a successful drug, epirubicin, as well as several promising candidates under clinical trials (1, 2). In contrast, only a few analogs have been generated by altering the anthracycline core, most of which were obtained by chemical synthesis. Therefore, more efforts toward analogs, especially through enzymatic modifications of the previously seldom-touched anthracycline core, are still urgently needed.

Naturally occurring anthracycline antibiotics, usually produced by *Streptomyces*, belong to a family of aromatic polyketides biosynthesized by type II polyketide synthases (PKSs) (3). During the last 3 decades, biosynthetic studies of this system in bacteria have gained a deeper insight into the anthracycline's molecular logic and enzymatic mechanism (4–6). In general, the nascent poly-β-ketone generated by minimal PKS undergoes carbon-9 (C-9) reduction first and then cyclizations and dehydrations mediated by cyclases, followed by oxidation of the second ring to afford the anthraquinone portion presented in all anthracyclines. The final hydrolytic release of the anthraquinone produces the nascent anthracycline core, which contains a C-4 hydroxyl group in D-ring (Fig. 1*A*) (3, 7). The anthracycline core is then decorated with various tailoring enzymes to generate types of anthracycline antibiotics (8–10). Therefore, most of the anthracyclines possess a C-4 hydroxyl group, and a very few C-4 deoxyanthracyclines have been isolated in nature.

Kosinostatin (KST, **1**), a rare C-4 deoxyanthracycline antibiotic produced by marine *Micromonospora* (*M.*) sp. TP-A0468, exhibits strong cytotoxicity against various cancer cell lines and an inhibition toward Gram-positive bacteria (11). During our previous studies, the anthracycline intermediate **4**, bearing a C-1 hydroxyl group in D-ring, was identified from the *kstB1*-inactivation mutant strain (Fig. 1*B*) (12). The high sequence identity between KST gene cluster and other anthracycline gene clusters indicates that KST may generate the C-4 hydroxyl anthracycline as primary anthracycline core; in addition, our labeled acetate feeding experiments further confirmed the prediction that KST has undergone similar assembly process to afford C-4 hydroxyl anthracycline (Fig. 1*B*) (12). If this is the case, an apparent hydroxyl regioisomerization of anthracycline must be involved in the KST biosynthesis, which is a chemically challenging transformation process. Here, we report a four-enzyme-catalyzed regioselective hydroxylation-dehydroxylation process resulting in the hydroxyl regioisomerization, which is totally distinct from currently known tailoring steps in type II PKS platforms.

Results

Cryptic Hydroxylation by KstA15/KstA16. Bioinformatic analysis of KST gene cluster revealed two closely linked genes, *kstA15* and *kstA16*. The gene product of former is evolutionarily related to polyketide cyclase, and the latter encodes a short-chain alcohol dehydrogenase. Furthermore, the KstA15/KstA16 pair is homologous to the AclR/AclQ and SnoaL2/SnoaW couples, which are

Significance

Enzymatic modifications of anthracycline antibiotics are urgently needed in the fields of biosynthesis, biocatalysis, and even medical chemistry. However, neither hydroxyl regioisomerization nor dehydroxylation of anthracycline core was described previously. Here, we discover an unprecedented hydroxyl regioisomerization process in the biosynthesis of a rare carbon-4 deoxyanthracycline, which includes three tailoring steps performed by a four-enzyme cascade: two-component hydroxylases mediated a cryptic hydroxylation, and two NmrA-like short-chain dehydrogenase/reductases catalyzed a reduction-dearomatization followed by a reduction-dehydration process. This study expands the enzymology and chemistry of type II polyketide synthase and provides tools to generate more analogs by engineering or enzymatic semisynthesis.

Author contributions: G.-L.T. designed research; Z.Z., Y.-K.G., Q.Z., Y.H., H.-M.M., and Y.-S.C. performed research; Y.I. contributed new reagents/analytic tools; Z.Z., Y.-K.G., L.P., and G.-L.T. analyzed data; and Z.Z., L.P., and G.-L.T. wrote the paper.

The authors declare no conflict of interest.

This article is a PNAS Direct Submission.

Data deposition: The atomic coordinates have been deposited in the Protein Data Bank, www.pdb.org (PDB ID code 5F5L and 5F5N).

[1]Z.Z. and Y.-K.G. contributed equally to this work.

[2]To whom correspondence may be addressed. Email: gltang@sioc.ac.cn or panlf@sioc.ac.cn.

This article contains supporting information online at www.pnas.org/lookup/suppl/doi:10.1073/pnas.1610097114/-/DCSupplemental.

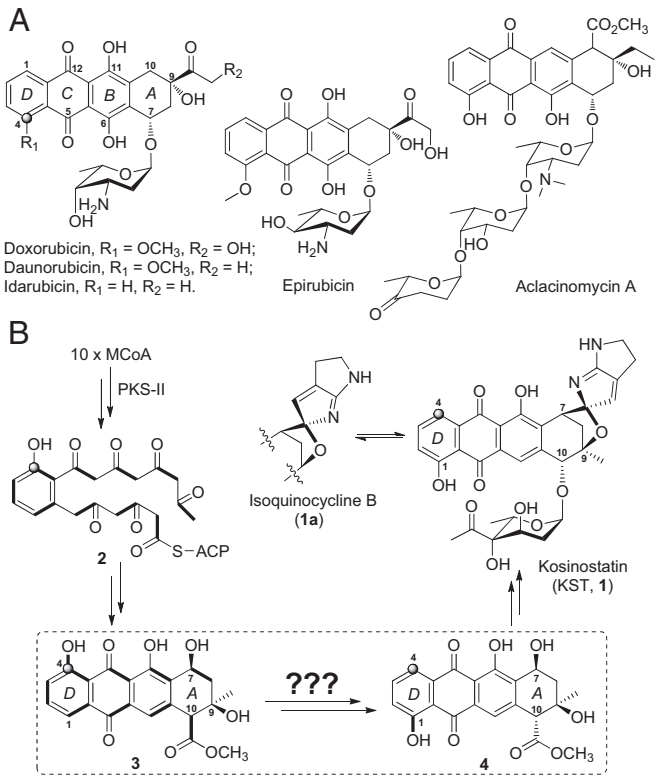

Fig. 1. Representative anticancer antibiotics of anthracycline family. (*A*) Structures of doxorubicin-like drugs and aclacinomycin A. (*B*) Biosynthetic pathway of kosinostatin (KST).

also encoded by adjacent genes in the aclacinomycin and nogalamycin biosynthetic gene clusters, respectively (*SI Appendix*, Fig. S1). AclR or SnoaL2 was previously discovered to be involved in the production of 1,4-dihydroxylated anthracyclines in vivo; however, in vitro experiment using AclR or SnoaL2 or cell-free lysate showed no bioconversion result (13). In addition, 1,4-dihydroxy-anthracyclines were also isolated from the aclacinomycin-producing strain (14). This evidence strongly implies that KstA15 and KstA16 are likely both involved in affording 1,4-dihydroxy-anthracycline, a possible intermediate relating to the bioconversion from **3** to **4** (Fig. 1*B*). To evaluate their functions, *kstA15* and *kstA16* were inactivated individually by gene replacement (*SI Appendix*, Fig. S2). The resultant mutant strains *M.* TG1711 (Δ*kstA15*) and *M.* TG1712 (Δ*kstA16*) exhibited similar production profiles: both abolished the production of KST and the isomer isoquinocycline (**1a**) while accumulating two compounds, **3** and **3g** (Fig. 2 *AIII* and *AIV*). Evaluations of the NMR and MS spectra (*SI Appendix*, Note S1 and Note S2) led to the successful identification of their chemical structures, both of which bear a C-4 hydroxyl group in the D-ring while being distinct from each other in the C-7 modification, where **3g** is glycosylated with a γ-branched octose (Fig. 2*C*). The isolation of **3** and **3g**, combining with characterized **4** and **4g** (Fig. 2 *AII* and *C*, *SI Appendix*, Note S4), leads to a confirmation that **3** is biosynthesized by the PKS as the first anthracycline core, and subsequently is modified into **4** as second anthracycline scaffold by unknown tailoring steps (Fig. 1*B*). Importantly, KstA15 and KstA16 may perform the first step of modification and synergistically catalyze 1-hydroxylation of **3** to yield 1, 4-dihydroxy-anthracycline.

To validate this hypothesis, KstA15 and KstA16 were expressed and purified as His_6-tagged proteins (*SI Appendix*, Fig. S4) and then incubated with **3** and NADH (or NADPH). Subsequent HPLC analysis showed a new peak appears dependent on both enzymes (Fig. 3*A*). The newly formed compound **5**, displaying an obvious red-shift on the UV/Vis spectrogram (Fig. 2*B*) and increased molecular weight by 16 Da compared with substrate **3**, is exactly in agreement with the expected 1,4-dihydroxy-anthracycline product (Fig. 2*C*). Structural elucidation of **5** provided by preparative enzymatic reactions confirmed **5** to be the 1,4-dihydroxy-anthracycline product (*SI Appendix*, Note S6). This evidence suggests KstA15/KstA16 function together to catalyze the C-1 hydroxylation.

To further explore the hydroxylation mechanism, KstA15 and KstA16 were purified under anaerobic conditions and performed the same enzymatic reaction anaerobically. Surprisingly, no production of **5** was observed, but a new compound **3d** with a decreased mass of 16 Da appeared, which mainly depended on the

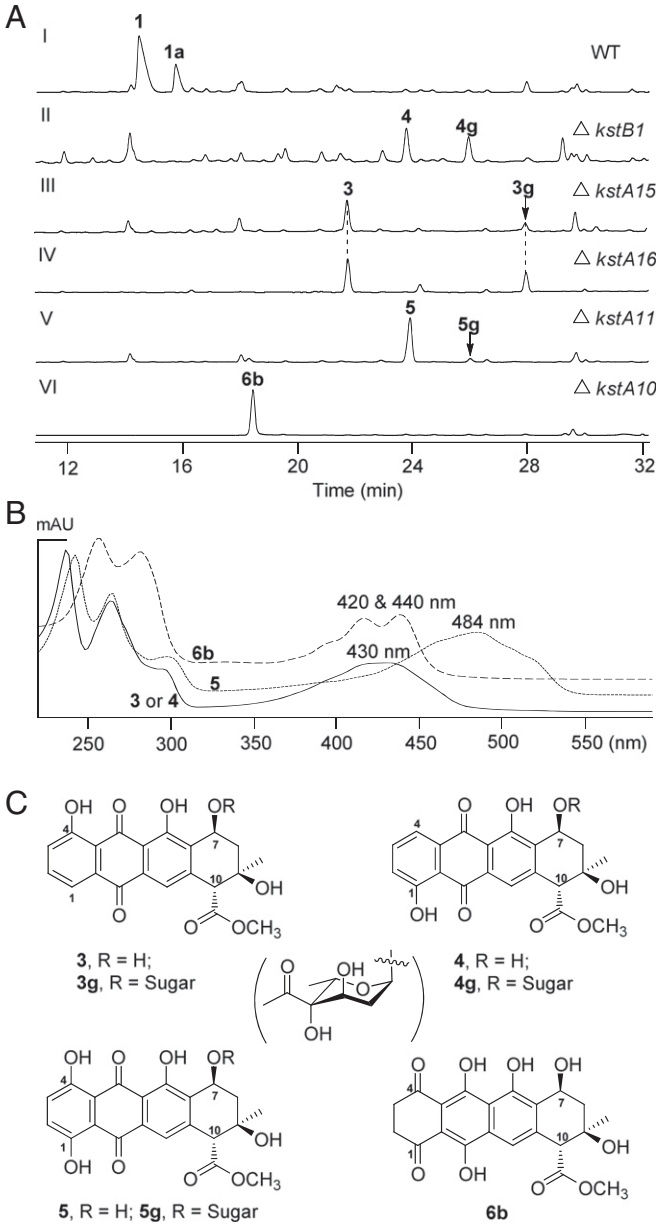

Fig. 2. Characterization of the biosynthetic intermediates in vivo. (*A*) HPLC analysis (UV at 254 nm) of KST relative metabolites by *Micromonospora* sp. strains. (*I*) Wild-type TP-A0468. (*II*) Mutant TG1708 (Δ*kstB1*). (*III*) Mutant TG1711 (Δ*kstA15*). (*IV*) Mutant TG1712 (Δ*kstA16*). (*V*) Mutant TG1713 (Δ*kstA11*). (*VI*) Mutant TG1714 (Δ*kstA10*). UV-Vis analysis (*B*) and chemical structures (*C*) of anthracycline metabolites produced by the mutants.

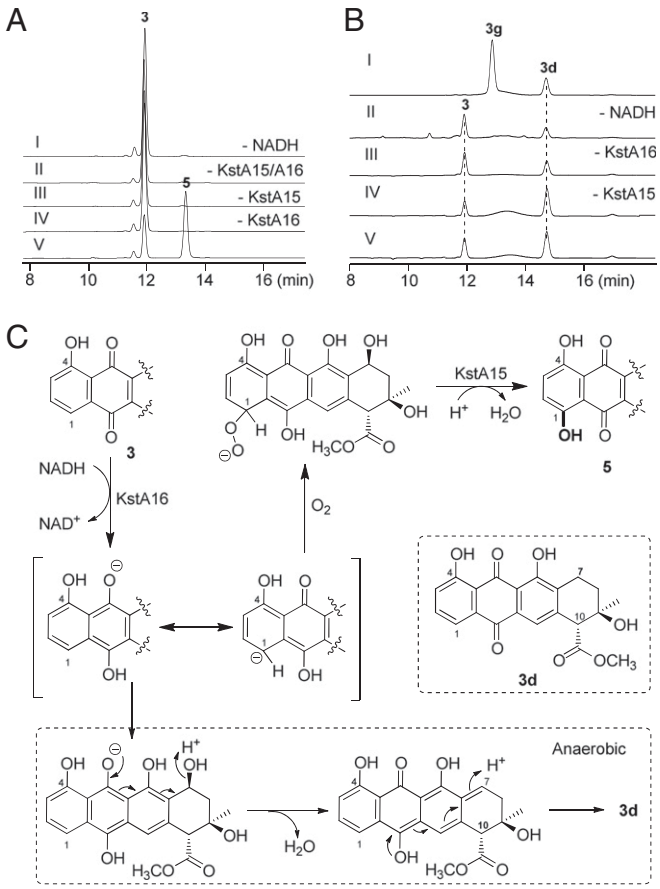

Fig. 3. In vitro biochemical characterization of KstA15/A16-catalyzed hydroxylation. HPLC analysis (UV at 254 nm) of normal enzymatic reaction (*A*) and anaerobic reaction (*B*). (*C*) Proposed enzymatic mechanism.

presence of KstA16 and NAD(P)H (Fig. 3*BII*–*V*). Further structural elucidation by the NMR and MS showed that **3d** was a C-7 dehydroxy-anthracycline shunt product (Fig. 3*C*, *SI Appendix*, Note S3). In addition, when **3g** was incubated with KstA15/KstA16 and NAD(P)H anaerobically, the same enzymatic product **3d** was observed through deglycosylation instead of dehydroxylation (Fig. 3*BI*). We also tested the formation of H_2O_2 to identify the existence of peroxyanthracycline intermediate. Expectedly, H_2O_2 can be well observed either in the KstA16 or the KstA16/KstA15-coupled reaction system; moreover, the KstA16 reaction system generated more H_2O_2 than the latter (*SI Appendix*, Figs. S5 and S6).

When we further investigated the enzymatic mechanism, a similar two-component monooxygenase SnoaW/SnoaL2 involved in nogalamycin biosynthesis was reported, and a reaction model was proposed (15). Our experiment results under anaerobic conditions, together with their proposal, led to replenishing the hydroxylation mechanism; the process resembles the reaction catalyzed by flavoenzymes, where the reduced flavin cofactor activates dioxygen to yield a semiquinone-superoxide radical pair (Fig. 3*C*). KstA16 first uses NAD(P)H to reduce the quinone moiety of the anthracycline; the reduced substrate then reacts with dioxygen to form highly reactive hydroperoxide intermediate, which then undergoes protonation in the presence of KstA15; the resulting hydroperoxide intermediate undergoes elimination of water to give a ketone followed by a tautomerization to afford the final 1,4-dihydroxylated product. Anaerobically, the resulted anion delocalized into C-7 through resonance over the aromatic ring system, eliminating the hydroxyl of **3** or the glycosyl group of **3g** to give **3d** (Fig. 3*C*).

Reduction-Dearomatization by KstA11. Our in vitro results unequivocally demonstrated that KstA15/A16 synergistically catalyze hydroxylation of **3** to produce **5**, which may serve as an intermediate during the hydroxyl regioisomerization process; thus, a dehydroxylation must be involved in the transformation from **5** to **4**. To the best of our knowledge, two enzymatic dehydroxylation pathways of aromatic ring had been reported: Birch-like one electron reduction mechanism, as exemplified by 4-hydroxybenzoyl-CoA reductase, which is a Mo-flavo-Fe/S-dependent protein (16, 17), and reduction-dehydration process-mediated dehydroxylation in the fungal melanin biosynthetic pathway, operated by 1,3,6,8-tetradroxynaphthalene reductase, 1,3,8-tridroxynaphthalene reductase, both belonging to the short-chain dehydrogenase/reductase (SDR) superfamily, and scytalone dehydratase (18–20). However, bioinformatic analysis revealed that neither Mo-flavo-Fe/S protein nor scytalone dehydratase homolog has been found in the KST pathway. Although we identified several genes encoding SDR family proteins within the *kst* cluster, sequential analysis cannot provide any clue about enzymes catalyzing dehydroxylation owing to the reaction flexibility of the SDR family (21). Thus, many efforts have been made to search for gene inactivation mutants producing the same metabolite **5**. Fortunately, **5** and its glycosylated relative **5g** were both observed from mutant *M*. TG1713 (Δ*kstA11*) (Fig. 2 *AV* and *C*, *SI Appendix*, Fig. S3), implying that KstA11 may perform the next step of tailoring modification, using **5** as the substrate.

Sequence analysis shows that KstA11 belongs to the NADB_Rossmann superfamily, bearing a conserved NAD(P)H binding motif (GxxGxxG), it also displays a high similarity with the NmrA family transcriptional regulator (22). To characterize the enzymatic function, substrate **5** was incubated with KstA11 purified from *Escherichia coli* (*SI Appendix*, Fig. S8) in the presence of NAD(P)H. Interestingly, different products were detected with prolonged reaction time (Fig. 4*A*). The intermediate **6a**, with a mass increase by 2 Da compared with substrate **5**, exhibits different UV/Vis absorption characteristics, and Vis_{max} of **6a** falls between **5** and **6b**, indicating a middle conjugated degree (Fig. 4*E*). The final product, **6b**, showing a totally different UV/Vis spectral property (Fig. 2*B*) and the same molecular weight as **6a**, is coincident with the dihydro-anthracycline. Structural elucidation of metastable **6b** provided by preparative enzymatic reactions confirms **6b** to be the 5,12-dihydroxy-2,3-tetrahydro-1,4-dione product (Fig. 2*C*, *SI Appendix*, Note S8). Unfortunately, other enzymatic intermediates are too labile and quickly change into **6b** during the extraction process, thereby preventing further purification and structural characterization. Collectively, our enzymatic results preliminarily demonstrated that KstA11 catalyzes the dearomatization of **5** to afford **6b**, indicating the dehydroxylation in KST biosynthesis is operated by a reductase-dehydratase pair.

Reduction-Dehydration by KstA10. Previous studies showed that **6b** was unstable and could convert into **5** at room temperature spontaneously. After optimizing the handing procedure, we detected the accumulation of **6b** as the major metabolite from mutant Δ*kstA10* (Fig. 2*AVI*, *SI Appendix*, Fig. S3). To verify the function of KstA10, we performed the biochemical assay of purified recombinant protein (*SI Appendix*, Fig. S10), using **6b** as substrate (Fig. 5*A*). Unexpectedly, the final product **4**, together with a shunt product **4d**, could be formed only in the presence of NAD(P)H (Fig. 5*BI*). Structural elucidation confirmed **4d** with the same hydroxyl modification of aromatic ring as **4**, but dehydroxylation at C-7 (Fig. 5*A*, *SI Appendix*, Note S5). These results preliminarily revealed that KstA10 catalyzes a reduction reaction followed by a dehydration process to rearomatize the D-ring, although less than 10% of **4** was produced after an overnight incubation, and more than 70% of **6b** was converted into **5** spontaneously (Fig. 5*BII* and *BIII*). Given that **6a** is more likely to be adopted by KstA10 than

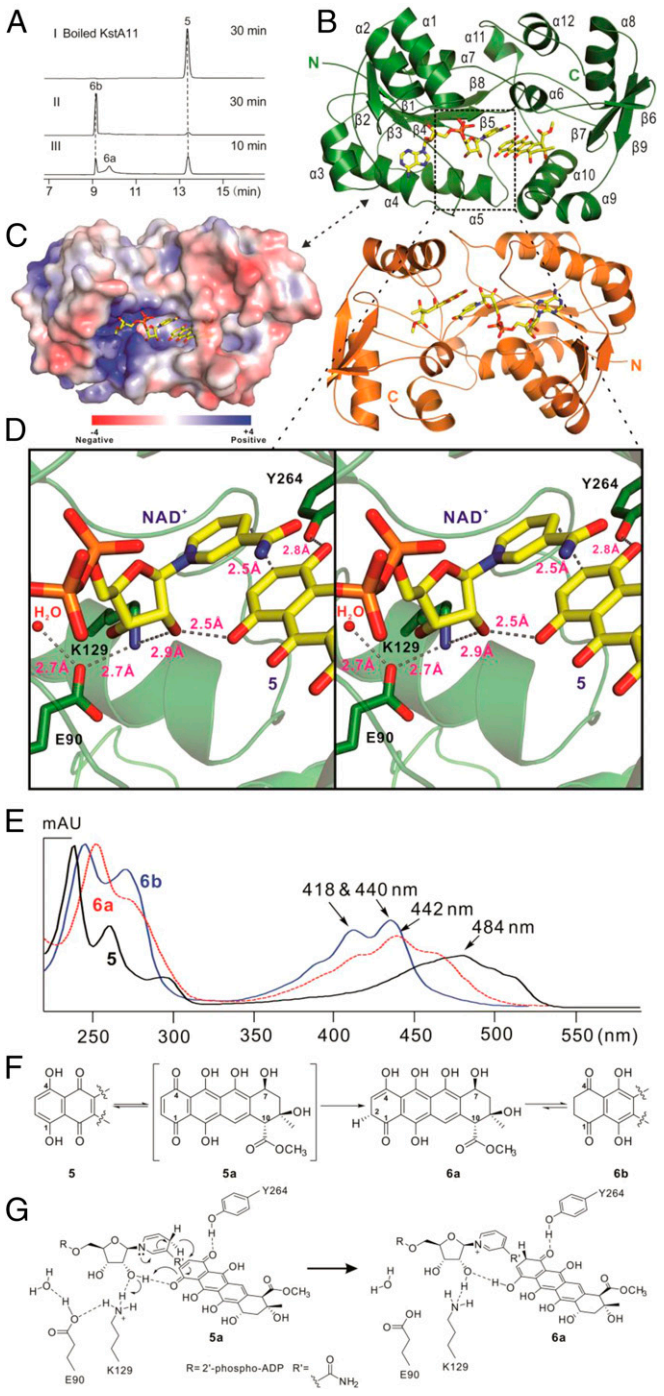

Fig. 4. Biochemical and structural characterizations of KstA11-catalyzed reduction-dearomatization. (*A*) HPLC analysis (UV at 254 nm) of enzymatic reaction with NADH. (*B*) The combined ribbon representation and stick model showing the overall structure of KstA11 in complex with cofactor NAD^+ and substrate. The bound cofactor NAD^+ and substrate are shown in the stick model. (*C*) The combined surface charge potential representation (contoured at ±4 kT/eV; blue/red) and the stick model showing the detailed interactions of KstA11 with NAD^+ and substrate. (*D*) Stereo view showing the detailed interactions among key residues of KstA11, NAD^+, and substrate. The hydrogen bonds involved in the binding are shown as dotted gray lines. (*E*) UV/Vis analysis of the reaction. (*F*) Proposed chemical reaction. (*G*) Proposed reaction mechanism from **5a** to **6a**.

6b, then we performed consecutive reactions in which the product of KstA11 acts as the substrate for KstA10 (Fig. 5*A*). Just as expected, more than 90% of substrate **5** was converted into the final product **4** within 1 h (Fig. 5*C*). Thus, the function of KstA10 as the third tailoring step was fully established in this hydroxyl regioisomerization reaction.

KstA10 is another NmrA-like enzyme belonging to the SDR family with a conserved NAD(P)H binding motif (GxxGxxG) (21, 22). Further analysis indicates that KstA10 is homologous to NAD^+-dependent nucleotide diphosphate sugar epimerases (23), which act on totally different substrates from that in KST biosynthesis. In addition, scytalone dehydratase in the fungal melanin

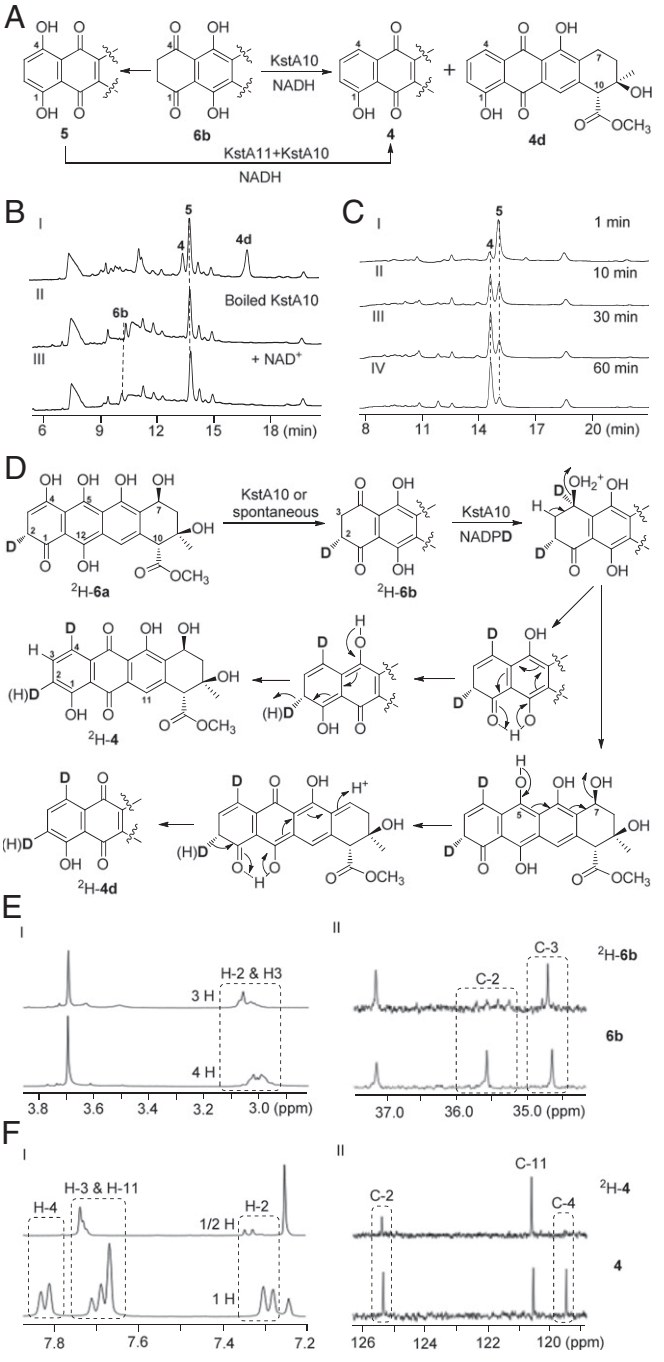

Fig. 5. Biochemical assay of KstA10-catalyzed dehydration-rearomatization. (*A*) Chemical reactions. HPLC analysis (UV at 254 nm) of enzymatic reactions using **6b** as the substrate by KstA10 (*B*) and **5** as the substrate by KstA11/KstA10 (*C*). (*D*) Proposed reaction mechanism. Comparison of the ^{1}H-NMR (*I*) and ^{13}C-NMR (*II*) spectra of ^{2}H-**6b** with **6b** (*E*) and ^{2}H-**4** with **4** (*F*).

biosynthesis is cofactor independent (18, 19). However, evidence obtained from our biochemical assays suggested that the dehydration catalyzed by KstA10 is dependent on NAD(P)H (*SI Appendix*, Fig. S11). To gain further insights into the enzymatic mechanism, KstA11 and KstA10 assays were conducted in the presence of (*S*)-[4-^{2}H]NADPH obtained by glucose dehydrogenase from *Bacillus megaterium* DSM 2894 BmGDH, using D-[1-^{2}H] glucose as the deuterium donor (24, 25), as the pro*S* hydrogen is the hydrogen transferred to the substrate during reduction observed from the cocrystal structure of KstA11 in complex with substrate **5** and NAD$^+$ (see *Structural Insight into the KstA11-Catalyzed Reaction*). Expectedly, a 1-Da shifted fragment ion at *m*/*z* 416.1103 was detected in a KstA11/BmGDH coupled assay (*SI Appendix*, Note S9), indicating a deuterium incorporation in **6b**; large-scale reactions were then performed to isolate ^{2}H-**6b** and elucidate the exact deuterium incorporation position. A comparison of ^{1}H-NMR and ^{13}C-NMR spectra of ^{2}H-**6b** and **6b** showing that C-2 of ^{2}H-**6b** has been split into three peaks (a triplet) and the relative hydrogen peak area has decreased confirmed the deuterium incorporation at C-2 of ^{2}H-**6b** (Fig. 5 *D* and *E*, *SI Appendix*, Note S9). A 1-Da shifted fragment ion at *m*/*z* 398.0997 and a 2-Da shifted fragment ion at *m*/*z* 399.1065 were both observed in the KstA11/KstA10/BmGDH coupled assay, implying that more than 1 deuterium had been incorporated into **4** (*SI Appendix*, Note S10). Similarly, we prepared ^{2}H-**4** by large-scale enzymatic reaction and elucidated ^{2}H-**4** by ^{1}H-NMR and ^{13}C-NMR. A head-to-head comparison of ^{1}H-NMR and ^{13}C-NMR spectra of ^{2}H-**4** and **4** showed the peak disappearance of C-4 and relative H-4 of ^{2}H-**4** and a peak attenuation of C-2 and relative H-2 (1/2 peak area), demonstrating the absolute deuterium incorporation at C-4 and partial deuterium incorporation at C-2 in ^{2}H-**4** (Fig. 5 *D* and *F*, *SI Appendix*, Note S10). According to the identification of shunt product and deuterium isotope experiments, we proposed that KstA10 functions as a ketoreductase and dehydratase, catalyzing a 1,2-nucleophilic addition, followed by dehydration to aromatize the D-ring. First, KstA10 binds **6a** as the real substrate and subsequently isomerizes it into **6b** in the active site; next is the nucleophilic addition of pro*S* hydrogen of NADPH to keto-carbonyl of C-4 to form a tetrahedral intermediate. Then the intermediate undergoes elimination of 4-OH, concomitant with hydrogen transferring from 12-OH to carbonyl of C1. Finally, deprotonation of 5-OH accompanied with leaving hydride at C-2 gives the final product **4**. In contrast, the formation of **4d** may result from deprotonation of 5-OH concomitant with leaving 7-OH, and then deprotonation at C-2 accompanied with protonation of C-7 (Fig. 5*D*).

Structural Insight into the KstA11-Catalyzed Reaction. To gain mechanistic insight into the unusual reaction catalyzed by KstA11, we determined the crystal structure of KstA11 in complex with substrate **5** and a relevant cofactor NAD$^+$ to 1.3-Å resolution (*SI Appendix*, Table S1). In the complex structure, two KstA11 molecules pack together to form a symmetric dimer, and each monomer contains 12α-h elixes (α1–α12) and 9 β-strands (β1–β9) and binds with one substrate **5** and one NAD$^+$ molecule in a 1:1:1 stoichiometry (Fig. 4*B*). Notably, **5** and NAD$^+$ directly contact with each other and pack extensively with a solvent-exposed elongated groove located at the middle region of KstA11 (Fig. 4 *B* and *C*). The specific interactions of KstA11 with substrate **5** and NAD$^+$ are mainly mediated by hydrophobic contacts and polar interactions (Fig. 4*C*, *SI Appendix*, Fig. S7). Specifically, the hydrophobic moiety of **5** packs extensively with the hydrophobic pocket formed by theV114, F126, F150, F155, W158, L171, I246, I252, M255, F256, and F259 residues of KstA11, and the oxygen located at the C-1 position of substrate **5** forms a hydrogen bond with the side chain of Y264 (*SI Appendix*, Fig. S7*A*). In parallel, the NAD$^+$ molecule forms a number of hydrogen bonds with the T14, T16, Q17, D58, T80, K129, and N154 residues, and its aromatic adenine and nicotinamide groups form a cation-π interaction with R37 and a π-π stacking with F151, respectively (*SI Appendix*, Fig. S7*B*). Subsequently, mutations that are expected to weaken the interaction between KstA11 and NADH, such as R37E and N154K, or interaction between KstA11 and substrate **5**, such as I252Y, all dramatically decrease the catalytic activity (*SI Appendix*, Figs. S8 and S9). In addition, the conformations of **5** and NAD$^+$ in the complex are further stabilized by a π-π stacking between **5** and the nicotinamide group of NAD$^+$, as well as a hydrogen bond between the C-4 oxygen of **5** and the 2′-OH group of NAD$^+$ (Fig. 4*D*).

Given the unique chemical structure of **5**, the transition state for the KstA11 catalyzed dearomatization reduction of **5** to **6b** would be expected to proceed from the 1,4-diketo tautomer of **5** (hereafter referred to as **5a**) (Fig. 4*F*). In the complex, **5a** is highly preferred, as the oxygen atoms located at the C-1 and C-4 positions of **5** are well positioned to form two hydrogen bonds with the side chain hydroxyl group of Y264 and the 2′-OH of NAD$^+$, respectively. Meanwhile, the 2′-OH of NAD$^+$ also forms a hydrogen bond with K129, which is further hydrogen bonded with the E90 residue to couple with a water molecule (Fig. 4*D*). Therefore, there is a hydrogen bonding network that proceeds from the water to the C-4 oxygen of substrate **5**. On the basis of the aforementioned biochemical and structural data, we proposed an enzymatic mechanism for the KstA11-catalyzed reduction of **5** to **6b** (Fig. 4 *F* and *G*). When substrate **5** and cofactor NADH are in complex with KstA11, the specific interactions among them not only induce the close contact between **5** and NADH but also stabilize the 1,4-diketo **5a**. Then, the pro*S* hydrogen of NADH (the hydrogen that is transferred as a hydride to the substrate in the reduction reaction) is directed toward the C-2 position of **5a**, as the C-4 of the nicotinamide ring of NAD$^+$ is highly close to the C-2 carbon of **5** in the complex structure (Fig. 4*D*). Importantly, aforementioned deuteration-based labeling studies confirmed this type of 1,4-addition reaction (Fig. 5*D*). Meanwhile, the 2′-OH of NADH, which is fed by the hydrogen bond network that includes K129, E90, and a water molecule, serve as the ultimate proton donor to the C-4 oxygen of **5a** to generate the product **6a** (Fig. 4*G*). Finally, **6a** is converted to **6b** through a chemical rearrangement because of the lower energy level of conjugated system in the latter (Fig. 4*F*). In line with this proposal, the substitution of the key catalytic K129 residue with Arg essentially abolished the enzymatic activity of KstA11 (*SI Appendix*, Fig. S9). Interestingly, the E90A mutation has little effect on the enzyme activity, suggesting the K129 may directly couple with a water molecule in the proton relay in this mutant.

Discussion

Combining in vivo genetic characterization and in vitro biochemical studies, we uncovered an unprecedented hydroxyl regioisomerization process operated on the aromatic ring of anthracycline leading to the 1-hydroxyl anthraquinone, an essential intermediate proposed to be a prerequisite for the spirocyclic formation during KST

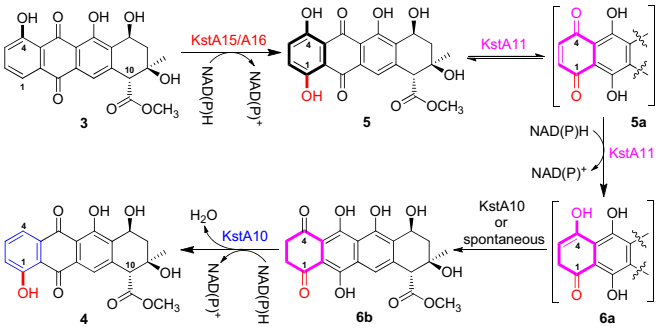

Fig. 6. Summary of the hydroxyl regioisomerization performed by KstA15/A16-KstA11-KstA10.

biosynthesis. This chemically challenging transformation has gone through a hydroxylation and a selective dehydroxylation by two tandem dearomatization and rearomatization processes, which include three tailoring steps acting on the anthracycline core: the primary core structure **3** synthesized by the PKS is catalyzed by KstA15/KstA16 to generate a 1, 4-dihydroxyl intermediate **5**; KstA11 performs an asymmetric dearomatization, using **5** as substrate to yield **6a**; and **6a** can isomerize into **6b** in the active site of KstA10, which then undergoes regioselectively reduction-dehydration to afford secondary core structure **4** mediated by KstA10 (Fig. 6).

Significantly, the dehydroxylation operated by KstA11 and KstA10, to the best of our knowledge, is the first enzymatic system realizing the dehydroxylation on the aromatic ring of anthracycline. 4-Demethoxydaunorbicin (idarubicin), a synthetic daunorubicin analog, displays superior fat solubility and cellular uptake compared with daunorubicin or doxorubicin, indicating the 4-deoxyanthrancycline core is vital for its antitumor activity (26). Accordingly, it is meaningful to develop an elaborate and versatile system of enzyme-mediated dehydroxylation on the aromatic ring of anthracycline. Our results now established feasibly enzymatic dehydroxylation on the aromatic ring of anthracycline. It is promising that this dehydroxylation could be used to provide aimed anthracycline analogs in the future by protein engineering. In addition, dearomatizations are chemically challenging in a sense both of chemistry and of biology (16, 17, 27), as the asymmetric hydrogenation of aromatic compounds, which was considered a versatile and practical synthetic strategy method to obtain chiral compound, has been an active and attractive field of methodology research (28, 29). Recently, characterization of the NADPH-dependent reductases involved in fungal 1,8-dihydroxynaphthalene melanin, monodictyphenone, and aflatoxin B1 biosynthesis expanded the substrates to hydroxynaphthoquinones and tricyclic anthrahydroquinones (30–33). The discovery of KstA11-catalyzed regio- and stereoselective hydrogenation of tetracyclic anthracyclines and regioselective dehydroxylation by KstA11/KstA10 couple are remarkable, which indicates that additional enzymes with broad substrate spectrum are waiting to be explored for biocatalysts. Significantly, as a tailoring modification acting on the anthracycline core, our results definitely broaden the tailoring spectrum to modify the previously seldom-touched anthracycline core to generate more analogs for future cancer drug studies.

Materials and Methods

Materials and methods are summarized in *SI Appendix, Materials and Methods*. Supporting data are provided in *SI Appendix*, Figs. S1–S11. X-ray crystallographic data collection, primers, strains and plasmids are summarized in *SI Appendix*, Tables S1–S3. Physicochemical characterizations of the compounds are provided in *SI Appendix*, Notes S1–S10.

ACKNOWLEDGMENTS. We thank Professor Ren-Xiao Wang of Shanghai Institute of Organic Chemistry for guiding the protein modeling; Professor Han-Jie Ying in Nanjing University of Technology for providing the plasmid pRSF-BmGDH; Professor Chang-Sheng Zhang of South China Sea Institute of Oceanology, Chinese Academy of Sciences, for kindly giving us D-[1-^{2}H]-glucose; Professor Michael Müller of Institut für Pharmazeutische Wissenschaften, Albert-Ludwigs-Universität Freiburg for helpful discussion, suggestion, and sharing unpublished data with us; and Shanghai Synchrotron Radiation Facility beamline BL17U and National Center for Protein Science Shanghai Beamline 19U1 for X-ray beam time. This work was supported in part by grants from Ministry of Science and Technology (2013CB836900), National Natural Science Foundation of China (81373307 and 31330003), Science and Technology Commission of Shanghai Municipality (14XD1404500 and 15JC1400400), Chinese Academy of Sciences (XDB20020200), and the "Thousand Talents Program" (L.P.).

1. Minotti G, Menna P, Salvatorelli E, Cairo G, Gianni L (2004) Anthracyclines: Molecular advances and pharmacologic developments in antitumor activity and cardiotoxicity. *Pharmacol Rev* 56(2):185–229.
2. Zhang G, et al. (2005) Syntheses and biological activities of disaccharide daunorubicins. *J Med Chem* 48(16):5269–5278.
3. Metsä-Ketelä M, Niemi J, Mäntsälä P, Schneider G (2008) Anthracycline biosynthesis: Genes, enzymes, and mechanisms. *Top Curr Chem* 282:101–140.
4. Shen B (2000) Biosynthesis of aromatic polyketides. *Top Curr Chem* 209:1–51.
5. Hertweck C, Luzhetskyy A, Rebets Y, Bechthold A (2007) Type II polyketide synthases: Gaining a deeper insight into enzymatic teamwork. *Nat Prod Rep* 24(1):162–190.
6. Das A, Khosla C (2009) Biosynthesis of aromatic polyketides in bacteria. *Acc Chem Res* 42(5):631–639.
7. Zhou H, Li Y, Tang Y (2010) Cyclization of aromatic polyketides from bacteria and fungi. *Nat Prod Rep* 27(6):839–868.
8. Niemi J, Metsä-Ketelä M, Schneider G, Mäntsälä P (2008) Biosynthetic anthracycline variants. *Top Curr Chem* 282:75–99.
9. Rix U, Fischer C, Remsing LL, Rohr J (2002) Modification of post-PKS tailoring steps through combinatorial biosynthesis. *Nat Prod Rep* 19(5):542–580.
10. Olano C, Méndez C, Salas JA (2010) Post-PKS tailoring steps in natural product-producing actinomycetes from the perspective of combinatorial biosynthesis. *Nat Prod Rep* 27(4): 571–616.
11. Furumai T, Igarashi Y, Higuchi H, Saito N, Oki T (2002) Kosinostatin, a quinocycline antibiotic with antitumor activity from *Micromonospora* sp. TP-A0468. *J Antibiot (Tokyo)* 55(2):128–133.
12. Ma HM, et al. (2013) Unconventional origin and hybrid system for construction of pyrrolopyrrole moiety in kosinostatin biosynthesis. *Chem Biol* 20(6):796–805.
13. Beinker P, et al. (2006) Crystal structures of SnoaL2 and AclR: Two putative hydroxylases in the biosynthesis of aromatic polyketide antibiotics. *J Mol Biol* 359(3): 728–740.
14. Oki T, et al. (1979) Antitumor anthracycline antibiotics, aclacinomycin a and analogues. II. Structural determination. *J Antibiot (Tokyo)* 32(8):801–819.
15. Siitonen V, Blauenburg B, Kallio P, Mäntsälä P, Metsä-Ketelä M (2012) Discovery of a two-component monooxygenase SnoaW/SnoaL2 involved in nogalamycin biosynthesis. *Chem Biol* 19(5):638–646.
16. Unciuleac M, Warkentin E, Page CC, Boll M, Ermler U (2004) Structure of a xanthine oxidase-related 4-hydroxybenzoyl-CoA reductase with an additional [4Fe-4S] cluster and an inverted electron flow. *Structure* 12(12):2249–2256.
17. Boll M (2005) Key enzymes in the anaerobic aromatic metabolism catalysing Birch-like reductions. *Biochim Biophys Acta* 1707(1):34–50.
18. Basarab GS, et al. (1999) Catalytic mechanism of scytalone dehydratase: Site-directed mutagenisis, kinetic isotope effects, and alternate substrates. *Biochemistry* 38(19): 6012–6024.
19. Thompson JE, et al. (2000) The second naphthol reductase of fungal melanin biosynthesis in Magnaporthe grisea: Tetrahydroxynaphthalene reductase. *J Biol Chem* 275(45):34867–34872.
20. Liao D, Basarab GS, Gatenby AA, Valent B, Jordan DB (2001) Structures of trihydroxynaphthalene reductase-fungicide complexes: Implications for structure-based design and catalysis. *Structure* 9(1):19–27.
21. Kavanagh KL, Jörnvall H, Persson B, Oppermann U (2008) Medium- and short-chain dehydrogenase/reductase gene and protein families : The SDR superfamily: Functional and structural diversity within a family of metabolic and regulatory enzymes. *Cell Mol Life Sci* 65(24):3895–3906.
22. Stammers DK, et al. (2001) The structure of the negative transcriptional regulator NmrA reveals a structural superfamily which includes the short-chain dehydrogenase/reductases. *EMBO J* 20(23):6619–6626.
23. Thoden JB, Holden HM (1998) Dramatic differences in the binding of UDP-galactose and UDP-glucose to UDP-galactose 4-epimerase from Escherichia coli. *Biochemistry* 37(33):11469–11477.
24. Zhang G, et al. (2014) Mechanistic insights into polycycle formation by reductive cyclization in ikarugamycin biosynthesis. *Angew Chem Int Ed Engl* 53(19):4840–4844.
25. Ye Q, et al. (2010) Construction and co-expression of a polycistronic plasmid encoding carbonyl reductase and glucose dehydrogenase for production of ethyl (*S*)-4-chloro-3-hydroxybutanoate. *Bioresour Technol* 101(17):6761–6767.
26. Adams N, et al. (1990) Synthesis and antitumor activity of novel 4-demethoxyanthracyclines. *J Med Chem* 33(9):2375–2379.
27. Eberlein C, et al. (2013) Identification and characterization of 2-naphthoyl-coenzyme A reductase, the prototype of a novel class of dearomatizing reductases. *Mol Microbiol* 88(5):1032–1039.
28. Zhuo CX, Zhang W, You SL (2012) Catalytic asymmetric dearomatization reactions. *Angew Chem Int Ed Engl* 51(51):12662–12686.
29. Wang DS, Chen QA, Lu SM, Zhou YG (2012) Asymmetric hydrogenation of heteroarenes and arenes. *Chem Rev* 112(4):2557–2590.
30. Schätzle MA, et al. (2012) Tetrahydroxynaphthalene reductase: Catalytic properties of an enzyme involved in reductive asymmetric naphthol dearomatization. *Angew Chem Int Ed Engl* 51(11):2643–2646.
31. Husain SM, Schätzle MA, Lüdeke S, Müller M (2014) Unprecedented role of hydronaphthoquinone tautomers in biosynthesis. *Angew Chem Int Ed Engl* 53(37): 9806–9811.
32. Schätzle MA, Husain SM, Ferlaino S, Müller M (2012) Tautomers of anthrahydroquinones: Enzymatic reduction and implications for chrysophanol, monodictyphenone, and related xanthone biosyntheses. *J Am Chem Soc* 134(36): 14742–14745.
33. Conradt D, Schätzle MA, Haas J, Townsend CA, Müller M (2015) New insights into the conversion of versicolorin A in the biosynthesis of aflatoxin B1. *J Am Chem Soc* 137(34):10867–10869.

Supporting Information

Hydroxyl regioisomerization of anthracycline catalyzed by a four-enzyme cascade

Zhuan Zhang[a,1], Yu-Kang Gong[a,1], Qiang Zhou[a], Yu Hu[a], Hong-Min Ma[a], Yong-Sheng Chen[a], Yasuhiro Igarashi[b], Li-Feng Pan[a,2], and Gong-Li Tang[a,2]

[a]State Key Laboratory of Bio-organic and Natural Products Chemistry, Shanghai Institute of Organic Chemistry, Chinese Academy of Sciences, 345 Lingling Road, Shanghai 200032, China

[b]Biotechnology Research Center, Toyama Prefectural University, 5180 Kurokawa, Imizu, Toyama 939-0398, Japan

[1]These authors contributed equally to this work.

[2]Correspondence: Gong-Li Tang, Email: gltang@sioc.ac.cn;

Li-Feng Pan, Email: panlf@sioc.ac.cn.

Table of contents

Materials

Biochemicals and media were purchased from Sinopharm Chemical Reagent Co., Ltd. (China); Oxoid Ltd. (UK); Sigma-Aldrich Corporation (USA); Shanghai Sangon Biotech Co. Ltd. (China) or Alibaba (China) unless otherwise stated. D-[1-^{2}H]-glucose was purchased from Cambridge Isotope Laboratories, Inc (USA); the H_2O_2 Quantitative Assay Kit was purchased from Shanghai Sangon Biotech Co. Ltd. (China). The enzymes for genetic manipulation were purchased from Thermo Fisher Scientific Co. Ltd. (USA); Takara Biotechnology Co. Ltd. (China) or New England Biolabs (USA). Chemical reagents were purchased from Sigma-Aldrich Corporation (USA), Merck KGaA (Germany). All the plasmids and strains are in *SI Appendix* Table S3. Atomic coordinates and structural factors for the reported crystal structures of KstA11 are deposited in the Protein Data Bank under the accession numbers 5F5L and 5F5N.

Methods

Construction of gene disruption and replacement mutants. *KstA15* and *kstA16* were disrupted by replacing the genes with apramycin resistance (Am^R) cassette. To construct the *kstA15* or *kstA16* gene replacement mutant, PCR amplification using primers A15dc-F/A15dc-R, A16dc-F/A16dc-R (*SI Appendix*, Table S2) gained gene disruption cassettes comprising Am^R gene *aac(3)IV*, *oriT*(RK2), FRT sites and 39-bp homology region of *kstA15* or *kstA16* at both ends. Library fosmid pTG1702 and gene disruption cassette were introduced into *E. coli* BW25114 (which was Am^R PCR-targeting host derived from BW25113) by transformation in sequence. Transformants were selected with Am (100 μg/mL) to get strains containing gene-replaced fosmids pTG1715 and pTG1716. Recombinant fosmids were put into *E. coli* S17-1 and then introduced into *M.* sp. TP-A0468 through conjugation. Am^R, chloramphenicol-sensitive strains were selected as gene-replaced mutants and the genotype was verified by PCR with primers A15e-F/A15e-R or A16e-F/A16e-R (*SI Appendix*, Fig. S2)

KstA10 and *kstA11* were inactivated by inserting pOJ260 derivative plasmids into the genes via homologous recombination. The constructions of gene disrupted mutants were as follow. 0.75 kb and 0.78 kb fragments of *kstA10* and *kstA11* were amplified from genomic DNA of *M.* sp. TP-A0468 via PCR with the primers A10d-F/A10d-R, A11d-F/A11d-R respectively (*SI Appendix*, Table S2). The fragments were introduced into pOJ260 to give plasmid pTG1717 and pTG1718.

Recombinant plasmids were transformed into *E. coli* S17-1 and sequentially introduced into *M*. sp TP-A0468 via conjugation. Correct conjugants were selected with Am (100 μg/mL), and further validated via PCR with primers M13-R/A10d-v or M13-R/A11d-v, giving 0.85 kb and 0.86 kb band respectively as expect (*SI Appendix*, Fig. S3).

Gene cloning, expression and protein purification. DNA isolation and manipulation in *E. coli* or *M.* strains were performed following standard methods. PCR amplifications were carried out on a Thermal Cycler (Applied Biosystems) by PrimeSTAR HS DNA polymerase (Takara Biotechnology Co., Ltd. Japan). DNA cloning and mutagenesis primers were ordered from Shanghai Sangon Biotech Co. Ltd. (China) or Shanghai Invitrogen Biotech Co., Ltd. (China). DNA sequencing was carried out at Shanghai Majorbio Biotech Co. Ltd. (China) or Shanghai Biosune Biotech Co. Ltd. (China).

Protein expression and purification. The genes encoding KstA15 and KstA16 were amplified by PCR from fosmid pTG1702 using the corresponding primers respectively. *KstA11* and *kstA10* were amplified by PCR from fosmid pTG1701 using the corresponding primers respectively. The sequences of primers are presented in *SI Appendix*, Table S2. PCR products were cloned, and confirmed by sequencing, digested with *Nde*I and *Hin*dIII (or *Xho*I) and then ligated into the vector pET28a (+) or pET37b (+). The resulting recombinant plasmids listed in *SI Appendix* Table S3, were transferred into *E. coli* BL21 (DE3) for overexpression. Cultures (0.8 L) in LB medium supplemented with 50 μg/mL of kanamycin were grown to an OD600 of 0.4~0.6 at 37°C and protein expression was induced by the addition of isopropyl-β-D-thiogalactopyranoside (IPTG) to a final concentration of 0.08 mM, followed by further incubation for 18 hr at 18°C. The cultures were centrifuged for 10 min at 5,000 rpm at 4°C, and then resuspended *E. coli* cell pellet in 30 mL of lysis buffer (50 mM NaH_2PO_4, 500 mM NaCl, 10 mM imidazole, 10% glycerol, pH 8.0), purified the His-tagged fusion protein with Ni-NTA affinity resin according to manufacturer's manual (Qiagen, Valencia, CA).The target protein was desalted using a PD-10 Desalting Column (GE Healthcare, USA) and the purified protein was concentrated using an Amicon Ultra-4 (10~30 K, GE Healthcare) and stored at -80 °C in buffer (50 mM NaH_2PO_4, 50~100 mM NaCl, 10% glycerol, pH 8.0~8.5) for use in assays. Bradford assay was used to determine the concentration of

protein.

KstA11 expression and purification. Recombinant proteins were expressed in BL21 (DE3) *E. coli* cells at 16°C. The bacterial cells were lysed by the ultrahigh-pressure homogenizer FB-110XNANO homogenizer machine (Shanghai Litu Machinery Equipment Engineering Co., Shanghai, China). Then the lysate was spun down by centrifugation at 18000 rpm (39191 g) for 30 minutes to remove the pellet fractions. His_6-tagged proteins were purified by Ni^{2+}-NTA agarose (GE Healthcare, 17–5318–03) affinity chromatography. After further purification using size-exclusion chromatography, the recombinant proteins were analyzed by SDS-PAGE, and concentrated using Stirred ultrafiltration cells (Millipore, USA) according to the manufacturer's protocol. The concentration of each protein was determined by NanoDrop 2000c (Thermo Scientific, USA).

To prepare the SeMet-labeled KstA11 protein, the cells were cultured in 1 L of M9 minimal medium at 37°C until they reached a density of 0.5 at $OD_{600\ nm}$. After supplementations with 0.06 g of SeMet (J&K Scientific Ltd., China), 0.1 g of lysine, threonine, and phenylalanine, and 0.5 g of leucine, isoleucine and valine, protein expression was induced by the addition of IPTG to a final concentration of 1 mM, followed by further incubation at 16°C overnight.

Protein crystallization and structural elucidation. Crystallization of the SeMet-KstA11 and KstA11-**5**-NAD^+ complex was performed using the sitting-drop, vapor-diffusion method at 16°C. To obtain SeMet-PyrI4 crystals, the solution composed of the SeMet-KstA11 protein (12 mg/mL in 20 mM Tris–HCl, pH 7.5, 100 mM NaCl, 1 mM DTT and 1 mM EDTA) was mixed with an equal volume of reservoir solution containing DL-Malic acid (100 mM, pH 6.5) and polyethylene glycol 3350 (20%, w/v) (HAMPTON RESEARCH CORP., HR2-098). Prior to the diffraction experiments, glycerol (15%) was added as the cryo-protectant. For the KstA11-**5**-NAD^+ complex, native KstA11 protein (16 mg/mL in 20 mM Tris–HCl, pH 7.5, 100 mM NaCl, 1 mM DTT and 1 mM EDTA) was saturated with substrate **5** (with a molar ratio up to 10 : 1 for **5** to KstA11) and co-factor NAD^+ (with a molar ratio up to 10 : 1 for NAD^+ to KstA11). Crystals of the KstA11-**5**-NAD^+ complex were harvested under the crystallization condition with 20 mM Magnesium chloride hexahydrate, 100 mM HEPES (pH=7.5) and 22% w/v Polyacrylic acid

sodium salt 5-100 (HAMPTON RESEARCH CORP., HR2-144). Prior to the diffraction experiments, the crystals were soaked in crystallization solution containing 5 mM **5**, 5 mM NAD^+ and 15% glycerol for cryo-protection.

All diffraction data sets were collected at the Shanghai Synchrotron Radiation Facility, and processed and scaled using HKL2000 (1) (*SI Appendix*, Table S1**)**. The single-wavelength anomalous diffraction phase was determined for the SeMet derivative dataset and a partial structural model was traced in AutoSol (2). The structure model was manually built based on the experimental phase and then refined using PHENIX (3). COOT was used for model rebuilding and adjustments (4). The phase problem of the complex was solved by the molecular replacement method using the structure of the SeMet-KstA11 protein with PHASER (5). The initial model was rebuilt manually and then refined using REFMAC (6). Further manual model building and adjustment were completed using COOT. The qualities of the final model were validated by MolProbity (7). The final refinement statistics are listed in *SI Appendix* Table S1. Structural diagrams were prepared using the program PyMOL (http://www.pymol.org/).

Site-specific mutation in KstA10 and KstA11. PCR amplifications were carried out using relative recombinant plasmids (*SI Appendix*, Table S2), after 18-cycle PCR amplification (using the primers listed in *SI Appendix*, Table S2) followed by subsequent *Dpn*I digestion, according to the standard procedure of the Quick Change Site-Directed Mutagenesis Kit purchased from Stratagene (USA). Each mutation was confirmed by sequencing. The recombined plasmids (*SI Appendix*, Table S3) were expressed in *E. coli* BL21 (DE3) according to the procedures described above for the native proteins.

Metabolite analysis. High performance liquid chromatography (HPLC) analysis was conducted on the Agilent 1200 HPLC system (Agilent Technologies Inc., USA) or Thermo Scientific Dionex Ultimate 3000 (Thermo Fisher Scientific Inc., USA) with a reverse-phase Alltima C18 column (5μ, 4.6×250 mm). Semi-preparative HPLC was performed on a Shimadzu LC-20-AT system. HPLC electrospray ionization MS (HPLC-ESI-MS) was performed on the Thermo Fisher LTQ Fleet ESI-MS spectrometer (Thermo Fisher Scientific Inc., USA). High-resolution ESI-MS analysis was conducted on the 6230B Accurate Mass TOF LC/MS System (Agilent Technologies Inc., USA).

NMR data were recorded on the BrukerAvance III AV400 (Cryo) spectrometers (Bruker Co. Ltd., Germany) or on the Agilent ProPlus 500 MHz NMR spectrometer (Agilent Technologies Inc., USA).

Production and analysis of KST and intermediates. *M.* sp. TP-A0468 wild-type and mutants were cultured in Y-22 medium (soluble starch 1%, glucose 0.5%, NZ-case plus 0.3%, yeast extract 0.2%, tryptone 0.5%, KH_2PO_4 0.1%, $MgSO_4$ 0.05%, $CaCO_3$ 0.3%, pH 7.0, and with 50 μg/mL apramycin for recombinant strains) at 30°C for 4–5 days. For fermentation, 3% inoculums were seeded in a 500 mL flask containing 100 mL of the fermentation broth (lactose 4%, cotton seed meal 2%) and incubated at 30°C for 2 days, then adding 4 g sterilized HP20 and incubation for another 2 days. The sediment after certification was extracted twice with acetone, and the extract was evaporated to remove acetone, extracted twice with ethyl acetate, evaporated, and finally dissolved with 500 μL methanol for analysis via HPLC and LC-MS. HPLC was performed using a reverse-phase Alltima C18 column (5μ, 4.6×250 mm) with UV detection at 254 nm under the following program: gradient elution of mobile phase A (H_2O supplemented with 0.1% formic acid and 10 mM ammonium acetate) and mobile phase B (acetonitrile supplemented with 0.1% formic acid) using a flow rate of 1 mL/min: 0-24 min, 24-60% phase B; 24-29 min, 60-80% phase B; 29-30 min, 80-95% phase B; 30-33 min, 95% phase B; 33-35 min, 95-24% phase B.

KstA15/KstA16 assay. The hydroxylation reaction was carried out in 50 mM NaH_2PO_4 containing 5 μM KstA15, 10 μM KstA16, 0.5 mM compound **3** and 1 mM NADH , in 50 μL of solution at pH 8.0. The reaction was incubated for 2 hr at 28°C then quenched by the addition of 3×50 μL of ethyl acetate, extracted by vortexing. The ethyl acetate layer (top layer) was evaporated to dryness in an eppendorf concentrator plus, the residue was dissolved in 50 μL methanol. The enzyme reaction was analyzed by HPLC with gradients of methanol in water using a flow rate of 0.8 mL/min: 0-5 min, 30-84% phase B; 5-20 min, 84-90% phase B; 20-22 min, 90-95% phase B; 22-25min, 95-30% phase B; UV detection at 254 nm. Control reactions lacking specific components were carried out to determine their necessity for enzymatic reaction.

Experiment under anaerobic. KstA15 and KstA16 were purified under anaerobic. The reaction

was performed in an anaerobic glove box (Coy Laboratory Product Inc., USA). 50 μL deoxygenized solution containing 50 mM NaH_2PO_4 (pH 8.0), 0.5 mM compound **3** or **3g** and 2 mM NADH. The reaction was initiated by adding KstA15 and KstA16, and performed at 28°C for overnight. Subsequent procedures were carried out according methods described in KstA15/KstA16 assay.

KstA11 assay. KstA11 activity was typically assayed with a reaction mixture volume of 50 μL, incubated at 28°C for 30min, and containing 0.25 mM compound **5**, with 0.5 mM NADH in 50 mM NaH_2PO_4, pH 6.0, and KstA11 was added to a final concentration of 1 μM. The aqueous mixture was extracted with 50 μL chloroform, and subjected to HPLC and LC-MS for analysis.

KstA10 assay. The single-step assay condition was in a total volume of 50 μL conversion buffer (50 mM NaH_2PO_4, pH 5.5), containing 0.5 mM **6b**, 1 mM NADH, KstA10 was added to a final concentration of 5 μM. The reaction was incubated at 26°C for two hours. Subsequent procedures were carried out according methods described in KstA15/KstA16 assay. During the multiple enzyme assay, firstly, the reaction was carried out in a reaction buffer (50 mM NaH_2PO_4, pH 5.5), 0.25 mM **5** served as the substrate, in the presence of 1 mM NADH and 10 μM KstA11, with a reaction mixture volume of 50 μL, incubated at 24°C for 10 min. Then adding KstA10 to a final concentration of 2.5 μM, the reaction was incubated at 24°C for another 1 hour. Subsequent procedures were carried out according methods described in KstA15/KstA16 assay.

Detection assumption of NADH. Using multiple enzyme assay, firstly, the reaction was carried out in 50 μL of reaction buffer (50 mM NaH_2PO_4, pH 5.5), 0.25 mM compound **5** served as the substrate, in the presence of 0.25 or 0.5 mM NADH and 10 μM KstA11, incubated at 24°C for 5 min. Then adding KstA10 or inactivated kstA10 to a final concentration of 10 μM, and incubated at 24°C for another 25 min. The reaction mixture was extracted with ethyl acetate, the organic phase and aqueous phase were separated by centrifugation (12000 rpm for 5 min). The aqueous phase was evaporated for 5 min in an eppendorf concentrator plus, to remove remanent ethyl acetate. The aqueous phase was analyzed by HPLC with gradients of methanol in water using a

flow rate of 0.8 mL/min: 0-10 min, 4% phase B; UV detection at 260 and 340 nm. Control reactions lacking specific components were carried out to determine their attributions and assumptions of NADH or NAD^+.

Isolation of metabolic intermediates. Intermediates **3** and **3g** were produced by *M.* sp. TG1711 using the same culture procedures as described for wild type. For isolation of intermediates **3** and **3g**, a total of 8 L of culture was prepared for fermentation. The culture broth was centrifugalized (5000 rpm for 10 min); all the mycelia including macro resin HP20 were collected followed by stirring extraction with acetone. The extract was evaporated to remove acetone, and then extracted twice with ethyl acetate, followed removal of the organic solvents by evaporation. The crude extracts were subjected to silica gel column (100-200 mesh), and successively eluted with ethyl acetate/petroleum ether (1/5, 2/5, 3/5, 4/5, 5/3, 5/2) and $CHCl_3/CH_3OH$ (100/0, 100/5, 100/10) to yield corresponding fractions. Fractions containing target components were combined and subjected to silica gel column (230-400 mesh), and eluted with $CHCl_3/CH_3OH$ (100/0, 100/1, 100/2, 100/3, 100/4, 100/5) to afford 60 mg **3** and 10 mg **3g**. The isolation **4g** with a yield of 2 mg/L from *M.* sp. TG1708 following the similar process (8). For isolation of intermediate **5g**, a total of 6 L of culture (*M.* sp. TG1713) was prepared and the same procedure described in the preparation of **3** and **3g** isolation, **5g** (200 mg) were obtained.

Preparation of the enzymatic products. 3d: Reactions were performed using 200 x 200 μL batches in an anaerobic glove box (Coy Laboratory Product Inc., USA). KstA15 and KstA16 were purified under anaerobic conditions. 200 μL deoxygenized buffer containing 50 mM NaH_2PO_4 (pH 8.0), 0.5 mM compound **3** and 2 mM NADH, incubated with KstA15 and KstA16, and performed at 28°C for overnight. All the reactions were combined and extracted with ethyl acetate; the extract was evaporated to remove the organic solvents. The crude extracts were purified by semi-preparative HPLC with isocratic elution of methanol in water using a flow rate of 2.8 mL/min (70% phase B). **5:** Reactions were performed using 200 x 200 μL batches carried out in 50 mM NaH_2PO_4 containing 10 μM KstA15, 20 μM KstA16, 0.5 mM compound **3** and 1.5 mM NADH, in 200 μL of solution at pH 8.0. The reaction was incubated for 5 hr at 28°C. All the reactions were combined and extracted with ethyl acetate; the extract was evaporated to remove

the organic solvents. The crude extracts were purified by semi-preparative HPLC with isocratic elution of methanol in water using a flow rate of 2.8 mL/min (60% phase B). **6b:** Reactions were carried out in 50 mM NaH_2PO_4 containing 100 μM KstA11, 1 mM compound **5** and 3 mM NADH, in 50 mL of solution at pH 6.0. The reaction was incubated for 2 hr at 28°C, and then extracted with $CHCl_3$ directly. The extract was evaporated to remove the organic solvents by evaporation. The crude extracts were subjected to silica gel column (230-400 mesh), and eluted with $CHCl_3$/CH_3OH (100/0, 100/1, 100/2, 100/3, 100/4, 100/5) to give **6b**. All the rotary evaporation processes were performed under ice-water bath. A large scale intermediates **6b** was produced by *M.* sp. TG1714 using the same culture procedures as described for wild type. For production of **6b**, a total of 6 L of culture was prepared for fermentation. The culture broth was centrifugalized (5000 rpm for 10 min); all the mycelia including macro resin HP20 were collected followed by stirring extraction with $CHCl_3$ directly. The extract was evaporated to remove the organic solvents by evaporation. The crude extracts were subjected to silica gel column (230-400 mesh), and eluted with $CHCl_3$/CH_3OH (100/0, 100/1, 100/2, 100/3, 100/4, 100/5) to give **6b (**3 mg/L**)**. All the rotary evaporation processes were performed under ice-water bath. **4d:** Reactions were carried out using 100×20 mL batches. Reaction mixture containing 50 mM NaH_2PO_4 (pH 5.5), 0.5mM compound **6b** and 2 mM NADH, incubated with KstA10 with a final concentration of 25 μM and performed at 25°C for overnight. Subsequent manipulations were consistent with previously described post-treatment for **3d**. Semi-preparative HPLC with isocratic elution of methanol in water using a flow rate of 2.8 mL/min (75% phase B). ^{2}H-**6b:** The reactions were carried out in a total volume of 4 x 5mL batches containing 50mM NaH_2PO_4 (pH 6.0), 2 mM $NADP^+$, 20 mM [1-^{2}H] D-glucose and 100 μM purified recombinant BmGDH, in 5 mL of solution at 37°C for 1h. Cool the reaction system to room temperature prior to adding 3 mg substrate **5** and KstA11 with a final concentration of 10 μM and incubated at 26°C until complete transformation of **5** (about 2 hours) and then extracted with $CHCl_3$ directly. The extract was evaporated to remove the organic solvents by evaporation. The crude extracts were subjected to silica gel column (230-400 mesh), and eluted with $CHCl_3$/CH_3OH (100/0, 100/1, 100/2, 100/3, 100/4, 100/5) to give 5 mg ^{2}H-**6b** for characterization. ^{2}H-**4**: The reactions were carried out in a total volume of 20 x 5mL batches containing 25mM NaH_2PO_4 (pH 6.0), 2 mM $NADP^+$, 30mM [1-^{2}H] D-glucose and 100 μM purified recombinant BmGDH, in 5 mL of solution at 37°C for 1h. Cool the reaction system to

room temperature prior to adding 3 mg substrate **5** and KstA11 with a final concentration of 10 μM and incubated at 26°C until complete transformation of **5** and then added 125 μL NaH_2PO_4 (pH 5.0) to adjust the reaction system to pH 5.5. Finally, KstA10 was added to the reaction mixture with a final concentration of 30 μM and incubated at 26°C for overnight. The reaction mixture was extracted with ethyl acetate directly. The extract was evaporated to remove the organic solvents by evaporation. The crude extracts were subjected to silica gel column (230-400 mesh), and eluted with $CHCl_3$/CH_3OH (100/0 -100/10) to yield 2 mg ^{2}H-**4**.

References

1. Otwinowski Z, Minor W (1997) Processing of X-ray diffraction data collected in oscillation mode. *Method Enzymol* 276:307–326.
2. Terwilliger TC, et al. (2009) Decision-making in structure solution using Bayesian estimates of map quality: the PHENIX AutoSol wizard. *Acta Crystallogr. D, Biol. Crystallogr* 65(Pt 6): 582–601.
3. Adams PD, et al. (2002) PHENIX: building new software for automated crystallographic structure determination. *Acta Crystallogr. D, Biol. Crystallogr* 58 (Pt 11):1948–1954.
4. Emsley P, Cowtan K (2004) Coot: model-building tools for molecular graphics. *Acta Crystallogr. D, Biol. Crystallogr* 60 (Pt 12 Pt 1):2126–2132.
5. Storoni LC, McCoy AJ, Read RJ (2004) Likelihood-enhanced fast rotation functions. *Acta Crystallogr. D, Biol. Crystallogr*. 60(Pt 3):432–438.
6. Murshudov GN, Vagin AA, Dodson EJ (1997) Refinement of macromolecular structures by the maximum-likelihood method. *Acta Crystallogr. D, Biol. Crystallogr* 53(Pt 3): 240–255.
7. Davis IW, et al. (2007) MolProbity: all-atom contacts and structure validation for proteins and nucleic acids. *Nucleic Acids Res* 35:W375–383.
8. Ma HM, et al. (2013) Unconventional origin and hybrid system for construction of pyrrolopyrrole moiety in kosinostatin biosynthesis. *Chem Biol* 20(6):796–805.

Supplementary Figures

Figure S1. Results of protein alignments.

A

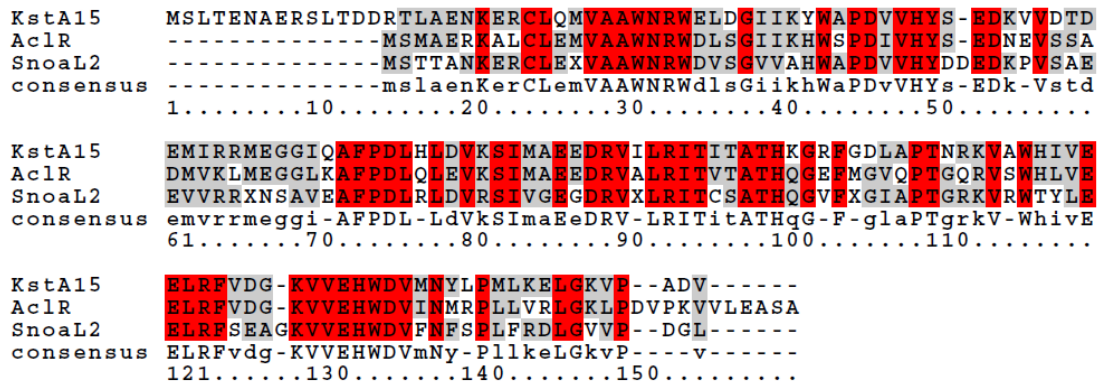

B

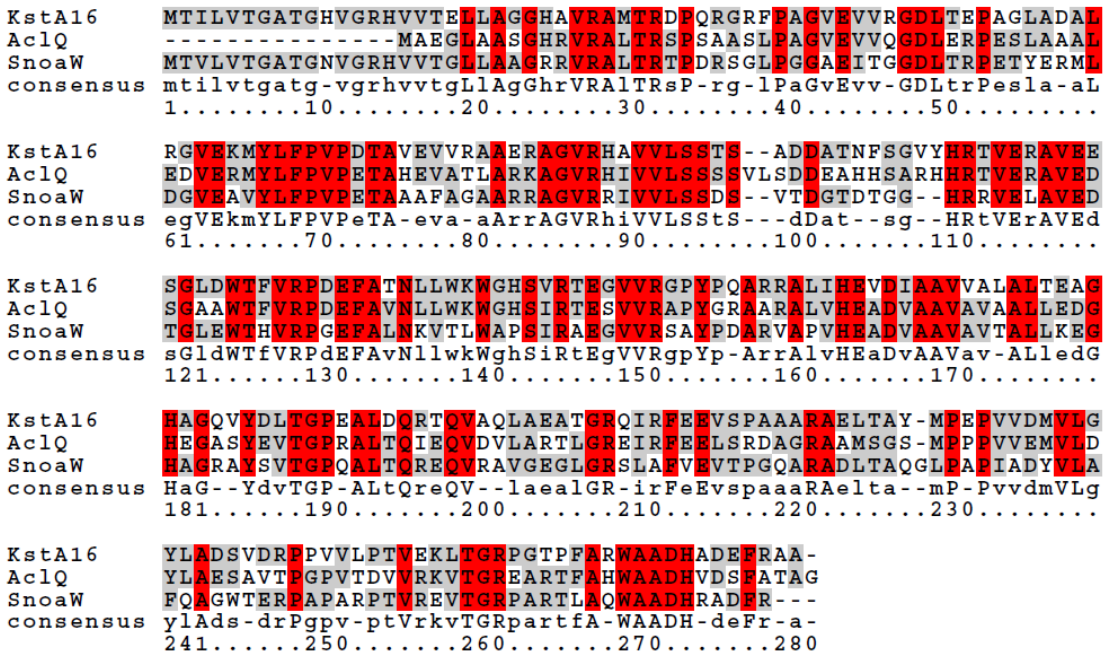

A, KstA15 with and AclR (identity/similarity, 68/86) and SnoaL2 (identity/similarity, 60/77).

B, KstA16 with AclQ (identity/similarity, 59/67) and SnoaW (identity/similarity, 54/65).

Figure S2. Construction and verification of *kstA15* and *kstA16* replacement mutant strains.

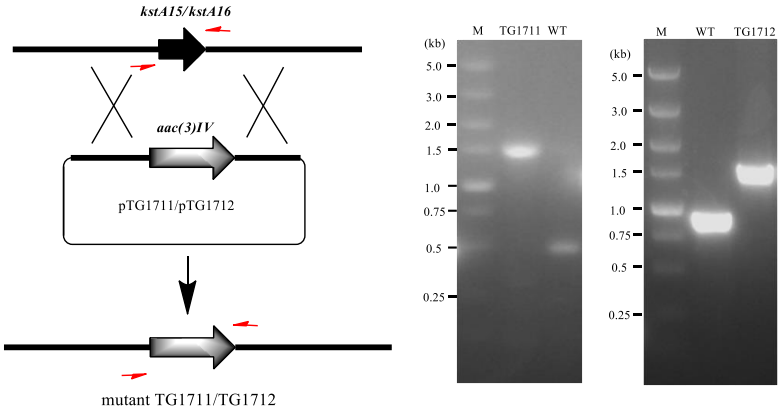

Figure S3. Construction and verification of *kstA10* and *kstA11* disruption mutant strains.

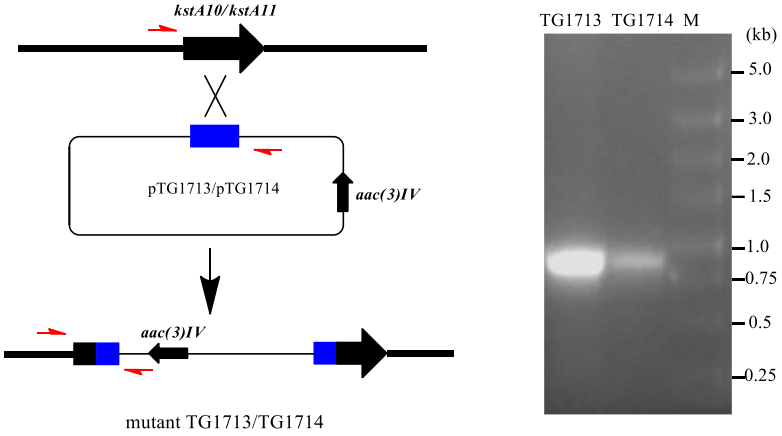

Figure S4. Analysis of purified proteins by SDS-PAGE (12 %).

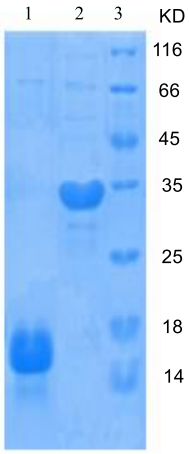

Line1, KstA15; line 2, KstA16; line 3, marker (116 KDa); the proteins were visualized by staining the gel with Coomassie Blue R250.

Figure S5. The time course of H_2O_2 formation.

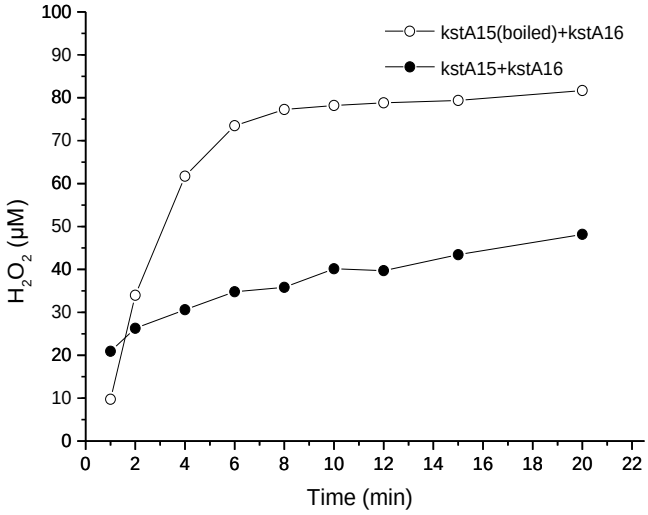

The reaction was carried out in 50 mM NaH_2PO_4, pH 7.5, 0.2 mM compound **3**, 0.4 mM NADH, 20 μM kstA15 and 10 μM kstA16. Formation of H_2O_2 was detected using H_2O_2 Quantitative Assay Kit at various reaction times (1, 2, 4, 6, 8, 10, 12, 14, 15, 20 min).

Figure S6. Effects of various concentrations of NADH on H_2O_2 formation.

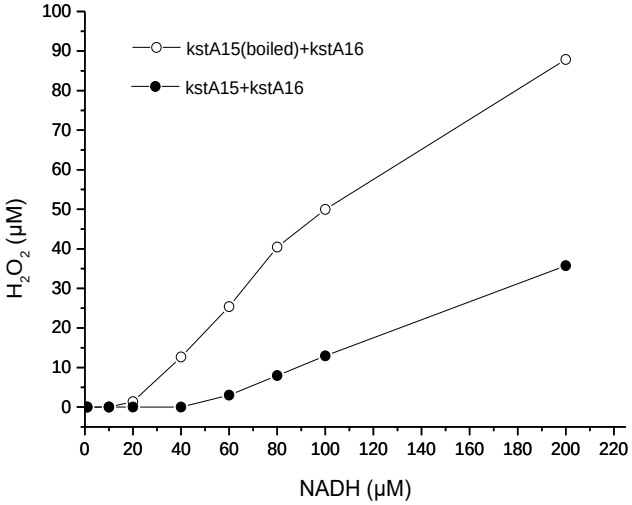

The reaction was carried out in 50 mM NaH_2PO_4, pH 7.5, 0.2 mM compound **3**, (0-0.2mM) NADH, 20 μM kstA15 and 10 μM kstA16. Formation of H_2O_2 was detected using H_2O_2 Quantitative Assay Kit at 10 min.

Figure S7. Detailed structural analysis of KstA11-NAD$^+$-5 complex.

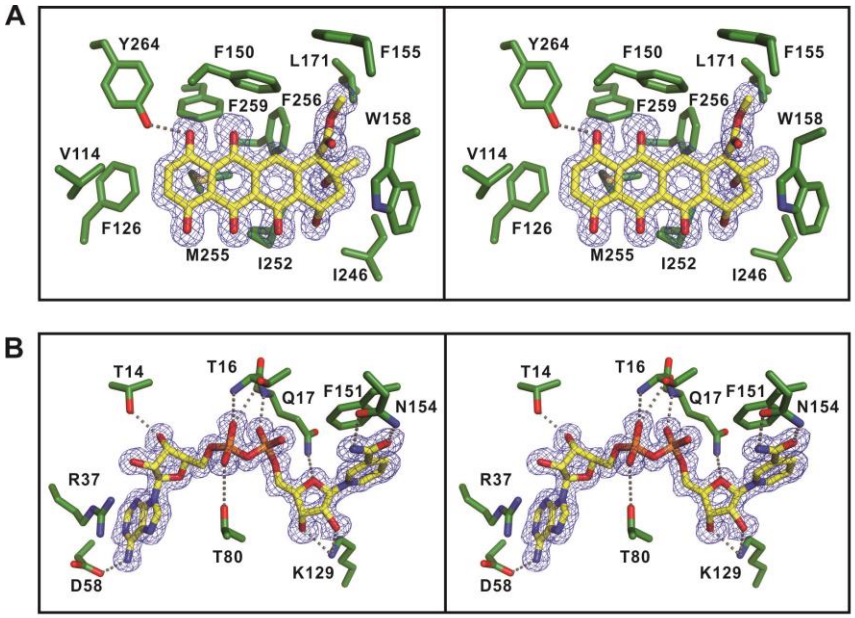

A, Stereo view showing the detailed interactions between KstA11 and substrate **5**. The hydrogen bonds involved in the binding are shown as dotted lines. Substrate **5** is overlaid with its refined F_o-F_c electron density map that is calculated by omitting the substrate **5** from the final PDB file (purple mesh, contoured at 3σ). **B**, Stereo view showing the detailed interactions between KstA11 and NAD$^+$. The hydrogen bonds involved in the binding are shown as dotted lines. NAD$^+$ is overlaid withits refined F_o-F_c electron density map that is calculated by omitting the substrate **5** from the final PDB file (purple mesh, contoured at 3σ).

Figure S8. Analysis of purified native and mutants of KstA11 by SDS-PAGE (12 %).

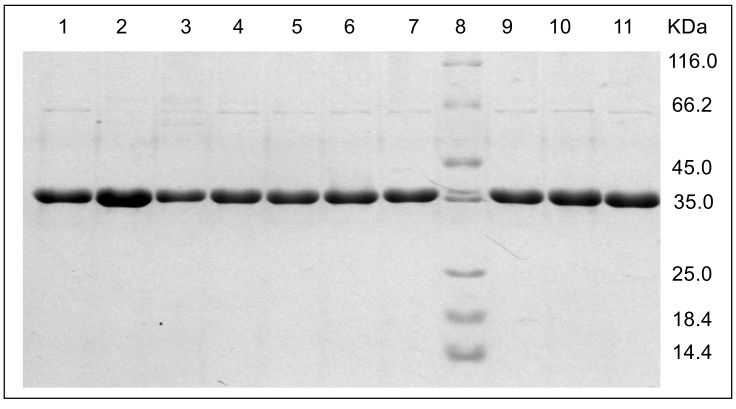

Line1, R37E; line 2, E90A; line 3, K129Q; line 4, K129R; line 5, F151A; line 6, N154D; line 7, N154K; line 8, Marker (116 KDa); line 9, N154L; line 10, I252Y; line 11, WT. The proteins were visualized by staining the gel with Coomassie Blue R250.

Figure S9. Enzymatic activities of KstA11 mutants.

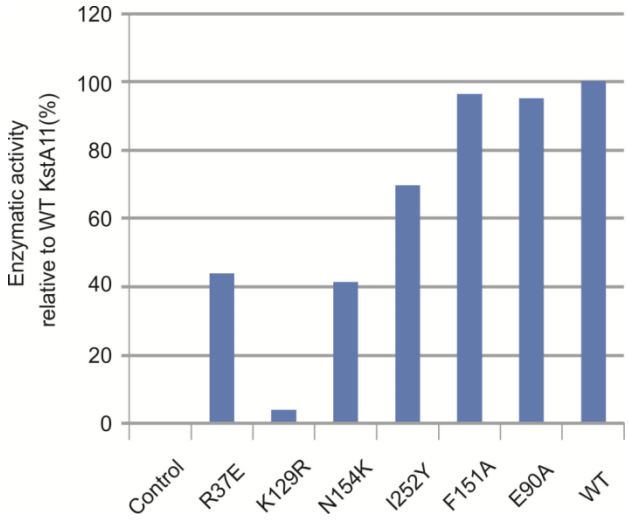

Figure S10. Analysis of purified KstA10 by SDS-PAGE (12 %).

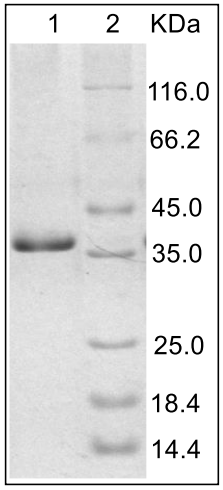

Line1, WT; line 2, Marker (116 KDa); The proteins were visualized by staining the gel with Coomassie Blue R250.

Figure S11. Dehydration catalyzed by KstA10 is dependent on NADH.

A **B**

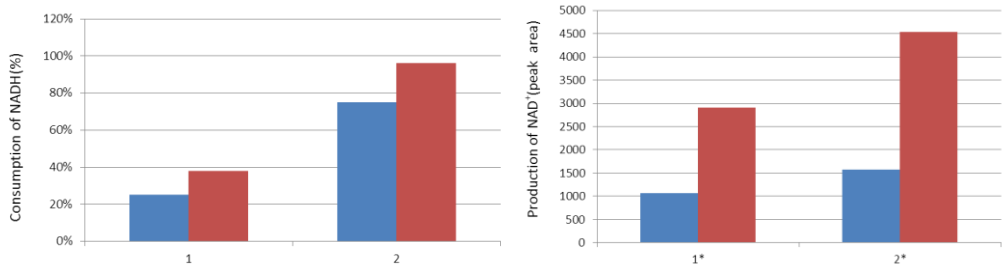

A: consumption of NADH: **1 blue**, 0.3 mM substrate **5**, 0.6 mM NADH, 12 μM KstA11, incubated for 5 min, then added 12 μM KstA10 (boiled) and incubated for another 25 min at 22°C; **1 red**, 0.3 mM substrate **5**, 0.6 mM NADH, 12 μM KstA11, incubated for 5 min at 22°C, then added 12 μM KstA10 and incubated for another 25 min at 22°C; **2 blue**, 0.3 mM substrate **5**, 0.3 mM NADH, 12 μM KstA11, incubated for 5 min, then added 12 μM KstA10 (boiled) and incubated for another 25 min at 22°C; **2 red**, 0.3 mM substrate **5**, 0.3 mM NADH, 12 μM KstA11, incubated for 5 min at 22°C, then added 12 μM KstA10 and incubated for another 25 min at 22°C.

B: production of NAD^+: **1* blue** correspondence with **1 blue**, **1* red** correspondence with **1 red**; **2* blue** correspondence with **2 blue**, **2* red** correspondence with **2 red**.

Supplementary Tables

Table S1. Statistics of X-ray crystallographic data collection and model refinements.

	SeMet-KstA11	KstA11-**5**-NAD^+complex
Data collection		
Wavelength (Å)	0.9791	0.9785
Space group	P 4 21 2	P 21 21 21
Cell dimensions		
a, b, c (Å)	93.7, 93.7, 71.2	56.5, 66.0, 176.3
α, β, γ (°)	90, 90, 90	90, 90, 90
Resolution range (Å)	50.00 - 1.68 (1.71 - 1.68)	50.00 - 1.30 (1.32 - 1.30)
R_{merge} (%)[a]	10.2 (96.1)	8.4 (38.6)
Mean I/sigma(I)	65.5 (4.6)	44.8 (8.2)
Completeness (%)	100.0 (100.0)	99.6 (99.9)
Redundancy	28.4 (28.7)	6.7 (6.8)
Structure refinement		
Resolution (Å)	39.2 - 1.68 (1.72 - 1.68)	31.1 - 1.30 (1.32 - 1.30)
R_{cryst}/ R_{free}(%)[b]	12.9 (14.5) / 17.7 (20.4)	14.3 (16.9) / 16.6 (20.0)
r.m.s.d bonds (Å) / angles (°)	0.011 / 1.357	0.006 / 1.194
Average B-factor(Å^2)	27.0	18.0
No. of atoms		
macromolecules	2202	4466
water	317	1042
ligands	38	239
Ramachandran plot[c]		
favored region (%)	97.96	98.66
allowed region (%)	1.70	1.34
outliers (%)	0.34	0.00

[a]$R_{merge}= \sum|I_i - I_m|/\sum I_i$, where I_i is the intensity of the measured reflection and Im is the mean intensity of all symmetry related reflections.

[b]$R_{cryst}= \Sigma||F_{obs}| - |F_{calc}||/\Sigma|F_{obs}|$, where F_{obs} and F_{calc} are observed and calculated structure factors.

$R_{free} = \Sigma_T||F_{obs}| - |F_{calc}||/\Sigma_T|F_{obs}|$, where T is a test data set of about 5% of the total reflections randomly chosen and set aside prior to refinement.

[c] Defined by Molprobity.

Numbers in parentheses represent the value for the highest resolution shell.

Table S2. List of PCR primers used in this study.

A15dc-F	ATGTCCCTGACCGAGAACGCGGAACGGTCCCTGACCGACATTCC GGGGATCCGTCGACC
A15dc-R	CACCTTGCCGAGCTCCTTGAGCATCGGCAGGTAGTTCATGTAGGC TGGAGCTGCTTC
A15e-F	TAAGAATTCCATATGTCCCTGACCGAGAAC
A15e-R	TTAAAGCTTTTACTCGAGGACGTCCGCCGGCACCTT
A16dc-F	ACCGGACACGTCGGCCGACACGTGGTCACGGAGCTGCTGATTCC GGGGATCCGTCGACC
A16dc-R	CACGGAGTCGGCCAGGTAGCCGAGCACCATGTCGACCACTGTAG GCTGGAGCTGCTTC
A16e-F	TAAGAATTCCATATGACGATCCTGGTGACG
A16e-R	TTAAAAGCTTTTACTCGAGGGCCGCGCGGAACTCGTC
A10d-F	TATTCTAGAAGGTGGGCAGGCACGTGGTG
A10d-R	TATAAGCTTCGAGCAGCCGCTCGACGGTG
A10d-v	CATTCCGTTTCCGACC
M13-R	CGCCAGGGTTTTCCCAGTCACGAC
A11d-F	TAT TCTAGAACCGCACCATCCTCGTCAC
A11d-R	TAT AAGCTTCGTACCCGTCGGTCTGGAAC
A11d-v	CACCTGTTCCGATGAC
M13-R	CGCCAGGGTTTTCCCAGTCACGAC
KstA10 for	ATA GAATTC CATATG ATCCTCGTCACCGGCGCG
KstA10 rev	ATA AAGCTT A CTCGAG TCGGAACAGGTGGGCGTGC
KstA11 for	ATA *GAATTC CATATG* GCCGACAGCAACCGCACCA
KstA11 rev	ATA AAGCTT A CTCGAG CCCGGCGGCGGGCGCC
KstA15 for	ATA GAATTC CATATG TCCCTGACCGAGAACGC
KstA15 rev	ATA AAGCTT A CTCGAG GACGTCCGCCGGCACCT
KstA16 for	ATA GAATTC CATATG ACGATCCTGGTGACGGGC
KstA16 rev	ATA AAGCTT A CTCGAG GGCCGCGCGGAACTCG
KstA11-R37E-for	GAAGACCCGGGCACCGAC
KstA11-R37E-rev	GACCAGGGCGCGCACCG
KstA11-D58A-for	TCGCTGGTGACCGGCGCA CTCAACGACCAGGCC
KstA11-D58A-rev	TGC GCCGGTCACCAGCGACACGCCGGCCGCGGC
KstA11-E90A-for	GGCGGGCTGGGCGCGGCGCTGCGCCAGGGC
KstA11-E90A-rev	CGCCGCGCCCAGCCCGCCGGGGGTCATGAA

KstA11-K129Q-for	CCGCACTTCGAGACCCAGTGGACGATCGAG
KstA11-K129Q-rev	CTGGGTCTCGAAGTGCGGCACCCCGCTGGC
KstA11-K129R-for	CCGCACTTCGAGACCCGCTGGACGATCGAG
KstA11-K129R-rev	GCGGGTCTCGAAGTGCGGCACCCCGCTGGC
KstA11-F151A-for	GCCATGGACAACTTCGCCG
KstA11-F151A-rev	GAAGGTGGGGCGCAGCAC
KstA11-N154D-for	GACTTCGCCGCCTGGGG
KstA11-N154D-rev	GTCCATGAAGAAGGTGGGGC
KstA11-N154K-for	AAGTTCGCCGCCTGGGG
KstA11-N154K-rev	GTCCATGAAGAAGGTGGGGC
KstA11-N154L-for	ACCTTCTTCATGGACCTCTTCGCCGCCTGGGGC
KstA11-N154L-rev	GAG GTCCATGAAGAAGGTGGGGCGCAGCACCGT
KstA11-I252Y-for	CCGTACAGCCACGAGTACGCGGTGATGTTCGAG
KstA11-I252Y-rev	GTA CTCGTGGCTGTACGGGATCCACGGGTCGGC
KstA11-Y264F-for	TTCGCCGCCGACATCG
KstA11-Y264F-rev	CCCGTCGGTCTGGAACCAC

Table S3. Strains and plasmids used in this study.

Strain/Plasmid	Characteristics	Reference
Strains		
E. coli DH5α	Host for general cloning	Invitrogen
E. coli BL21(DE3)	Host for protein expression	Invitrogen
E. coli S17-1	Donor strain for conjugation between *E. coli* and *Micromonospora*	1
E. coli BW 25113	Host for PCR-targeting gene replacement on fosmids	2
Micromonospora (*M.*) sp. TP-A0468	Wild type strain	3
M. sp. TG1708	Δ*kstB1* gene replacement mutant, **4** and **4g** producer	4
M. sp. TG1711	Δ*kstA15* gene replacement mutant, **3** and **3g** producer	This work
M. sp. TG1712	Δ*kstA16* gene replacement mutant, **3** and **3g** producer	This work
M. sp. TG1713	Δ*kstA11* gene disruption mutant, **5** and **5g** producer	This work
M. sp. TG1714	Δ*kstA10* gene disruption mutant, **6b** producer	This work
Plasmids		
pSP72	Ap^R, *E. coli* subcloning vector	Promega
pANT841	Ap^R, *E. coli* subcloning vector	AF438749
pET28a	Km^R, heterologous expression vector in *E. coli*	Invitrogen
pET37b	Km^R, heterologous expression vector in *E. coli*	Invitrogen
pCC1FOS-1™	fosmid vector for genomic library construction	Epicentre
pOJ260	Am^R, shuttle vector for gene inactivation	1
pTG1701	Fosmid containing *kst* gene cluster (left part)	4
pTG1702	Fosmid containing *kst* gene cluster (right part)	4
pRSF-BmGDH	Expression vector for D-Glucose dehydrogenase from *Bacillus megaterium* (BmGDH)	5
pTG1715	pTG1702 derivative for gene replacement of *kstA15*	This work
pTG1716	pTG1702 derivative for gene replacement of *kstA16*	This work
pTG1717	pOJ260 derivative for gene disruption of *kstA10*	This work
pTG1718	pOJ260 derivative for gene disruption of *kstA11*	This work
pTG1719	pET28a containing *kstA15* for protein expression	This work
pTG1720	pET28a containing *kstA16* for protein expression	This work
pTG1721	pET37b containing *kstA10* for protein expression	This work

pTG1722	pET28a containing *kstA11* for protein expression	This work
pTG1723	pTG1722 derivative for expression of KstA11-R37E	This work
pTG1724	pTG1722 derivative for expression of KstA11-D58A	This work
pTG1725	pTG1722 derivative for expression of KstA11-E90A	This work
pTG1726	pTG1722 derivative for expression of KstA11-K129Q	This work
pTG1727	pTG1722 derivative for expression of KstA11-K129R	This work
pTG1728	pTG1722 derivative for expression of KstA11-F151A	This work
pTG1729	pTG1722 derivative for expression of KstA11-N154D	This work
pTG1730	pTG1722 derivative for expression of KstA11-N154K	This work
pTG1731	pTG1722 derivative for expression of KstA11-N154L	This work
pTG1732	pTG1722 derivative for expression of KstA11-I252Y	This work
pTG1733	pTG1722 derivative for expression of KstA11-Y264F	This work

Ap^R, ampicillin resistance; Km^R, kanamycin resistance; Am^R, apramycin resistance.

References

1. Kieser, T., Bibb, M. J., Buttner, M. J., Chater, K. F. & Hopwood, D. A. *Practical Streptomyces Genetics* (John Innes Foundation, Norwich, UK) (2000)
2. Gust, B., Challis, G. L., Fowler, K., Kieser, T. & Chater, K. F. PCR-targeted *Streptomyces* gene replacement identifies a protein domain needed for biosynthesis of the sesquiterpene soil odor geosmin. *Proc. Natl. Acad. Sci. USA* **100**, 1541-1546 (2003).
3. Igarashi, Y., Higuchi, H., Oki, T. & Furumai, T. Kosinostatin, a quinocycline antibiotic with antitumor activity from *Micromonospora* sp. TP-A0468. *J. Antibiot.* (Tokyo) **55**, 128-133 (2002).
4. Ma, H.-M. *et al.* Unconventional origin and hybrid system for construction of pyrrolopyrrole moiety in kosinostatin biosynthesis. *Chem. Biol.* **20**, 796-805 (2013).
5. Ye, Q. *et al.* Construction and co-expression of a polycistronic plasmid encoding carbonylreductase and glucose dehydrogenase for production of ethyl (*S*)-4-chloro-3-hydroxybutanoate. *Bioresour. Technol*. **101**, 6761-6767 (2010).

Supplementary Notes

Note S1. Physicochemical and structure characterization data of compound 3.

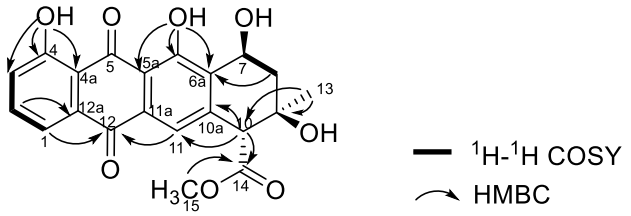

3

HRMS (ESI): m/z = 397.1929 ([M-H]$^-$), m/z (calculated [calcd.]) = 397.0929 ([M-H]$^-$) consistent with the molecular formula $C_{21}H_{18}O_8$; UV max (in CH_3OH/H_2O = 87:13): 228 nm, 258 nm, 288 nm, 432 nm. The stereochemistry of **3** was determined by comparing with **5**.

NMR spectroscopic data for compound 3.

Position	δH(mult., J in Hz)	δc	mutl.
1	7.79 (d, J = 7.6 Hz, 1H)	120.4	CH
2	7.67 (t, J = 8.0 Hz, 1H)	137.7	CH
3	7.31 (d, J = 8.4 Hz, 1H)	125.0	CH
4		162.8	C
4a		115.9	C
5		192.9	C
5a		114.8	C
6		161.3	C
6a		132.8	C
7	5.36 (d, J = 4.4 Hz, 1H)	62.7	CH
8	2.61 (dd, J = 15.2, 5.2 Hz, 1H), 2.21 – 2.24 (m, 1H)	37.1	CH_2
9		70.0	C
10	4.05 (s, 1H)	58.1	CH
10a		142.5	C
11	7.65 (s, 1H)	121.4	CH
11a		132.8	C
12		181.4	C
12a		133.6	C
13	1.42 (s, 3H)	27.6	CH_3
14		171.5	C
15	3.72 (s, 3H)	52.7	CH_3
4-OH	12.52 (s, 1H)		
6-OH	13.27 (s, 1H)		

In $CDCl_3$, 400 MHz for ^{1}H and 101 MHz for ^{13}C NMR; Chemical shifts are reported in ppm.
All signals are determined by ^{1}H -^{1}H COSY, HMBC and DEPT135 correlation.

NMR spectra of compound 3.

^{1}H NMR spectrum of 3.

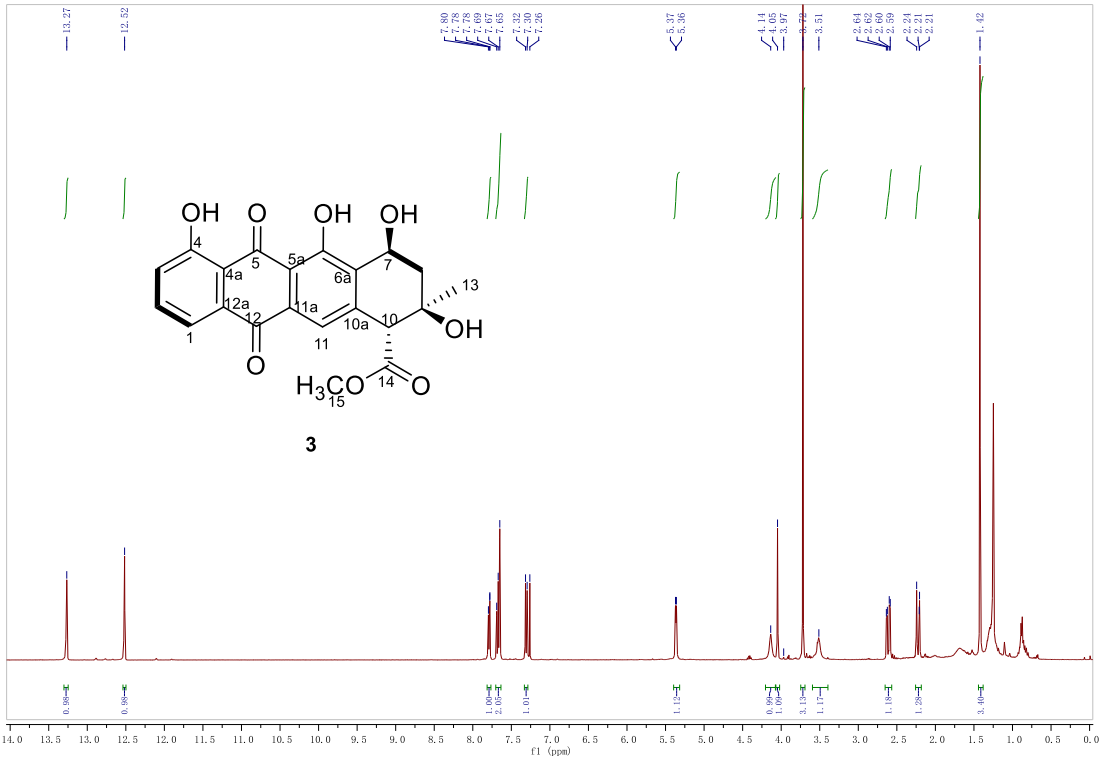

^{13}C NMR spectrum of 3.

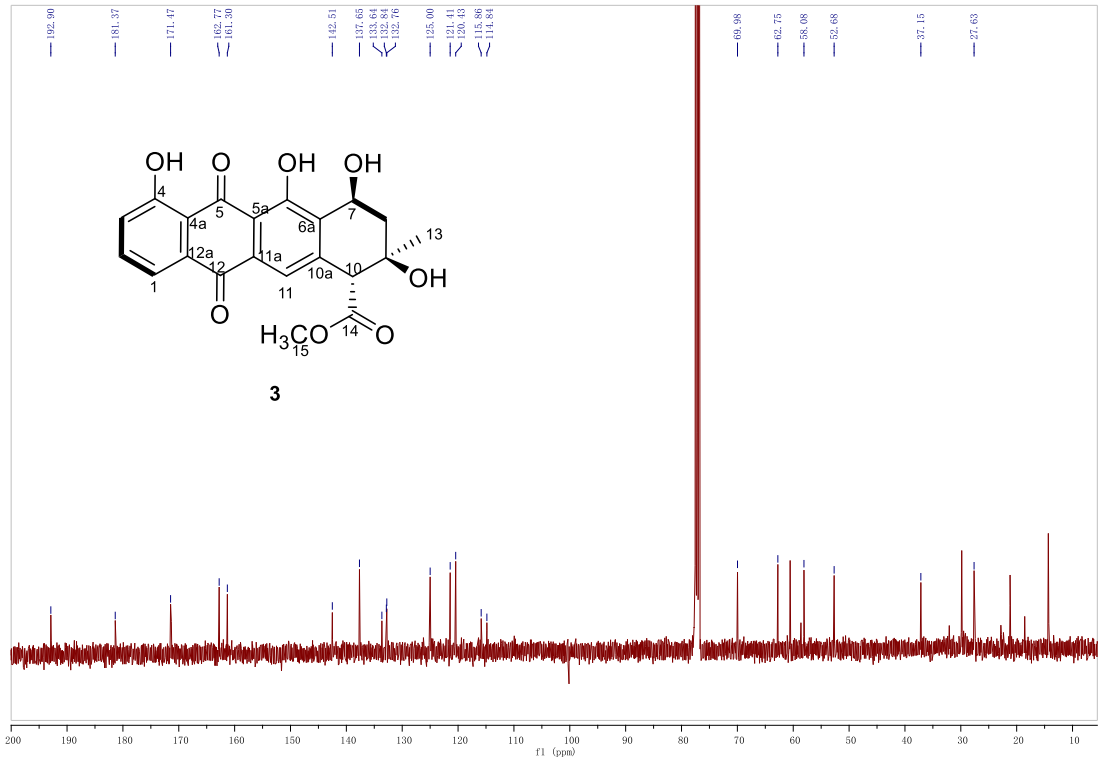

Note S2. Physicochemical and structure characterization data of compound 3g.

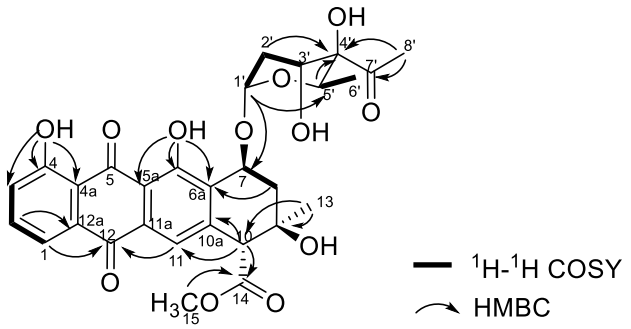

3g

HRMS (ESI): m/z = 569.1632 ([M-H]$^-$), m/z (calculated [calcd.]) = 569.1664 ([M-H]$^-$) consistent with the molecular formula $C_{29}H_{30}O_{12}$; UV max (in CH_3OH/H_2O = 87:13): 228 nm, 258 nm, 288 nm, 432 nm. The stereochemistry of **3g** was determined by NOESY and comparing with **5.**

NMR spectroscopic data for 3g.

Position	δH(mult., J in Hz)	δc	mutl.
1	7.82(d, J = 7.5 Hz, 1H)	120.4	CH
2	7.69 (d, J = 8.5 Hz, 1H)	137.5	CH
3	7.30 (d, J = 8.5 Hz, 1H)	125.0	CH
4		162.7	C
4a		115.9	C
5		192.8	C
5a		114.9	C
6		162.2	C
6a		131.2	C
7	5.21 (s, 1H)	70.7	CH
8	2.61 (dd, J = 15.5, 4.0 Hz, 1H)	36.7	CH_2
	2.33(m, 1H)		
9		69.9	C
10	4.07 (s, 1H)	58.2	CH
10a		142.6	C
11	7.65 (s, 1H),	121.0	CH
11a		133.6	C
12		181.4	C
12a		133.0	C
13	1.44 (s, 3H)	27.4	CH_3
14		171.5	C
15	3.71 (s, 3H)	52.7	CH_3
1’	5.51 (s, 1H)	100.7	CH
2’	2.31(m, 1H)	31.6	CH_2
	1.89 (d, J = 14.0 Hz, 1H)		
3’	3.67 (m, 1H)	69.7	CH
4’		79.4	C
5’	4.92 (d, J = 6.0 Hz, 1H)	63.4	CH
6’	1.13 (d, J = 6.0 Hz, 3H)	14.2	CH_3
7’		211.7	C
8’	2.37 (s, 3H)	27.4	CH_3
4-OH	11.99 (s, 1H)		
6-OH	12.69(s, 1H)		

In $CDCl_3$, 500 MHz for ^1H and 126 MHz for ^{13}C NMR; Chemical shifts are reported in ppm. All signals are determined by ^1H -^1H COSY, HMBC and HSQC correlation.

NMR spectra of compound 3g.

^{1}H NMR spectrum of 3g.

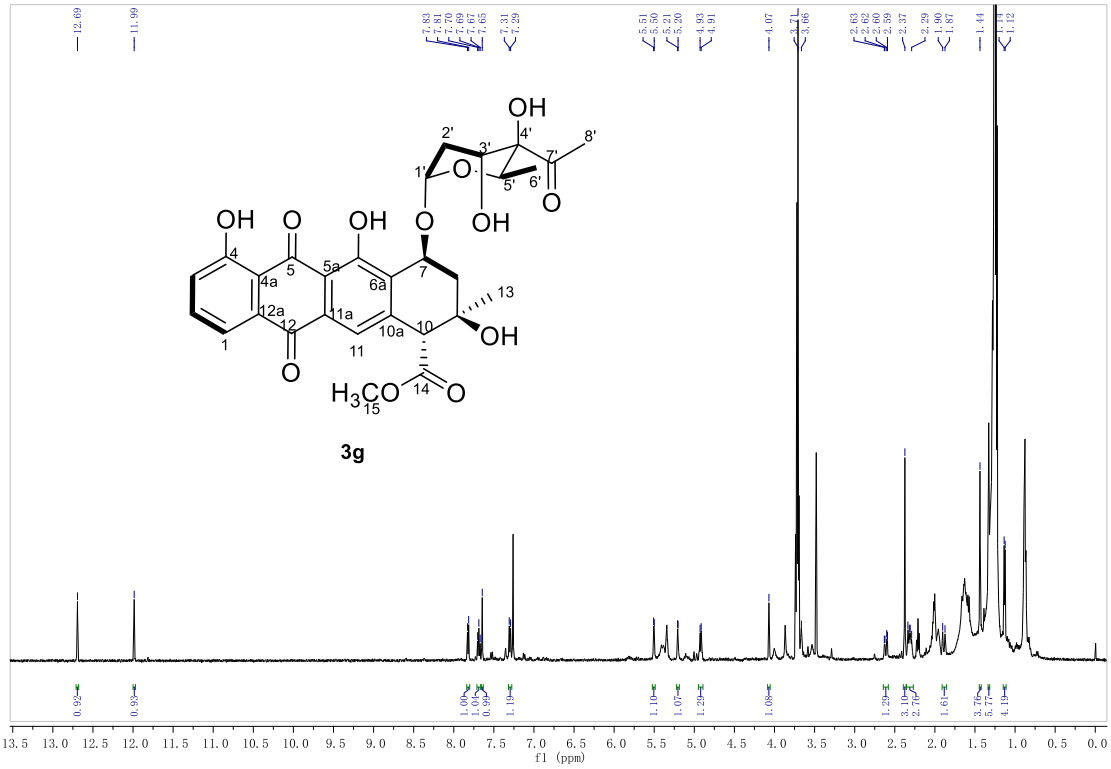

^{13}C NMR spectrum of 3g.

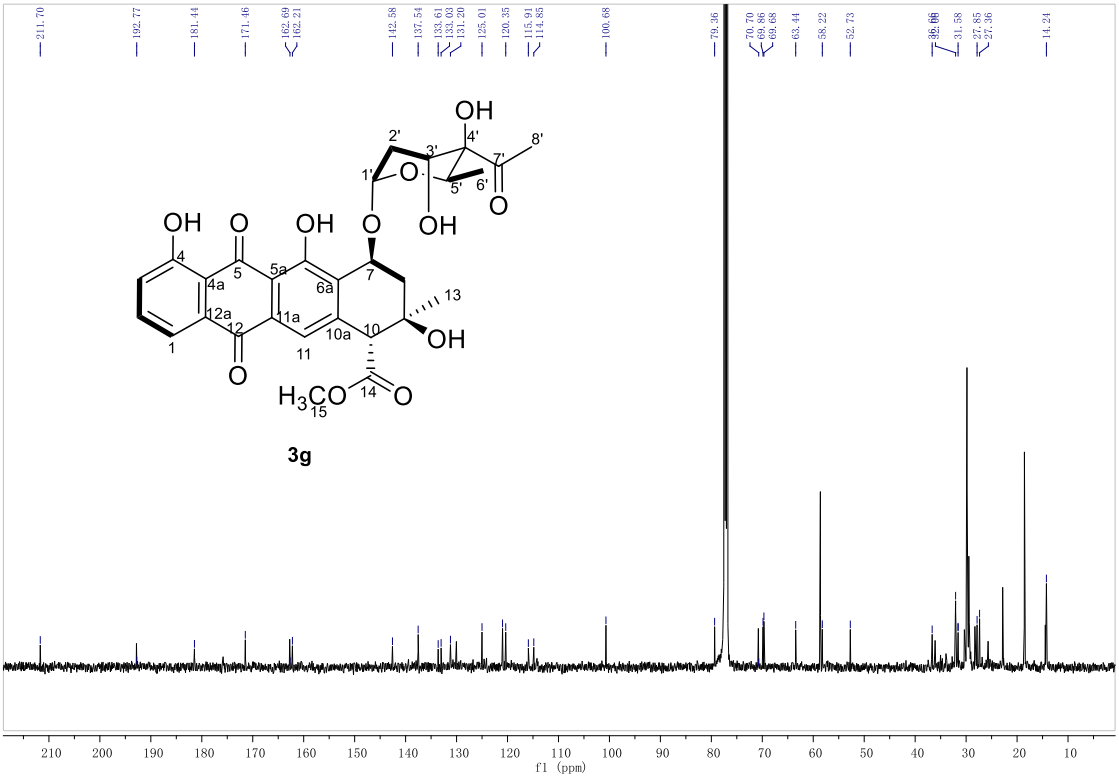

^{1}H-^{1}H COSY spectrum of 3g.

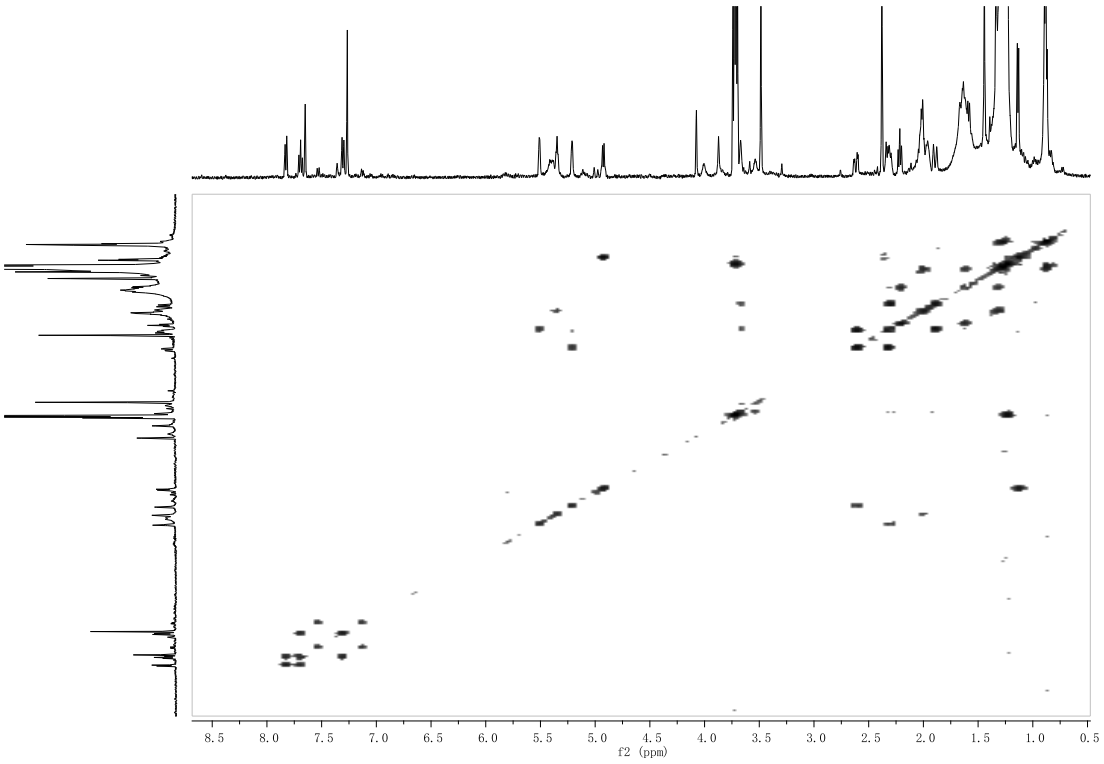

^{1}H-^{13}C HSQC spectrum of 3g.

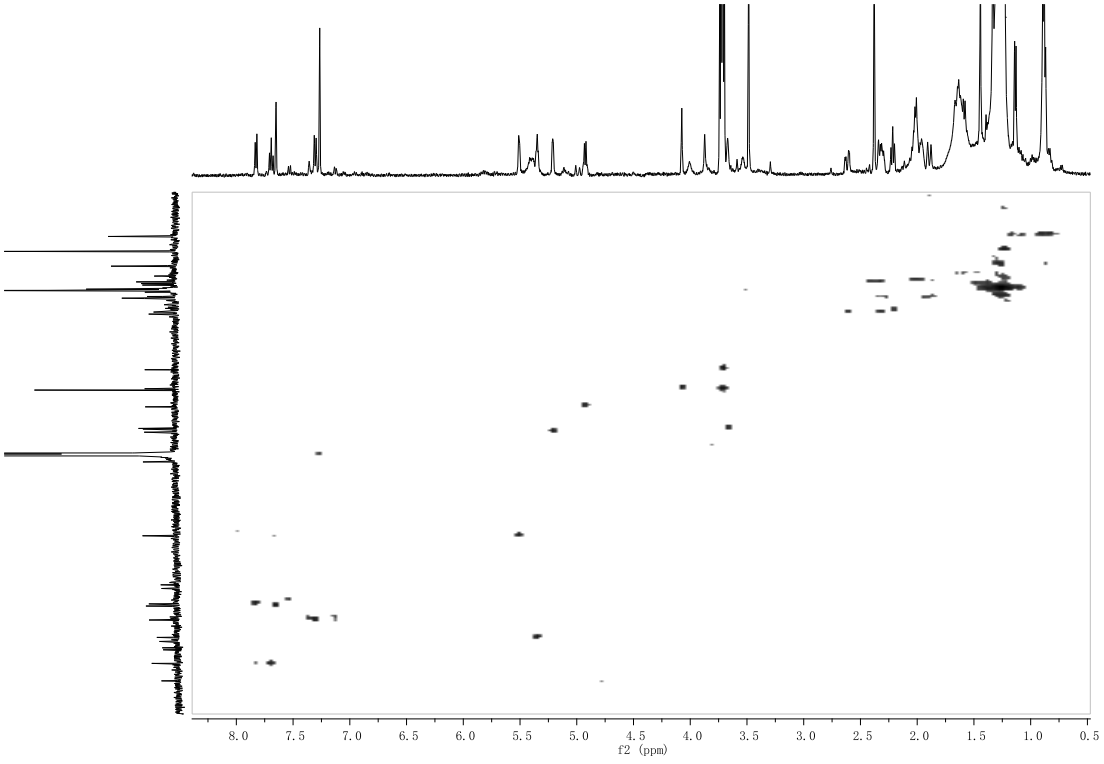

^{1}H-^{13}C HMBC spectrum of 3g.

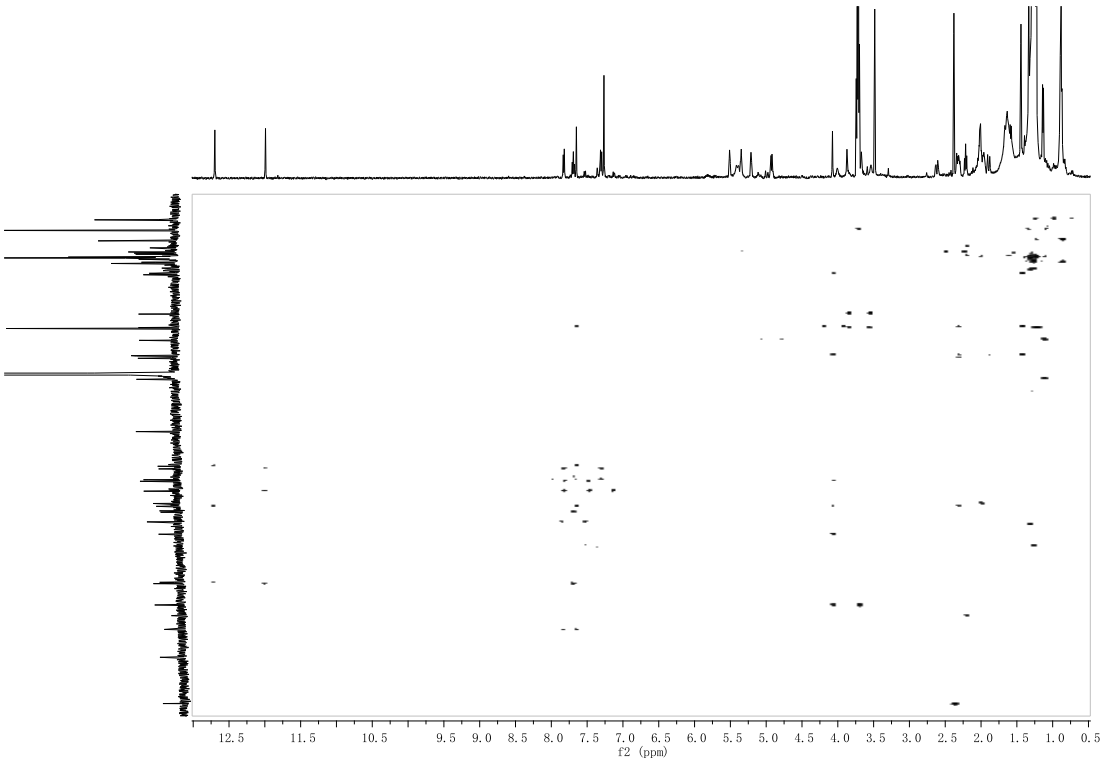

^{1}H-^{1}H NOESY spectrum of 3g.

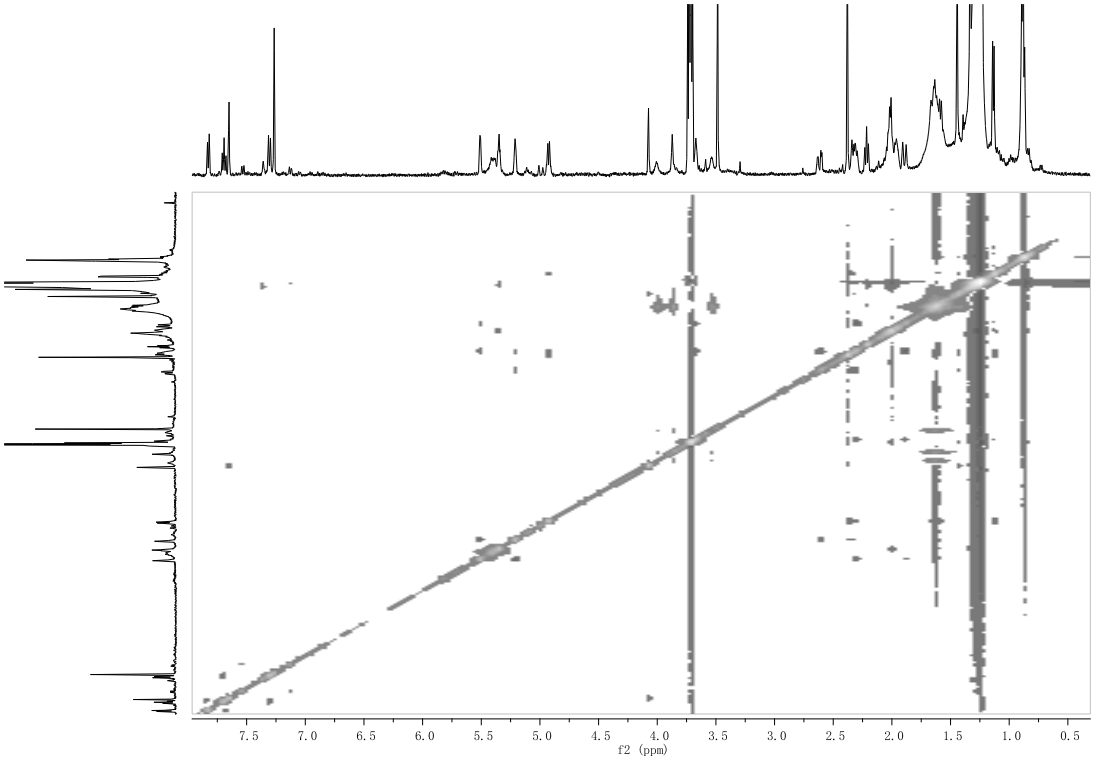

Note S3. Physicochemical and structure characterization data of compound 3d.

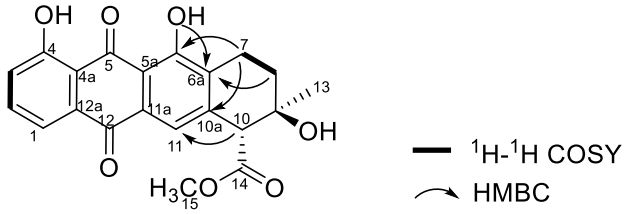

3d

HRMS (ESI): m/z = 381.0980 ([M-H]$^-$), m/z (calculated [calcd.]) = 381.0980 ([M-H]$^-$) consistent with the molecular formula $C_{21}H_{18}O_7$; UV max (in CH_3OH/H_2O = 88:12): 228 nm, 260 nm, 432 nm. The stereochemistry of **3d** was determined by comparing with **3**.

NMR spectroscopic data for compound 3d.

Position	*δH*(mult., *J* in Hz)	δc	mutl.
1	7.82 (d, *J* = 7.4 Hz, 1H)	120.1	CH
2	7.67 (t, *J* = 8.0 Hz, 1H)	137.3	CH
3	7.29 (d, *J* = 8.3 Hz, 1H)	124.7	CH
4		162.6	C
4a		116.1	C
5		193.0	C
5a		113.8	C
6		161.2	C
6a		133.9	C
7	3.05 (ddd, *J* = 19.0, 6.7, 2.8 Hz, 1H)	20.3	CH_2
	2.87 (ddd, *J* = 19.0, 10.0, 6.5Hz 1H)		
8	2.32 (dd, *J* = 10.0, 7.0 Hz, 1H)	31.0	CH_2
	1.92 (dd, *J* = 13.5, 6.3 Hz, 1H)		
9		69.8	C
10	3.91 (s, 1H)	57.6	CH
10a		142.1	C
11	7.63 (s, 1H)	121.3	CH
11a		130.9	C
12		181.8	C
12a		133.7	C
13	1.42 (s, 4H)	27.6	CH_3
14		171.8	C
15	3.75 (s, 3H)	52.7	CH_3
4-OH	12.09 (s, 1H)		
6-OH	12.50 (s, 1H)		

In $CDCl_3$, 500 MHz for ^{1}H and 101 MHz for ^{13}C NMR; Chemical shifts are reported in ppm.
All signals are determined by ^{1}H -^{1}H COSY, HMBC and HSQC correlation.

NMR spectra of compound 3d.

^{1}H NMR spectrum of 3d.

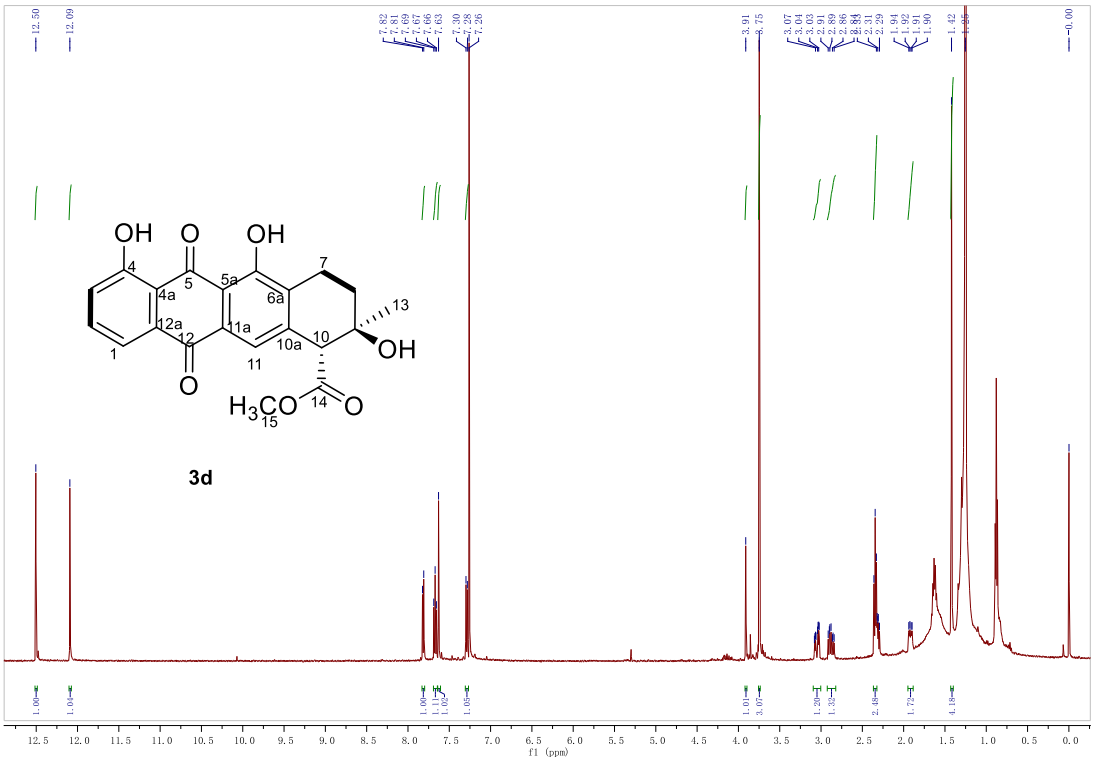

^{13}CNMR spectrum of 3d.

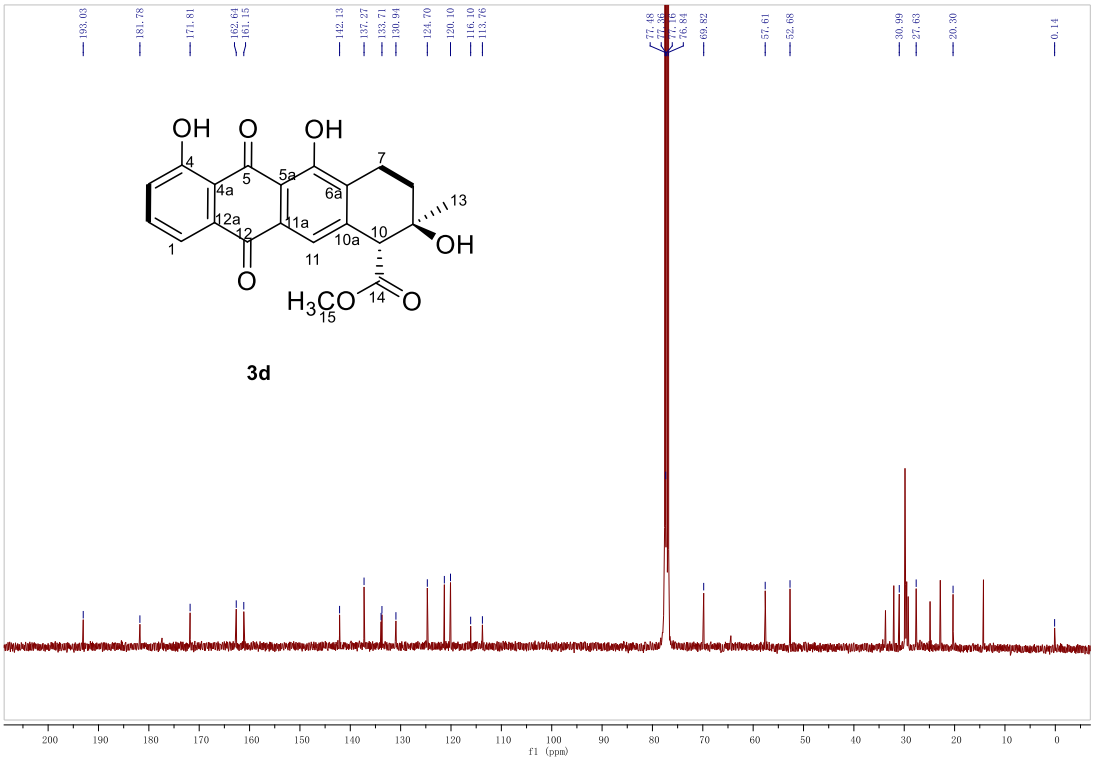

^{1}H-^{1}H COSY spectrum of 3d.

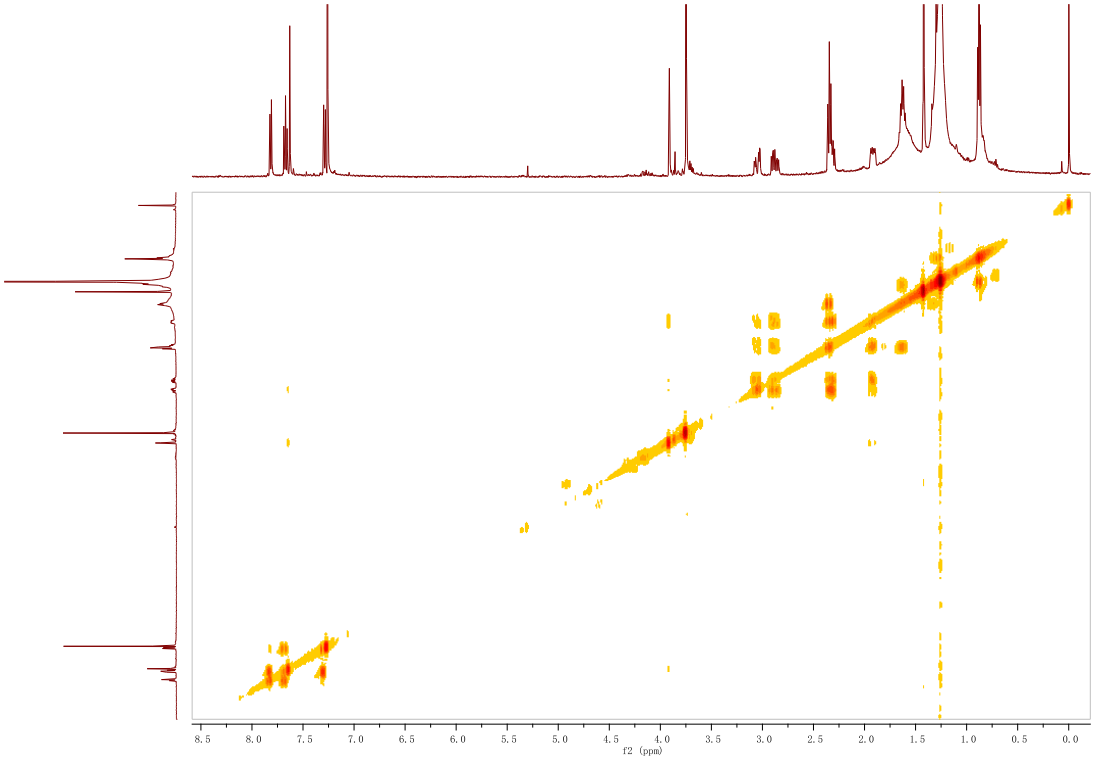

^{1}H-^{13}C HSQC spectrum of 3d.

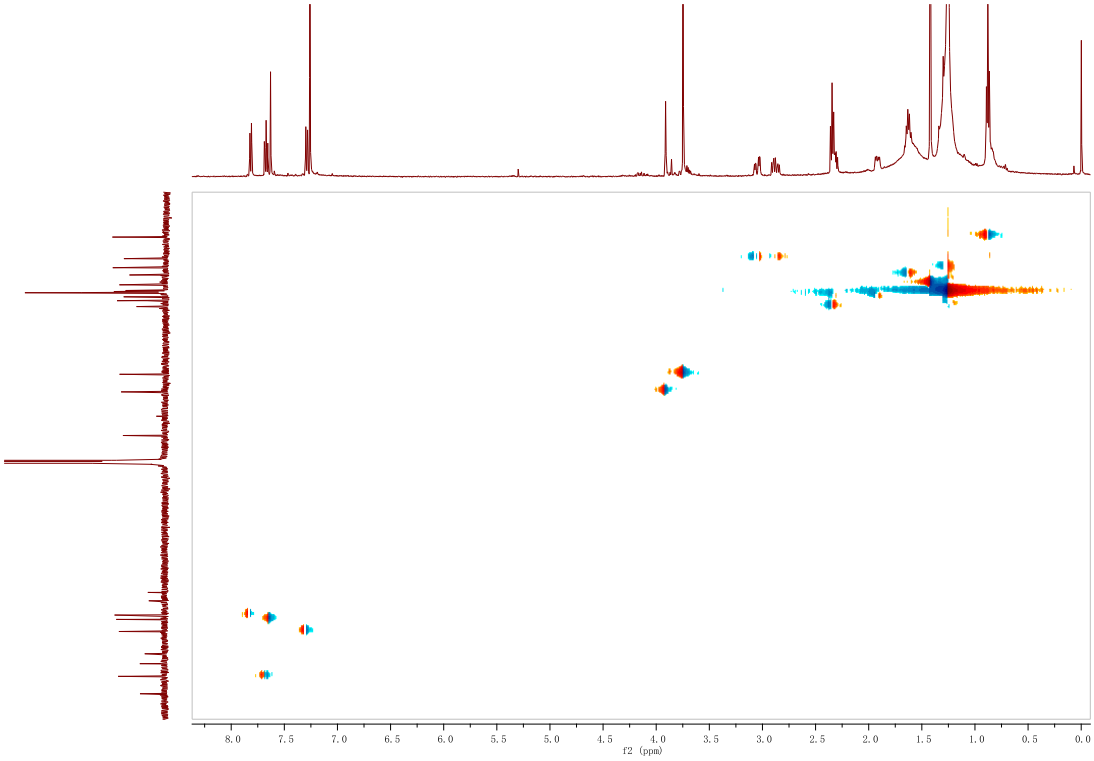

^{1}H-^{13}C HMBC spectrum of 3d.

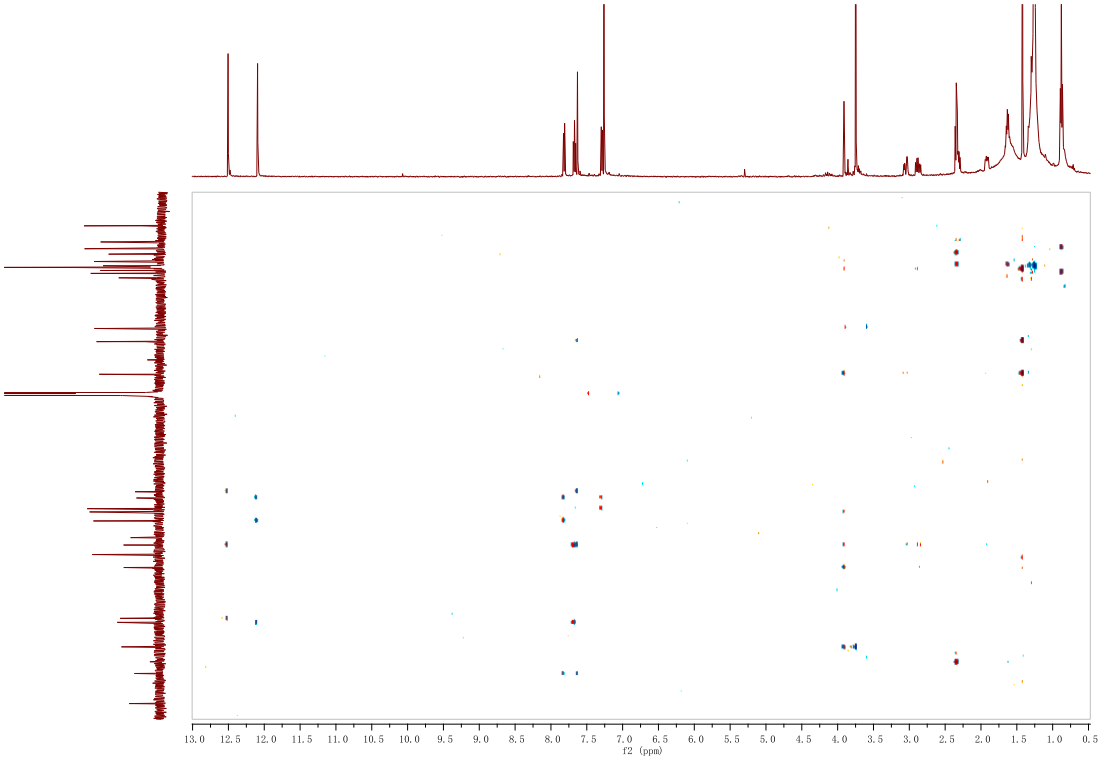

Note S4. Physicochemical and structure characterization data of compound 4g.

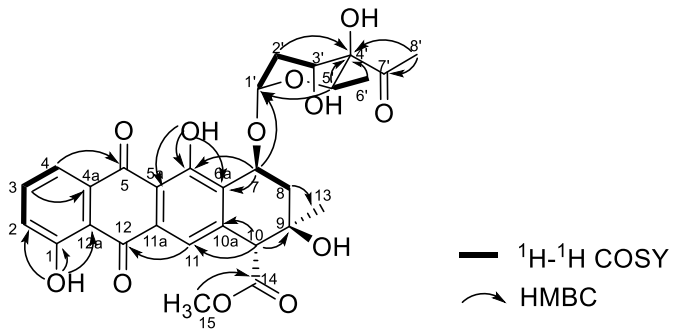

4g

HRMS (ESI): m/z = 569.1632 ([M-H]$^-$), m/z (calculated [calcd.]) = 569.1664 ([M-H]$^-$) consistent with the molecular formula $C_{29}H_{30}O_{12}$; UV max (in CH_3OH/H_2O = 88:12): 230 nm, 258 nm, 292 nm, 432 nm. The stereochemistry of **4g** was determined by comparing with **KST.**

NMR spectroscopic data for 4g.

Position	δH(mult., J in Hz)	δc	mutl.
1		162.8	C
2	7.03 (d, J = 8.0 Hz, 1H)	124.9	CH
3	7.42 (t, J = 8.0 Hz, 1H)	137.1	CH
4	7.52 (d, J = 8.0 Hz, 1H)	119.4	CH
4a		132.7	C
5		187.2	C
5a		114.6	C
6		162.3	C
6a		131.5	C
7	5.14 (d, J = 3.0 Hz, 1H)	70.1	CH
8	2.54 (dd, J = 15.0, 3.0 Hz, 1H)	36.5	CH_2
	2.27 (d, J = 15.0 Hz, 1H)		
9		69.5	C
10	3.90 (s, 1H)	58.2	CH
10a		141.7	C
11	7.32 (s, 1H),	119.9	CH
11a		132.1	C
12		186.9	C
12a		115.5	C
13	1.39 (s, 3H)	28.6	CH_3
14		171.4	C
15	3.69 (s, 3H)	52.7	CH_3
1’	5.50 (s, 1H)	100.5	CH
2’	2.36 (dt, J = 14.5, 3.5 Hz,1H)	32.0	CH_2
	1.98 (d, J = 14.5 Hz, 1H)		
3’	3.71 (s, 1H)	70.3	CH
4’		79.5	C
5’	4.96 (q, J = 12.0, 6.0 Hz, 1H)	63.4	CH
6’	1.15 (d, J = 6.0 Hz, 3H)	14.5	CH_3
7’		211.5	C
8’	2.40 (s, 3H)	27.9	CH_3
4-OH	12.25 (s, 1H)		
6-OH	13.13(s, 1H)		

In $CDCl_3$, 500 MHz for ^1H and 126 MHz for ^{13}C NMR; Chemical shifts are reported in ppm.
All signals are determined by ^1H -^1H COSY, HMBC and HSQC correlation.

NMR spectra of compound 4g.

^{1}H NMR spectrum of 4g.

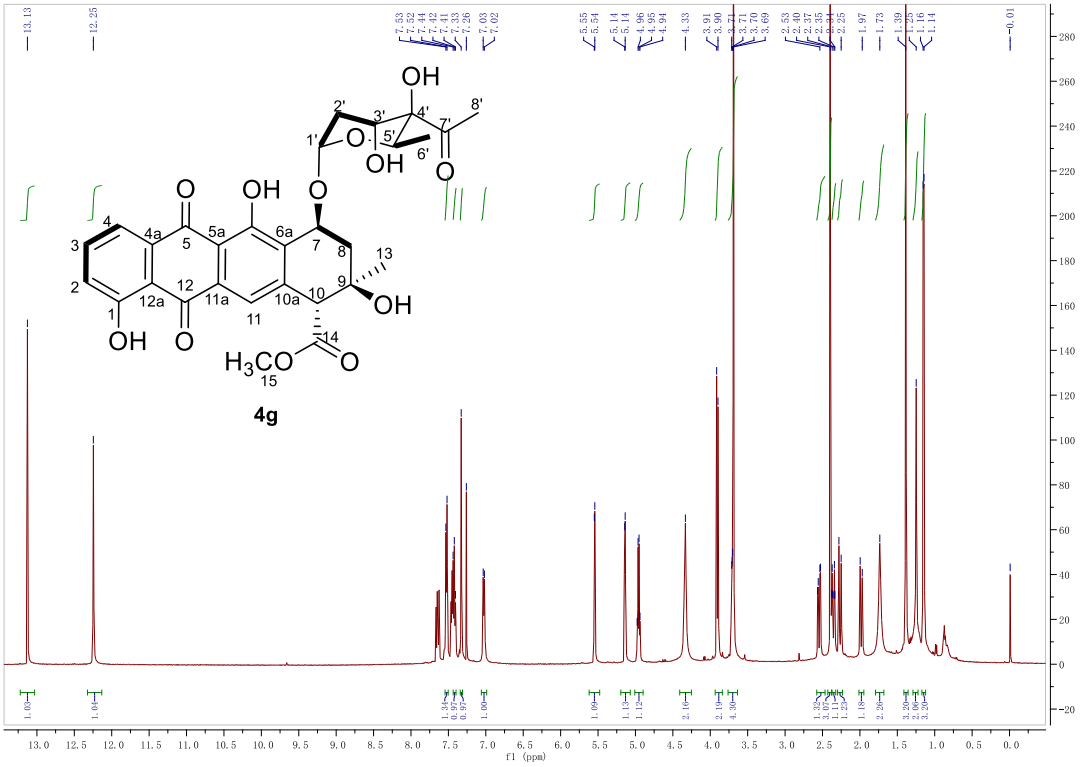

^{13}C NMR spectrum of 4g.

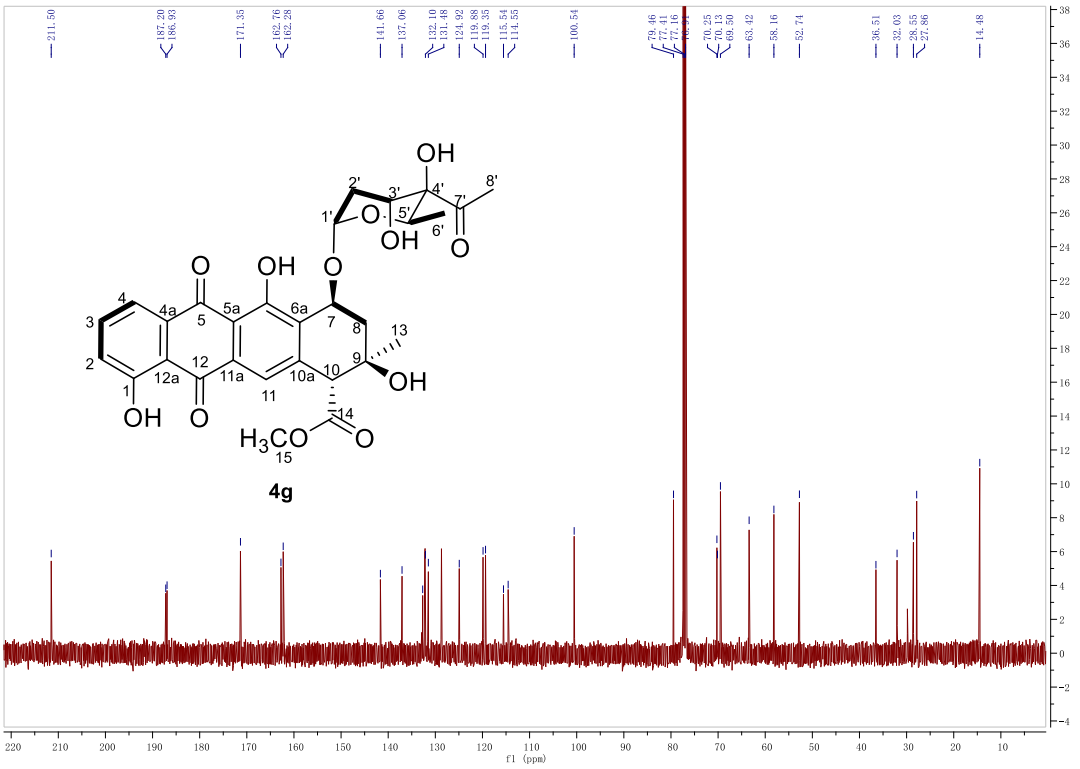

^{1}H-^{1}H COSY spectrum of 4g.

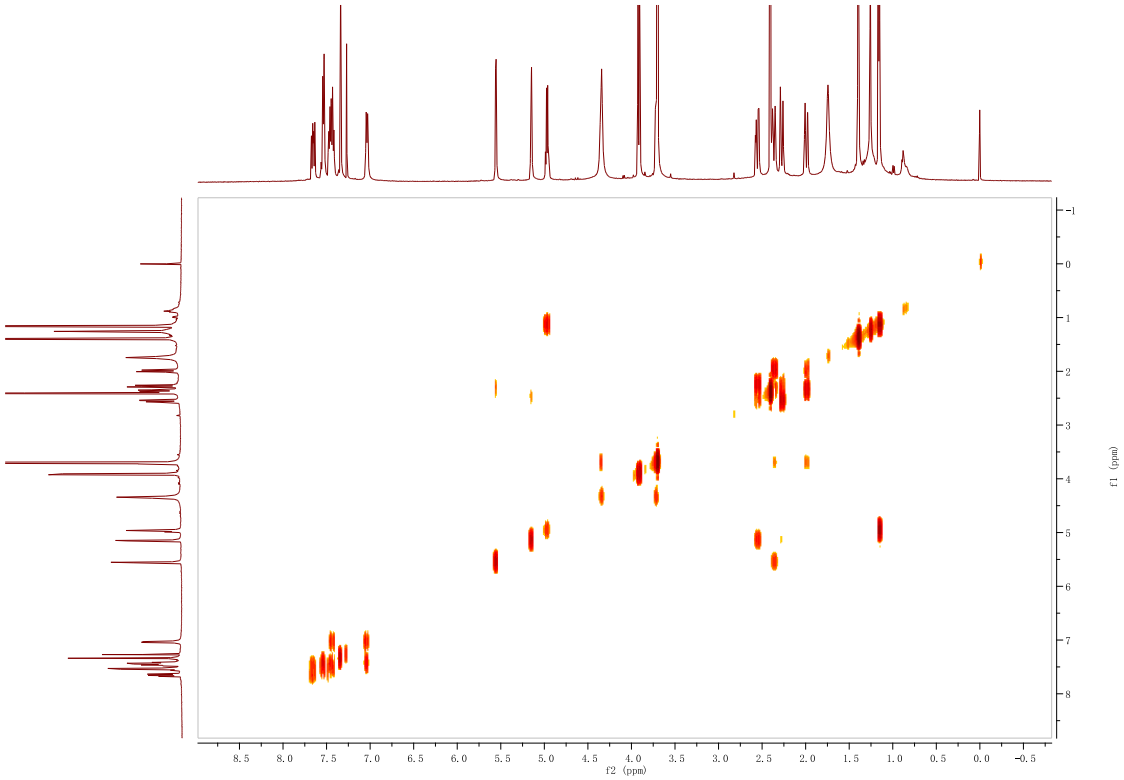

^{1}H-^{13}C HSQC spectrum of 4g.

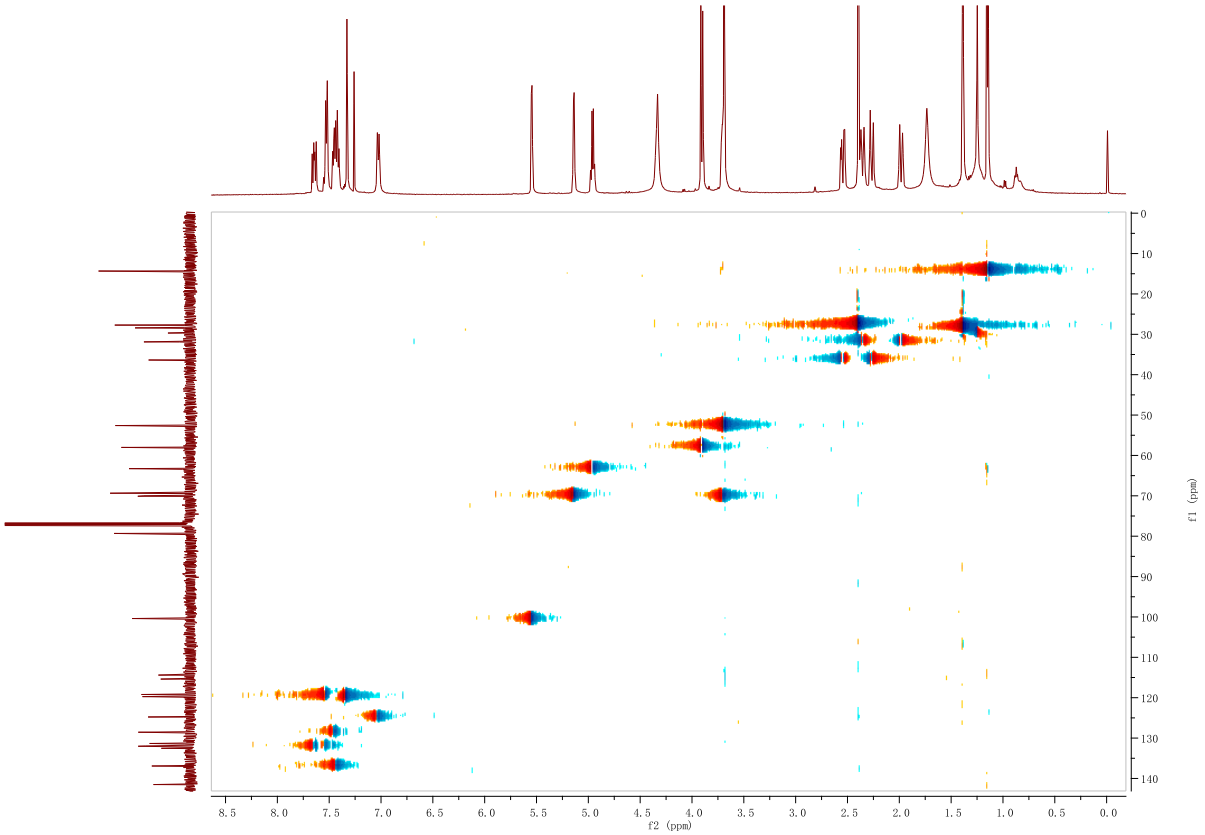

^{1}H-^{13}C HMBC spectrum of 4g.

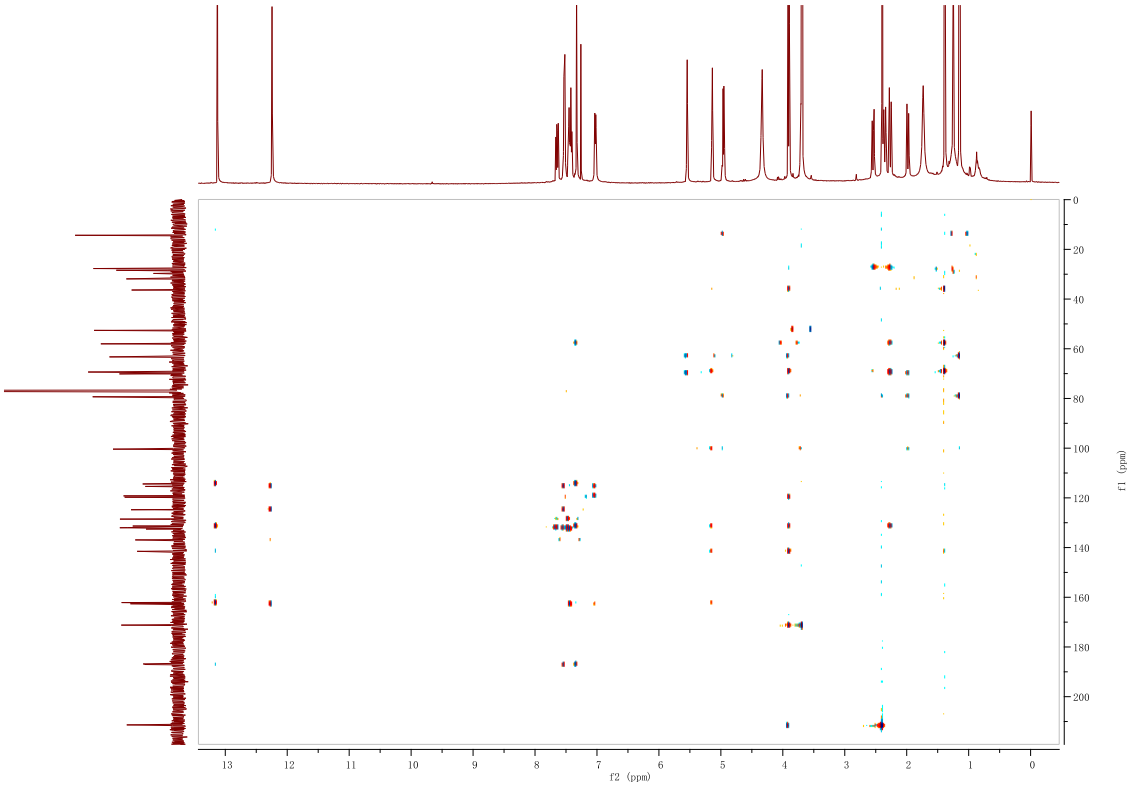

Note S5. Physicochemical and structure characterization data of compound 4d.

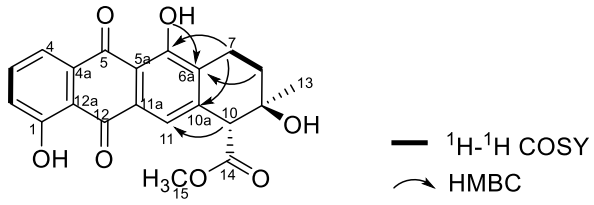

4d

HRMS (ESI): m/z = 381.0953 ([M-H]$^-$), m/z (calculated [calcd.]) = 381.0980 ([M-H]$^-$) consistent with the molecular formula $C_{21}H_{18}O_7$; UV max (in CH_3OH/H_2O = 88:12): 228 nm, 258 nm, 292 nm, 434 nm. The stereochemistry of **4d** was determined by comparing with **5**.

NMR spectroscopic data for compound 4d.

Position	δH(mult., J in Hz)	δc	mutl.
1		162.8	C
2	7.28 (t, J = 8.5 Hz, 1H)	125.0	CH
3	7.65 (d, J = 8.0 Hz, 1H)	136.8	CH
4	7.78(d, J = 7.5 Hz, 1H)	119.4	CH
4a		113.4	C
5		187.8	C
5a		113.9	C
6		161.4	C
6a		134.3	C
7	3.05 (ddd, J = 19.5, 7.0, 3.0 Hz, 1H)	20.4	CH_2
	2.88 (ddd, J = 19.0, 10.0, 7.0 Hz 1H)		
8	2.32 (dd, J = 18.0, 10.0, 7.0 Hz, 1H)	31.0	CH_2
	1.92 (m, 1H)		
9		69.8	C
10	3.90 (s, 1H)	57.6	CH
10a		141.5	C
11	7.59 (s, 1H)	120.6	CH
11a		130.4	C
12		187.9	C
12a		116.2	C
13	1.42 (s, 4H)	27.6	CH_3
14		171.8	C
15	3.75 (s, 3H)	52.7	CH_3
1-OH	12.63 (s, 1H)		
6-OH	13.04 (s, 1H)		

In $CDCl_3$, 500 MHz for ^{1}H and 126 MHz for ^{13}C NMR; Chemical shifts are reported in ppm.
All signals are determined by ^{1}H -^{1}H COSY, HMBC and HSQC correlation.

NMR spectra of compound 4d.

^{1}H NMR spectrum of 4d

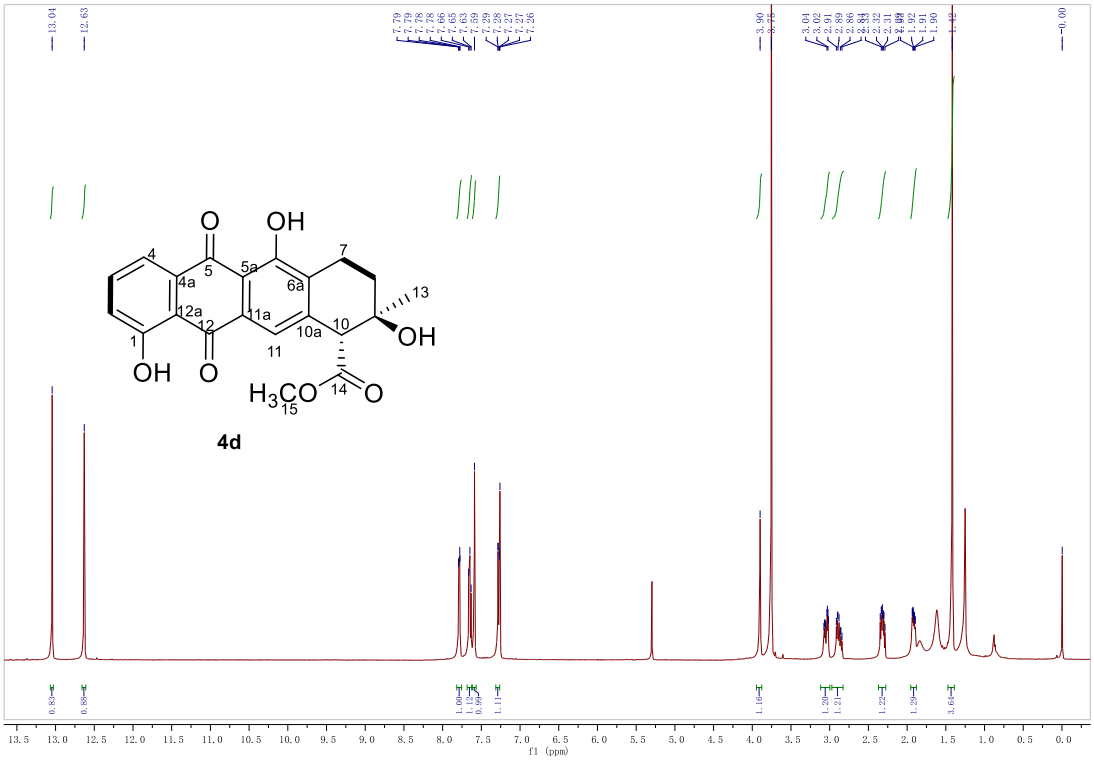

^{13}C NMR spectrum of 4d.

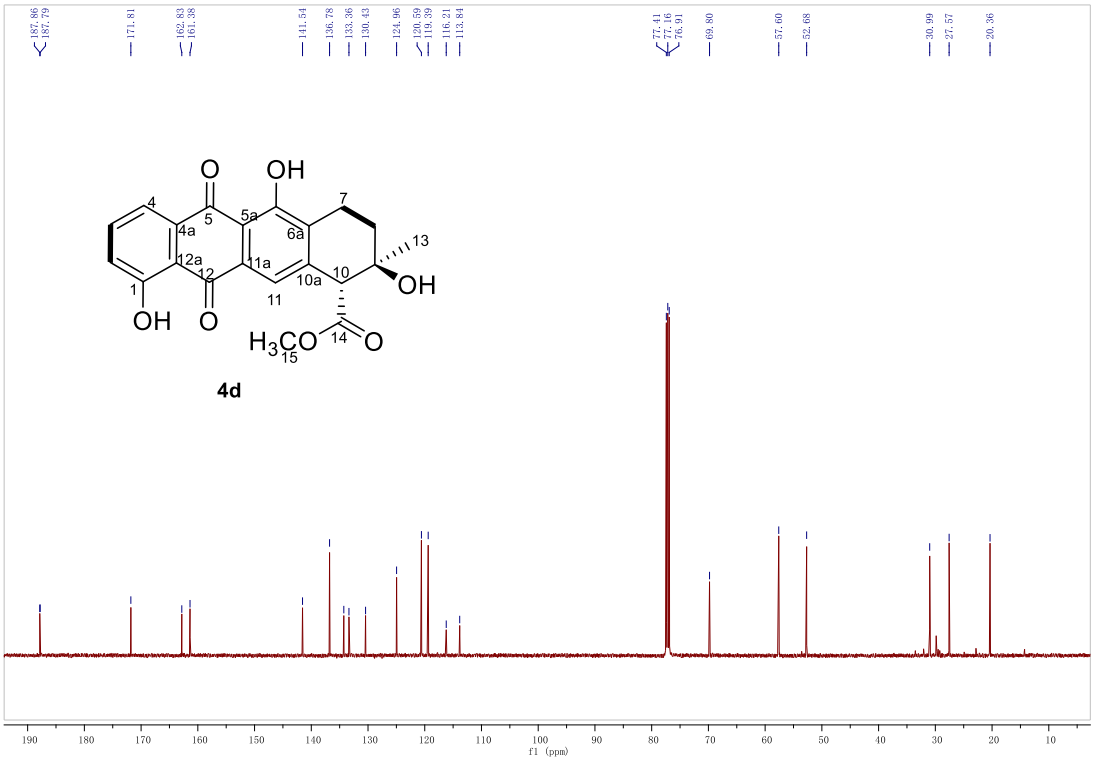

^{1}H-^{1}H COSY spectrum of 4d.

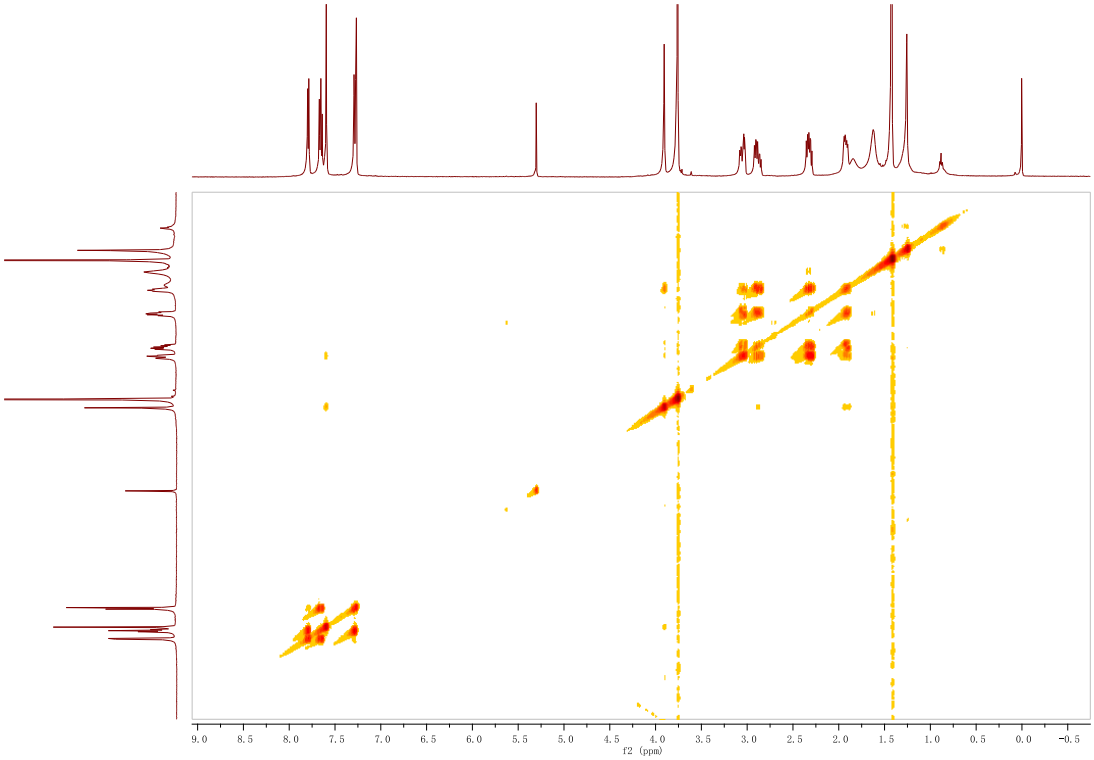

^{1}H-^{13}C HSQC spectrum of 4d.

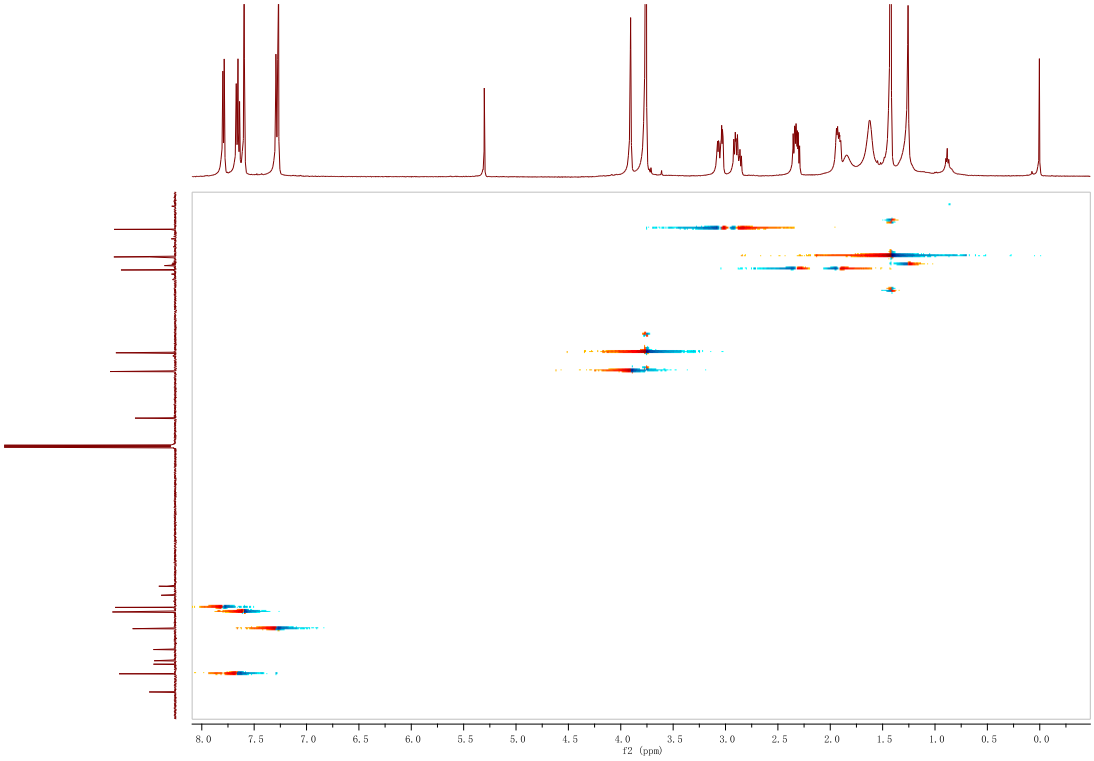

^{1}H-^{13}C HMBC spectrum of 4d.

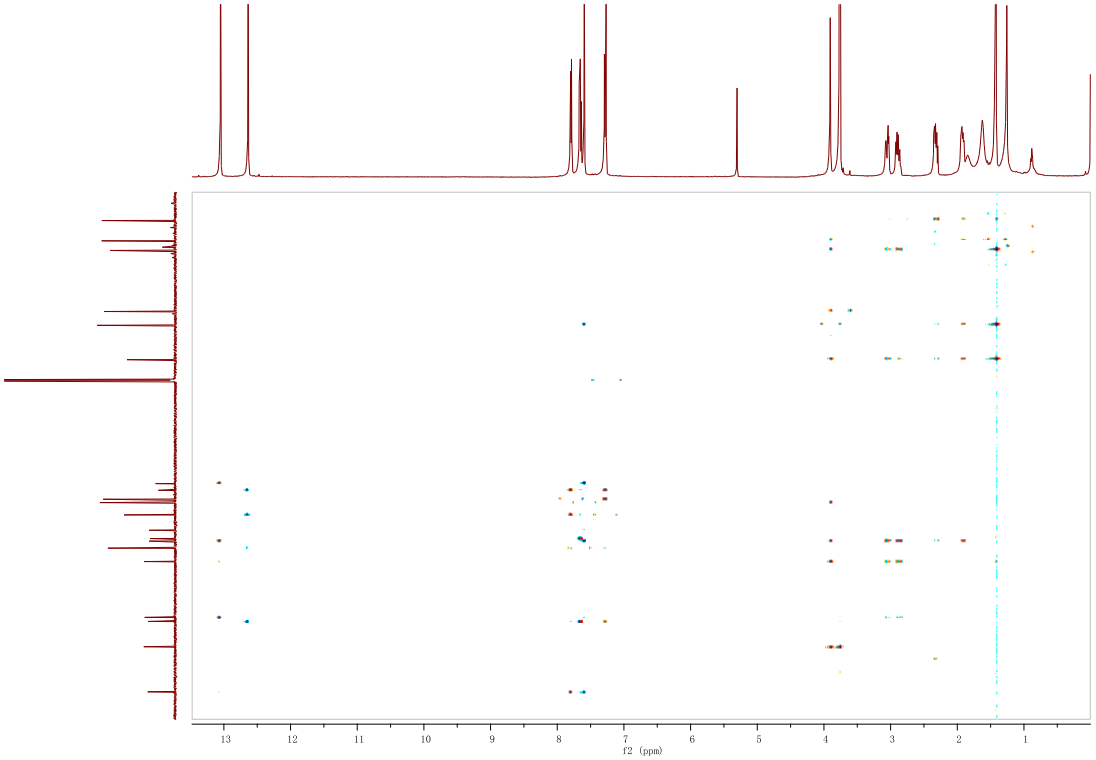

Note S6. Physicochemical and structure characterization data of compound 5.

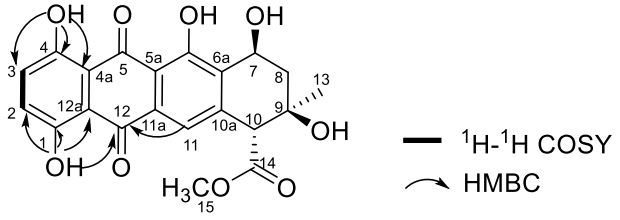

5

HRMS (ESI): m/z = 413.1175 ([M-H]$^-$), m/z (calculated [calcd.]) = 413.0878 ([M-H]$^-$) consistent with the molecular formula $C_{21}H_{18}O_9$; UV max (in CH_3OH/H_2O =87:13): 234 nm, 256 nm, 292 nm, 490 nm. The stereochemistry of **5** was determined by cocrystal.

NMR spectroscopic data for 5.

Position	*δH*(mult., *J* in Hz)	δc	mutl.
1		158.3	C
2	7.16 (d, *J* = 9.2 Hz, 1H)	130.4	CH
3	7.19 (d, *J* = 9.2 Hz, 1H)	129.9	CH
4		157.9	C
4a		111.9	C
5		190.1	C
5a		114.5	C
6		161.3	C
6a		133.0	C
7	5.30 (d, *J* = 6.2 Hz, 1H)	62.5	CH
8	2.58 (dd, *J* = 14.9, 4.8 Hz, 1H)	37.1	CH_2
	2.22 (d, *J* = 14.8 Hz, 1H)		
9		70.1	C
10	4.04 (s, 1H)	58.0	CH
10a		142.2	C
11	7.51 (s, 1H)	120.7	CH
11a		132.2	C
12		185.3	C
12a		112.0	C
13	1.43 (s, 3H)	27.6	CH_3
14		171.4	C
15	3.72 (s, 3H)	52.7	CH_3
1-OH	12.69 (s, 1H)		
4-OH	11.90 (s, 1H)		
6-OH	12.54 (s, 1H)		
7-OH	3.84 (d, *J* = 3.2 Hz, 1H)		
9-OH	4.39 (s, 1H)		

In $CDCl_3$, 400 MHz for ^{1}H and 101 MHz for ^{13}C NMR; Chemical shifts are reported in ppm.
All signals are determined by ^{1}H -^{1}H COSY, HMBC and HSQC correlation.

NMR spectra of compound 5.

^{1}H NMR spectrum of 5.

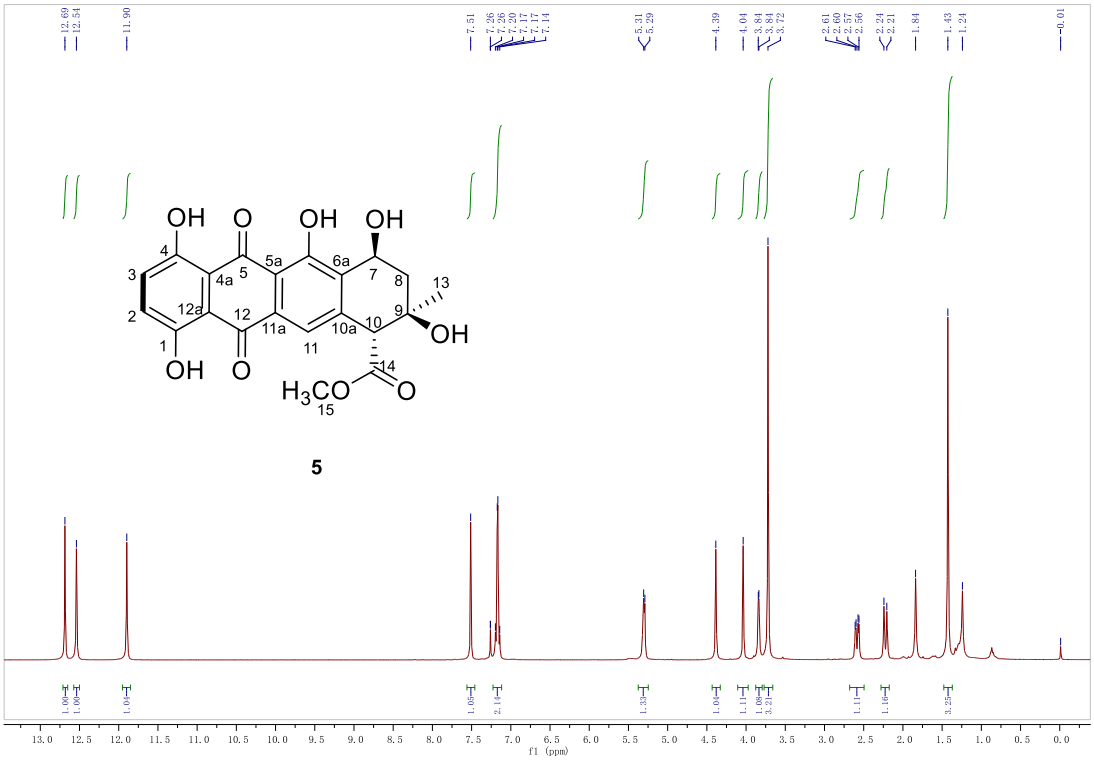

^{13}C NMR spectrum of 5.

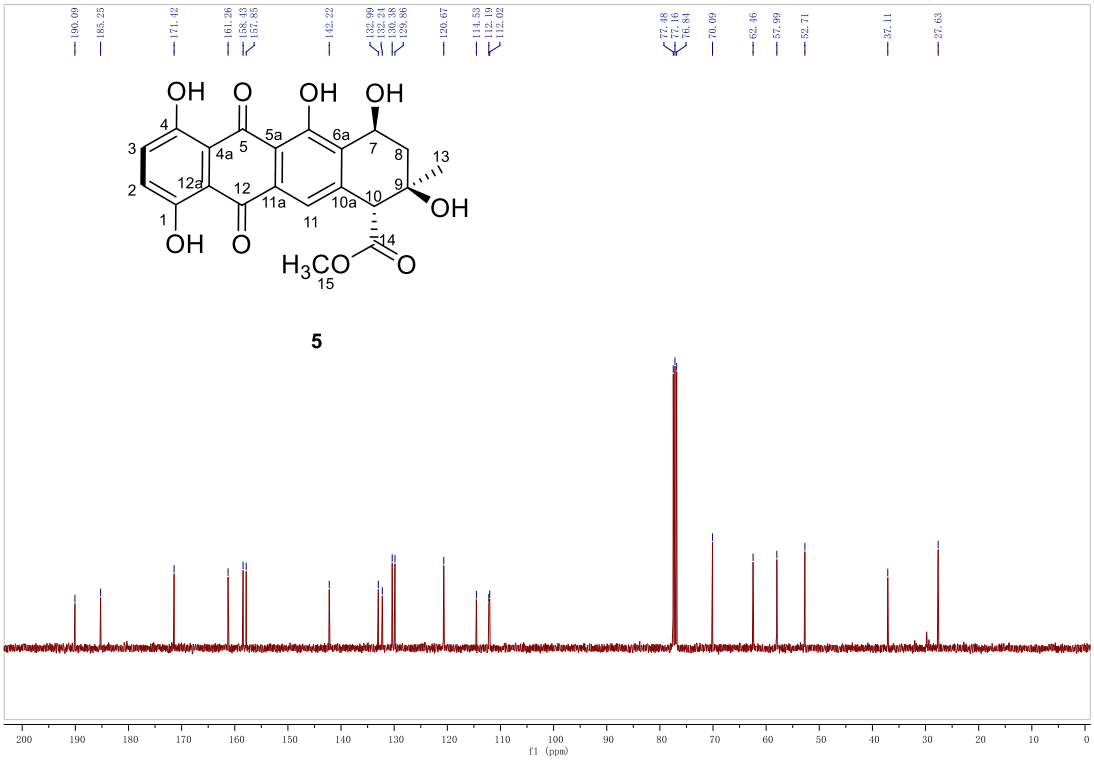

^{1}H-^{1}H COSY spectrum of 5.

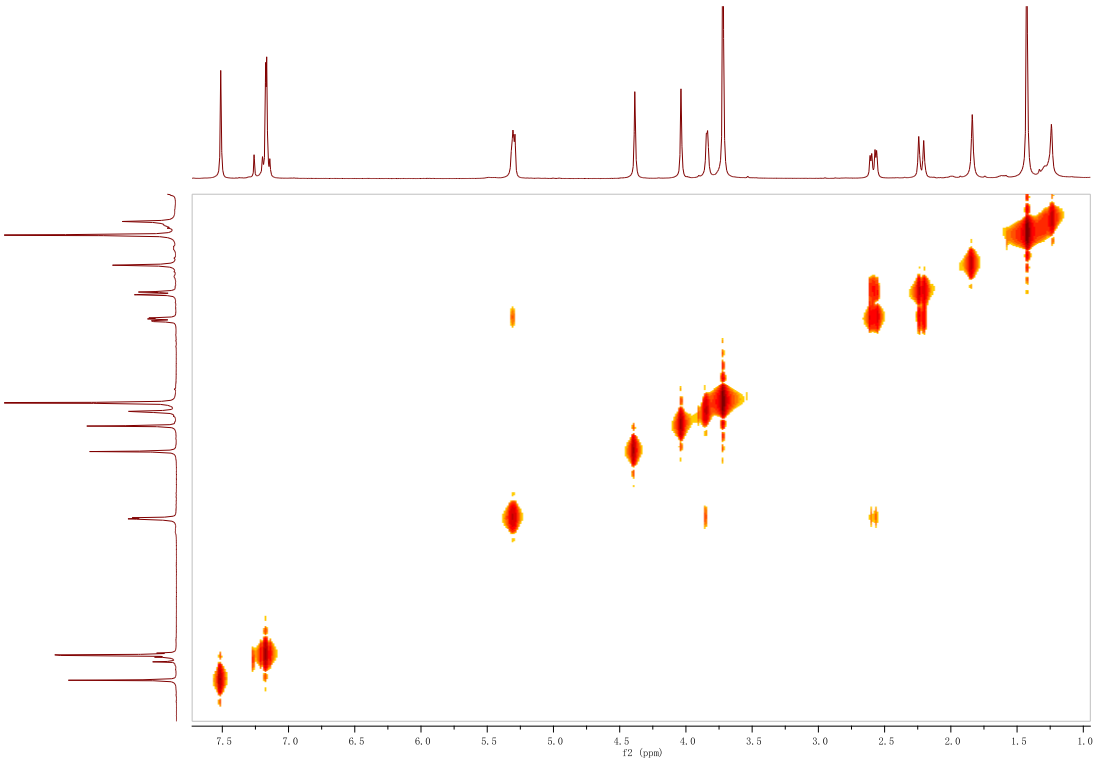

^{1}H-^{13}C HSQC spectrum of 5.

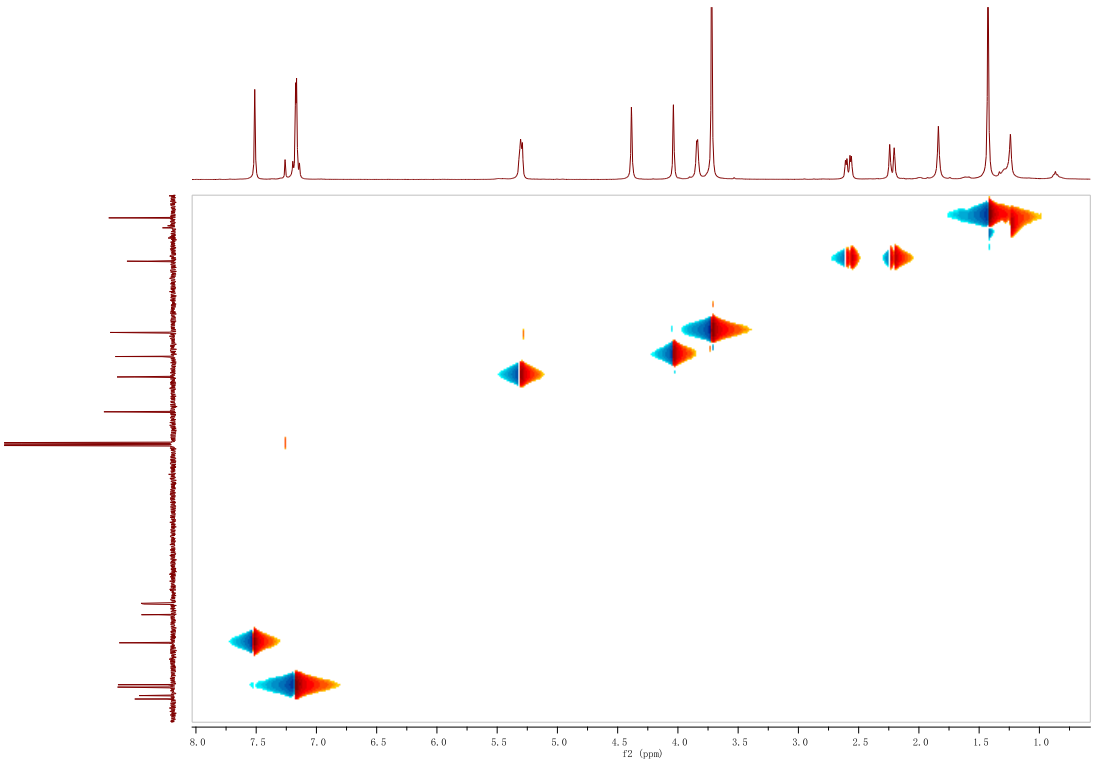

^{1}H-^{13}C HMBC spectrum of 5.

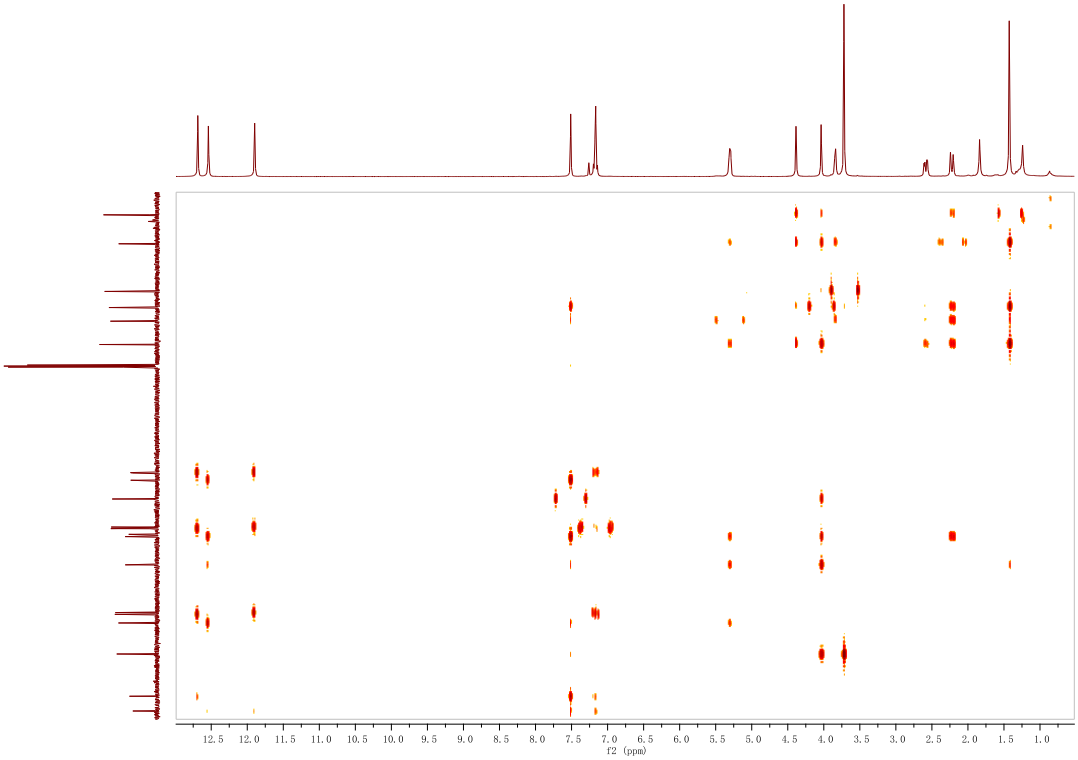

Note S7. Physicochemical and structure characterization data of compound 5g.

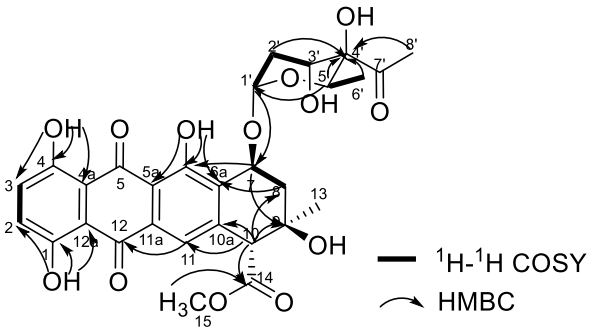

5g

HRMS (ESI): m/z = 585.1623 ($[M-H]^-$), m/z (calculated [calcd.]) = 585.1614 ($[M-H]^-$) consistent with the molecular formula $C_{29}H_{29}O_{13}$; UV max (in CH_3OH/H_2O = 88:12): 234 nm, 258 nm, 294 nm, 492 nm. The stereochemistry of **5g** was determined by comparing with **5** and **KST.**

NMR spectroscopic data for 5g.

Position	δH(mult., J in Hz)	δc	mutl.
1		158.4	C
2	6.97 (m, 1H)	130.0	CH
3	6.97 (m, 1H)	129.8	CH
4		157.8	C
4a		111.7	C
5		190.0	C
5a		114.4	C
6		162.1	C
6a		131.0	C
7	5.13 (d, J = 3.5 Hz, 1H)	70.1	CH
8	2.59 (dd, J = 15.0, 4.9 Hz, 1H)	36.3	CH_2
	2.28 (d, J = 15.0 Hz, 1H)		
9		69.4	C
10	3.94 (s, 1H)	57.9	CH
10a		141.8	C
11	7.53 (s, 1H),	119.8	CH
11a		132.3	C
12		185.0	C
12a		115.8	C
13	1.40 (s, 3H)	28.4	CH_3
14		171.2	C
15	3.71 (s, 3H)	52.7	CH_3
1’	5.53 (d, J = 3.5 Hz,1H)	100.5	CH
2’	2.35 (dt, J = 15.0, 3.5 Hz,1H)	31.7	CH_2
	2.02 (d, J = 15.0 Hz, 1H)		
3’	3.71 (s, 1H)	70.3	CH
4’		79.3	C
5’	4.95 (q, J = 12.5, 6.0 Hz, 1H)	63.3	CH
6’	1.15 (d, J = 6.0 Hz, 3H)	14.4	CH_3
7’		211.4	C
8’	2.40 (s, 3H)	27.7	CH_3
1-OH	12.81 (s, 1H)		
4-OH	12.00 (s, 1H)		
6-OH	12.66 (s, 1H)		

In $CDCl_3$, 500 MHz for ^1H and 101 MHz for ^{13}C NMR; Chemical shifts are reported in ppm.
All signals are determined by ^1H -^1H COSY, HMBC and HSQC correlation.

NMR spectra of compound 5g.

^{1}H NMR spectrum of 5g.

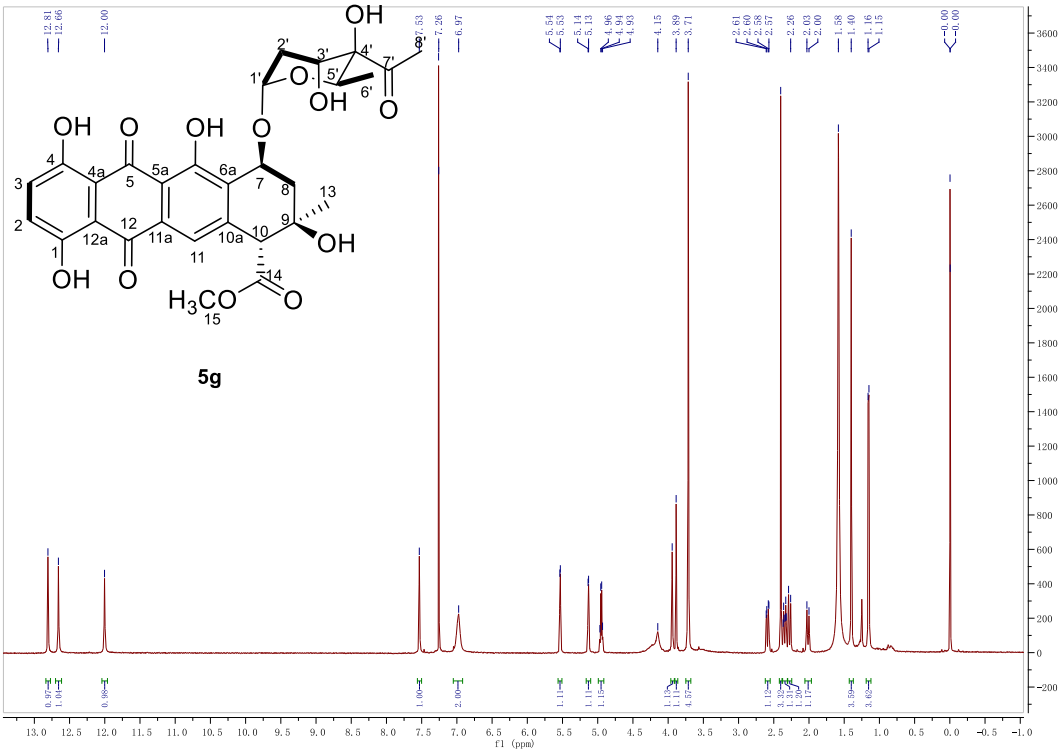

^{13}C NMR spectrum of 5g.

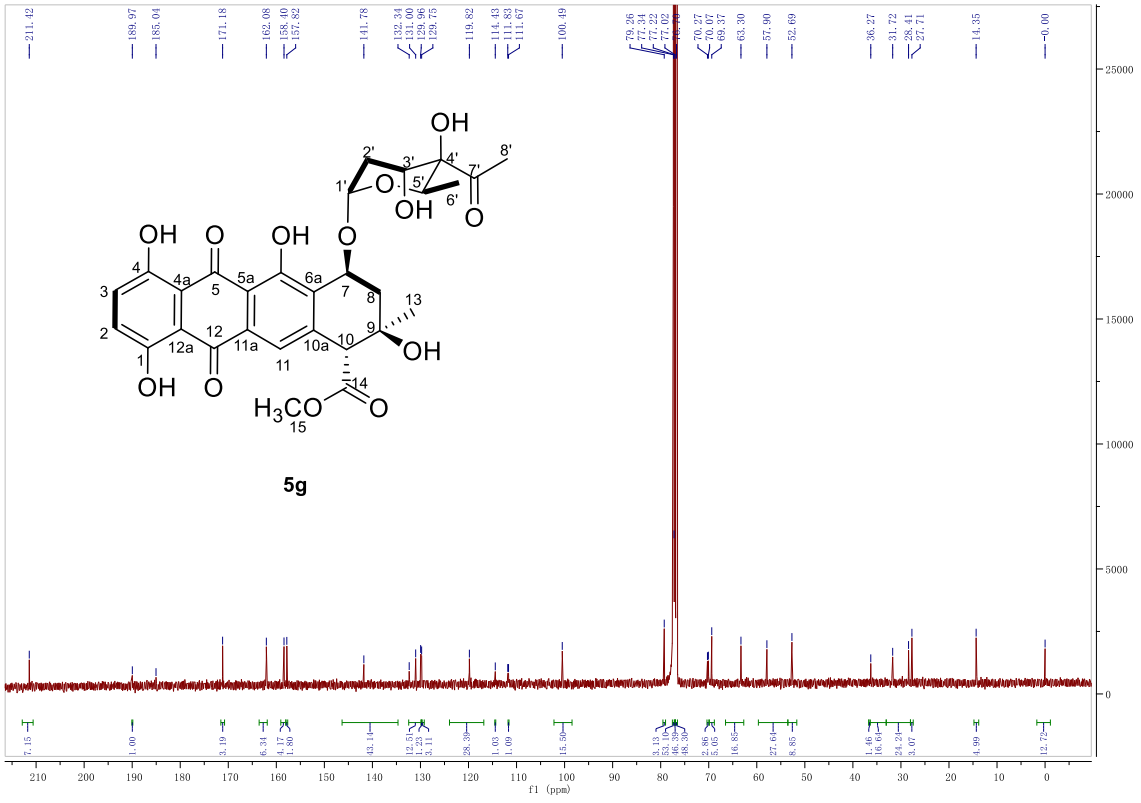

^{1}H-^{1}H COSY spectrum of 5g.

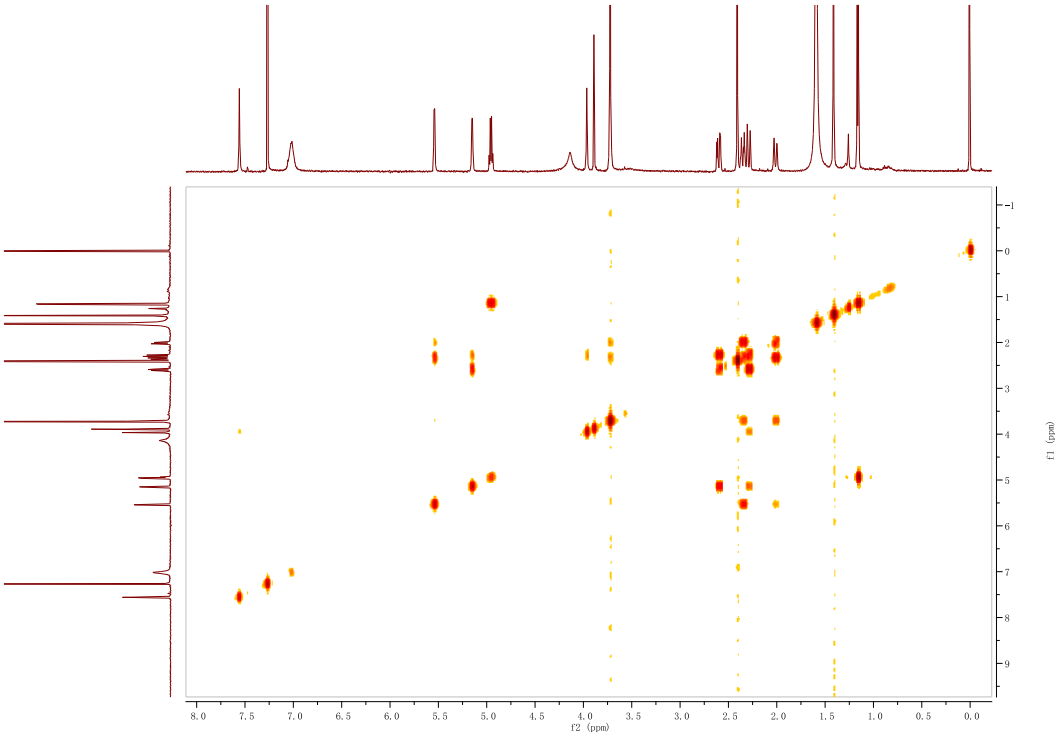

^{1}H-^{13}C HSQC spectrum of 5g.

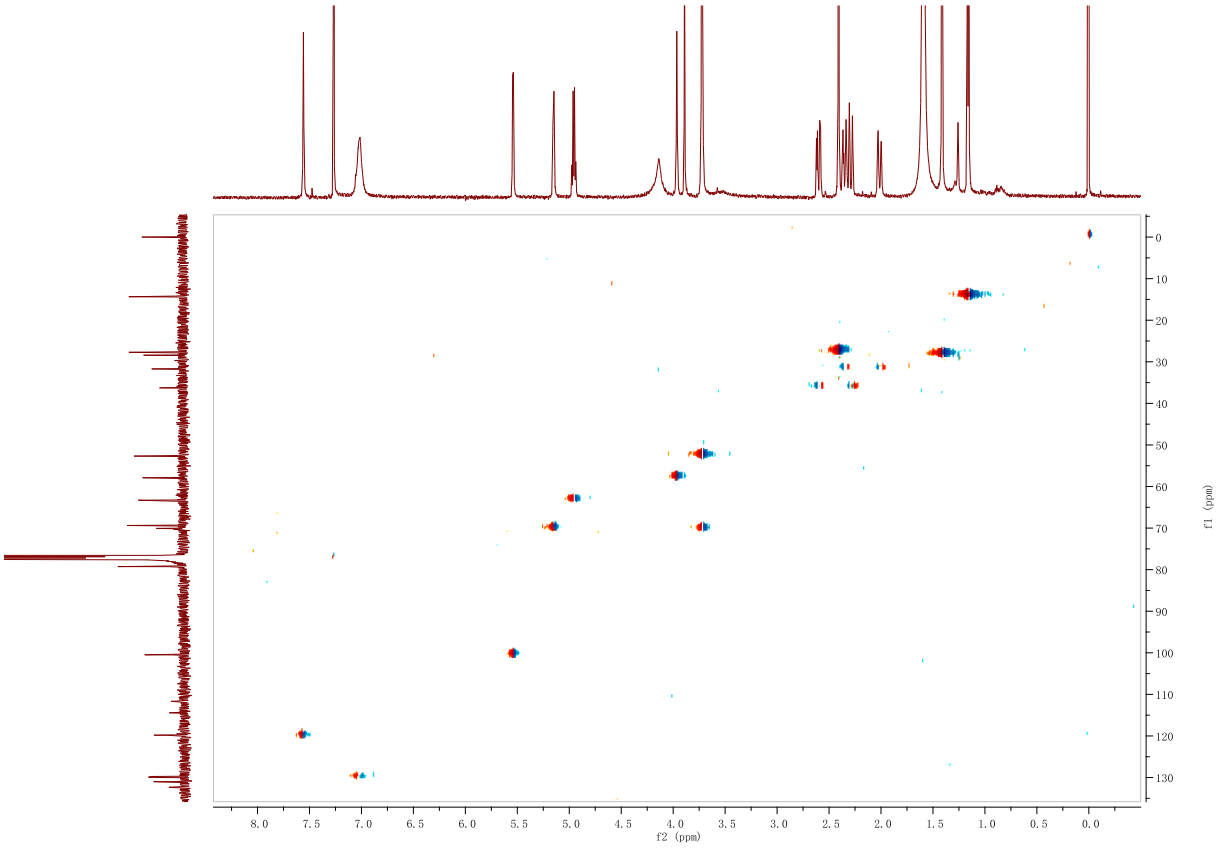

^{1}H-^{13}C HMBC spectrum of 5g.

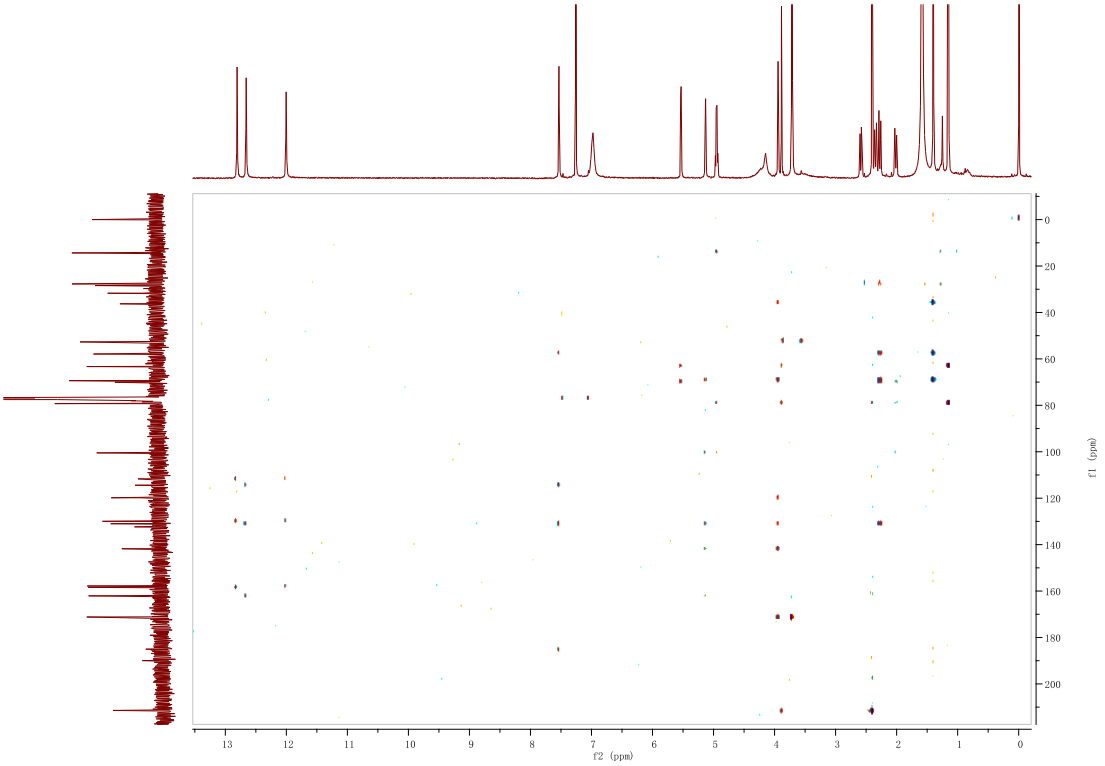

Note S8. Physicochemical and structure characterization data of compound 6b.

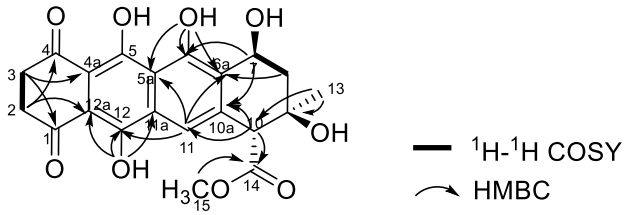

6b

HRMS (ESI): m/z = 415.1030 ([M-H]$^-$), m/z (calculated [calcd.]) = 415.1035 ([M-H]$^-$) consistent with the molecular formula $C_{21}H_{20}O_9$; UV max (in CH_3OH/H_2O = 85:15): 250 nm, 276 nm, 418 nm, 440 nm. The stereochemistry of **6b** was determined by comparing with **5**.

NMR spectroscopic data for compound 6b.

Position	δH(mult., J in Hz)	δc	mutl.
1		200.4	C
2	3.00 (m, 2H)	35.6	CH_2
3	3.00 (m, 2H)	34.7	CH_2
4		199.4	C
4a		106.2	C
5		159.8	C
5a		115.0	C
6		157.0	C
6a		126.2	C
7	5.39 (d, J = 4.2 Hz, 1H)	63.0	CH
8	2.64 (dd, J = 14.9, 5.0 Hz, 1H)	37.2	CH_2
	2.22 (d, J = 14.9 Hz, 1H)		
9		70.1	C
10	4.11 (s, 1H)	57.8	CH
10a		138.5	C
11	7.66 (s, 1H)	117.2	CH
11a		130.2	C
12		154.7	C
12a		106.7	C
13	1.42 (s, 3H)	27.7	CH_3
14		172.1	C
15	3.70 (s, 3H)	52.5	CH_3
5-OH	15.63 (s, 1H)		
6-OH	10.33 (s, 1H)		
12-OH	13.39 (s, 1H)		

In $CDCl_3$, 400 MHz for ^{1}H and 101 MHz for ^{13}C NMR; Chemical shifts are reported in ppm.
All signals are determined by ^{1}H -^{1}H COSY, HMBC, HSQC and DEPT135 correlation.

NMR spectra of compound 6b.

^{1}H NMR spectrum of 6b.

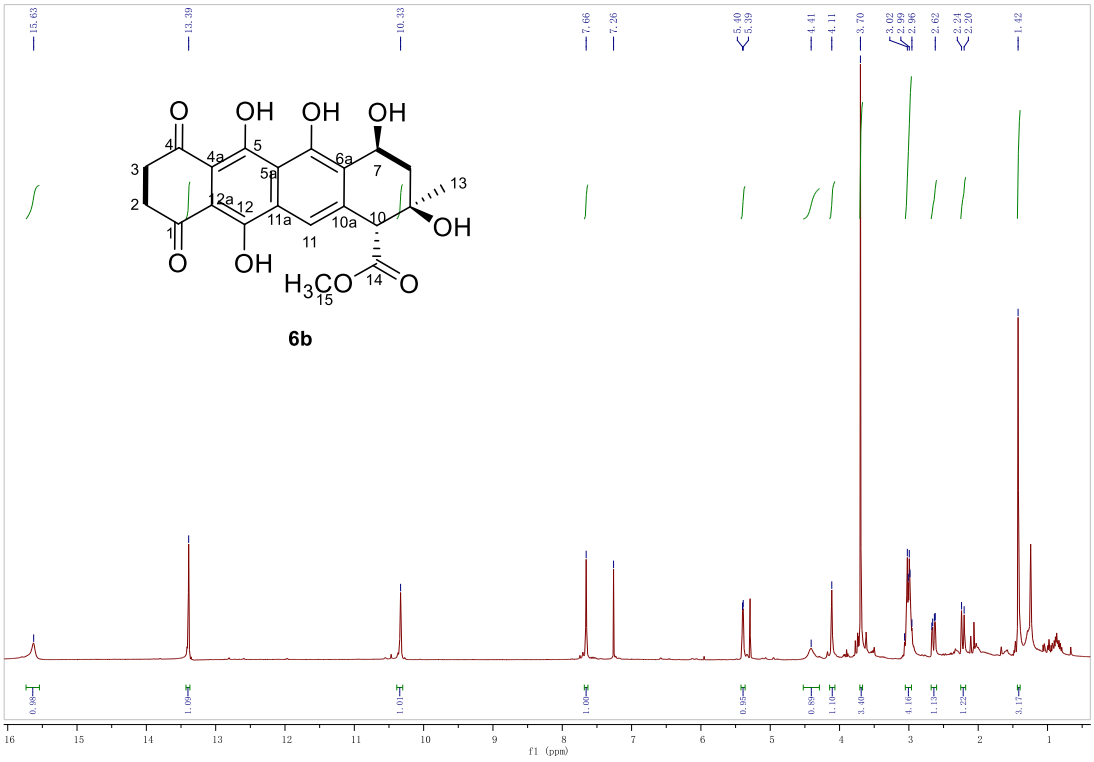

^{13}C NMR spectrum of 6b.

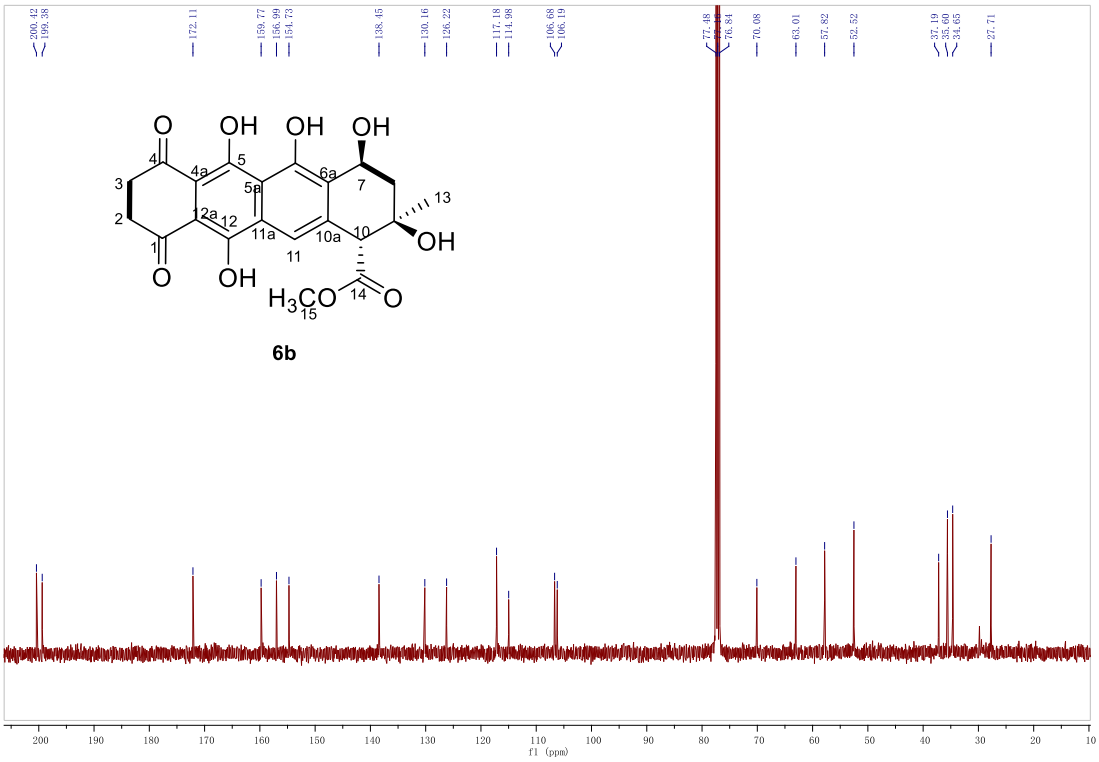

DEPT135 spectrum of 6b

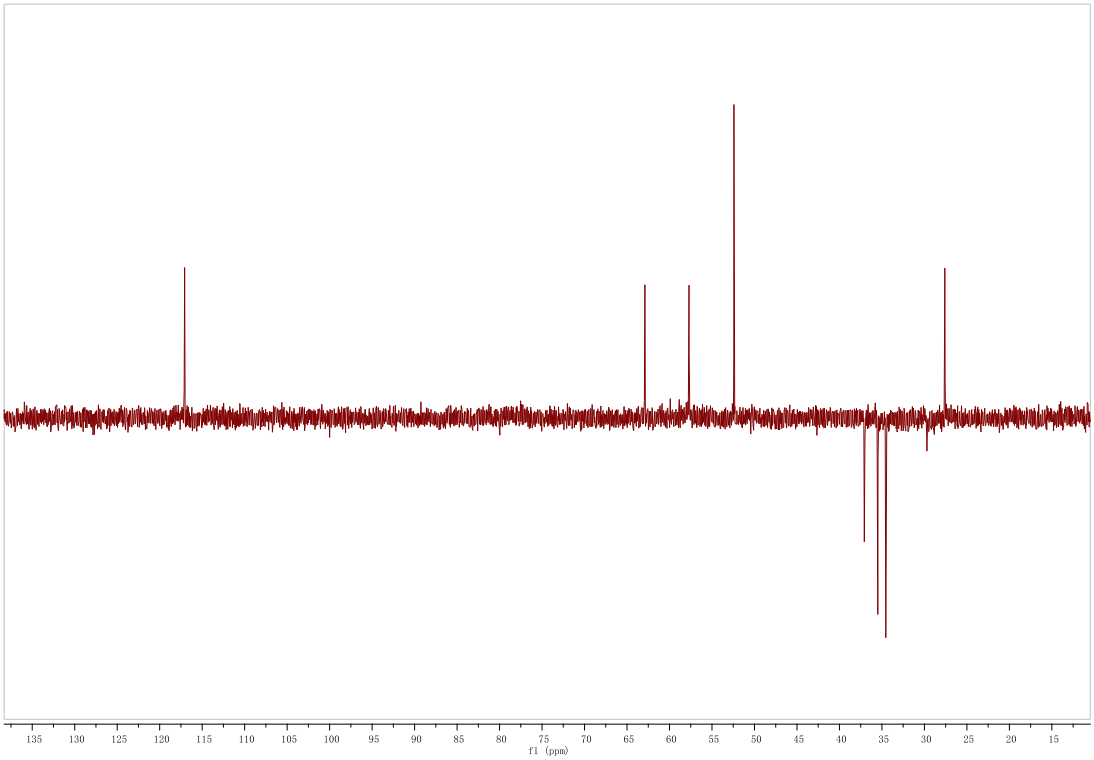

^{1}H-^{13}C HSQC spectrum of 6b.

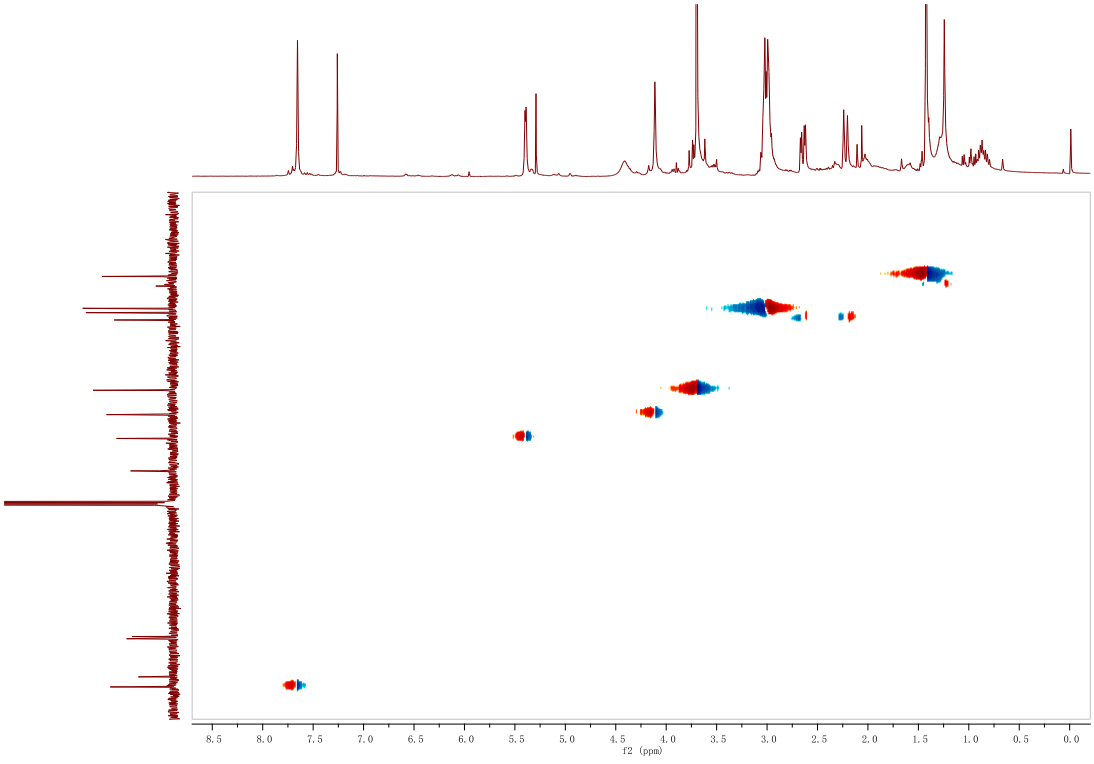

^{1}H-^{13}C HMBC spectrum of 6b.

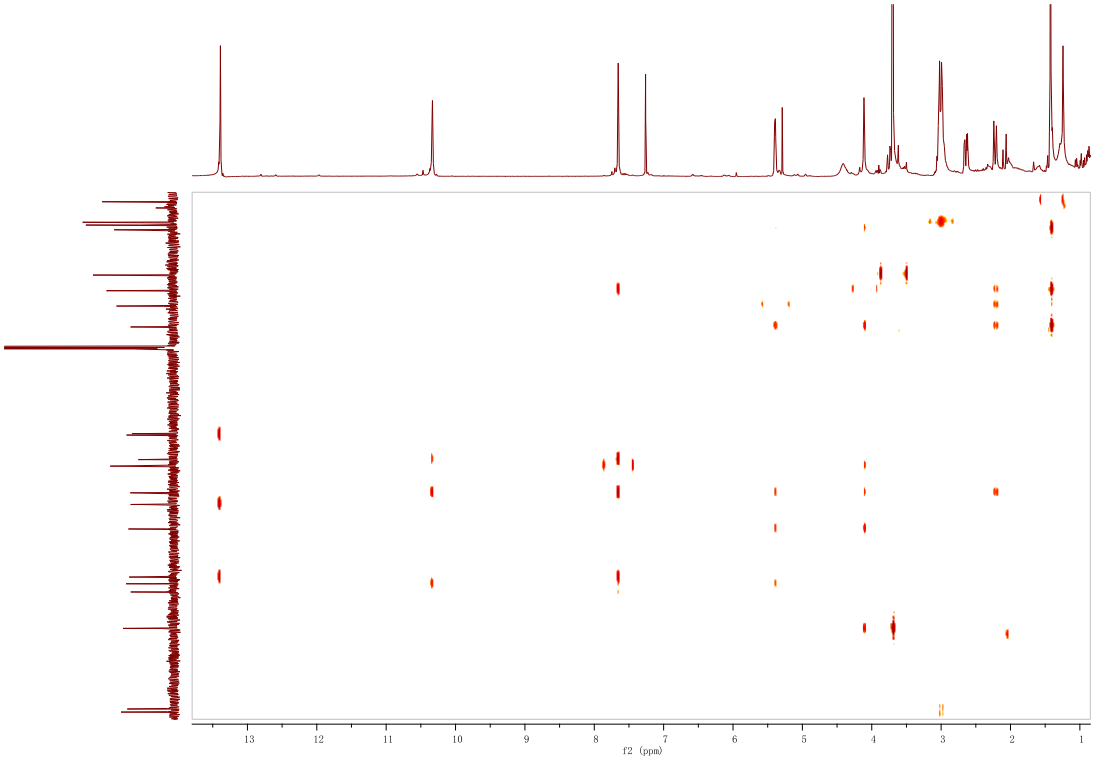

^{1}H-^{1}H COSY spectrum of 6b

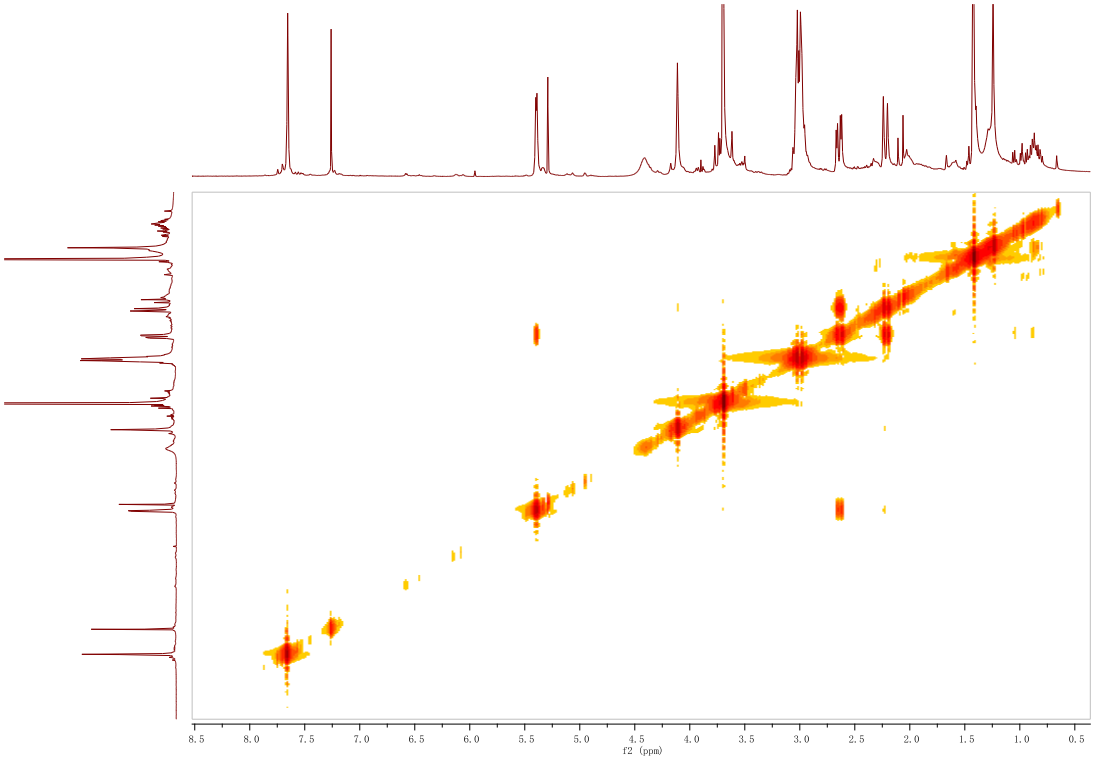

Note S9.Comparison of the $^{1}H(^{13}C)$ NMR spectra of ^{2}H-416b and 416b

HR-ESI-MS of ^{2}H-**6b**

Elemental composition search on mass 416.11

m/z= 411.11-421.11

m/z	Theo. Mass	Delta (ppm)	RDB equiv.	Composition
416.1103	416.1109	-1.26	17.5	$C_{24}H_{14}{}^{2}H_{2}O_{6}N$
	416.1097	1.46	12.5	$C_{21}H_{18}{}^{2}HO_{9}$
	416.1113	-2.26	12.0	$C_{21}H_{20}O_{9}$
	416.1124	-4.98	17.0	$C_{24}H_{16}{}^{2}HO_{6}N$

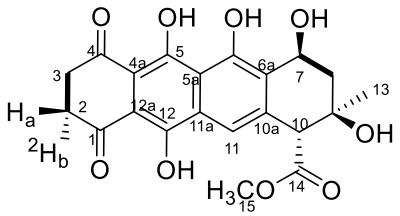

^{2}H-**6b**

Chemical Formular: $C_{21}H_{19}{}^{2}H_{1}O_{9}$

calculated for $[M-H]^{-}$: 416.1109

Comparison of the ^{1}H NMR spectra of ^{2}H-416b and 416b

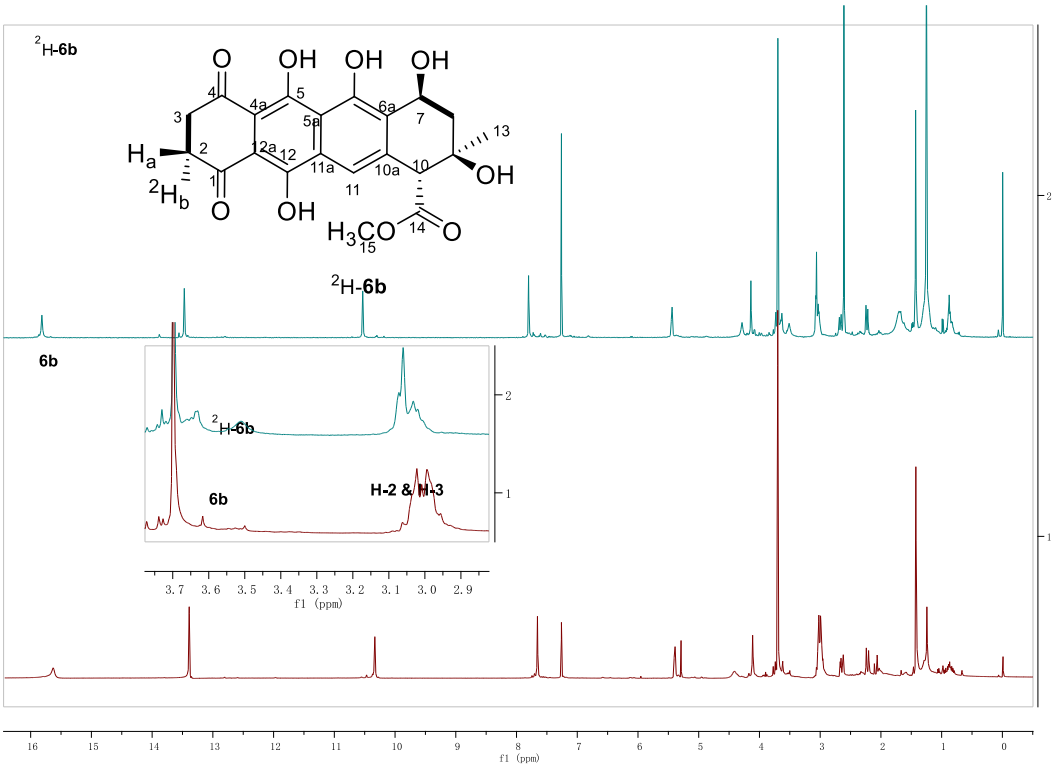

Comparison of the ^{13}C NMR spectra of ^{2}H-416b and 416b

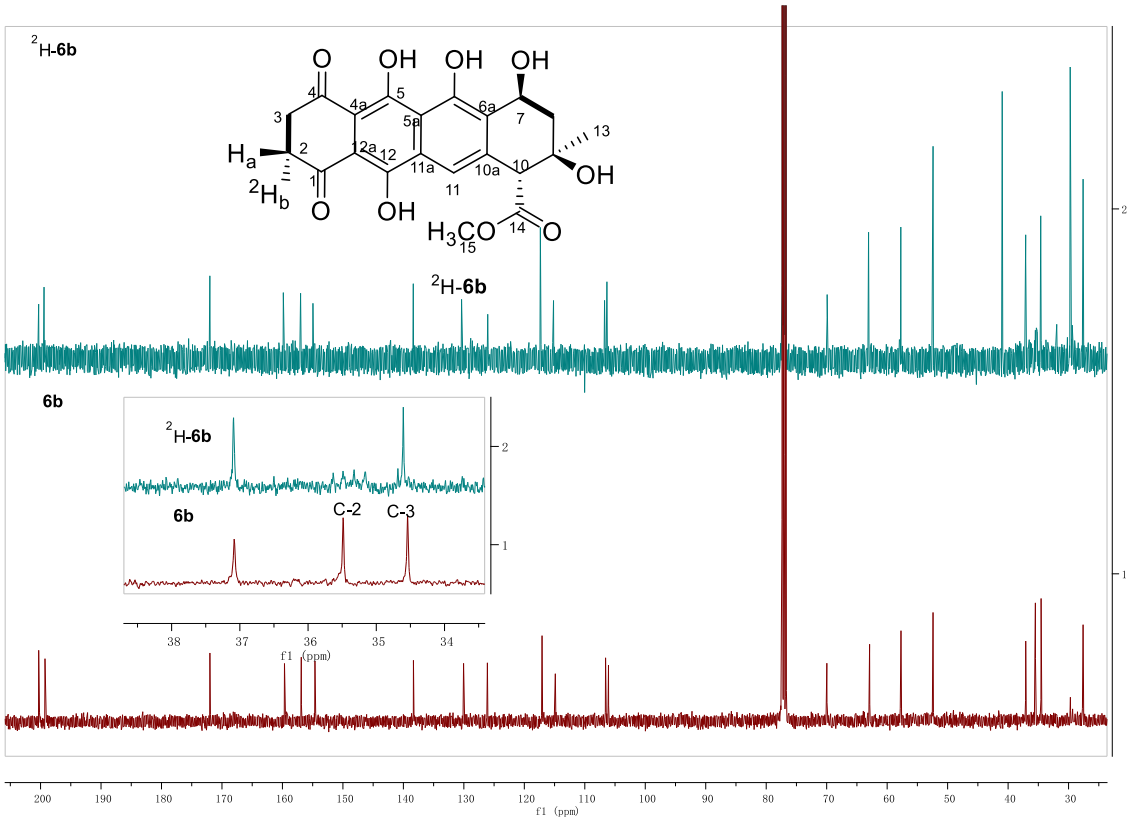

Note S10. Comparison of the $^{1}H(^{13}C)$ NMR spectra of ^{2}H-4 and 4

HR-ESI-MS of ^{2}H-**4**

Elemental composition search on mass 398.10

m/z= 393.10-403.10

m/z	Theo. Mass	Delta (ppm)	RDB equiv.	Composition
398.0997	398.1003	-1.40	18.5	$C_{24}H_{12}{}^{2}H_{2}O_{5}N$
	398.0992	1.44	13.5	$C_{21}H_{16}{}^{2}HO_{8}$
	398.1007	-2.45	13.0	$C_{21}H_{18}O_{8}$

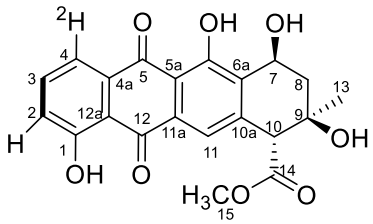

^{2}H-**4**

Chemical Formular: $C_{21}H_{17}{}^{2}H_{1}O_{8}$
calculated for $[M-H]^{-}$: 398.0992

Elemental composition search on mass 399.11

m/z= 394.11-404.11

m/z	Theo. Mass	Delta (ppm)	RDB equiv.	Composition
399.1065	399.1070	-1.13	13.0	$C_{21}H_{17}{}^{2}HO_{8}$
	399.1054	2.75	13.5	$C_{21}H_{15}{}^{2}H_{2}O_{8}$
	399.1053	2.99	26.0	$C_{31}H_{13}N$
	399.1081	-3.97	18.0	$C_{24}H_{13}{}^{2}H_{2}O_{5}N$

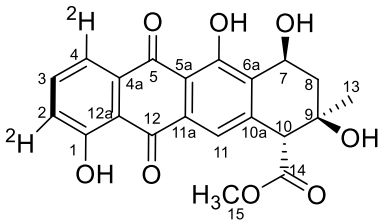

^{2}H-**4**

Chemical Formular: $C_{21}H_{16}{}^{2}H_{2}O_{8}$
calculated for $[M-H]^{-}$: 399.1054

Comparison of the ^{1}H NMR spectra of ^{2}H-4 and 4

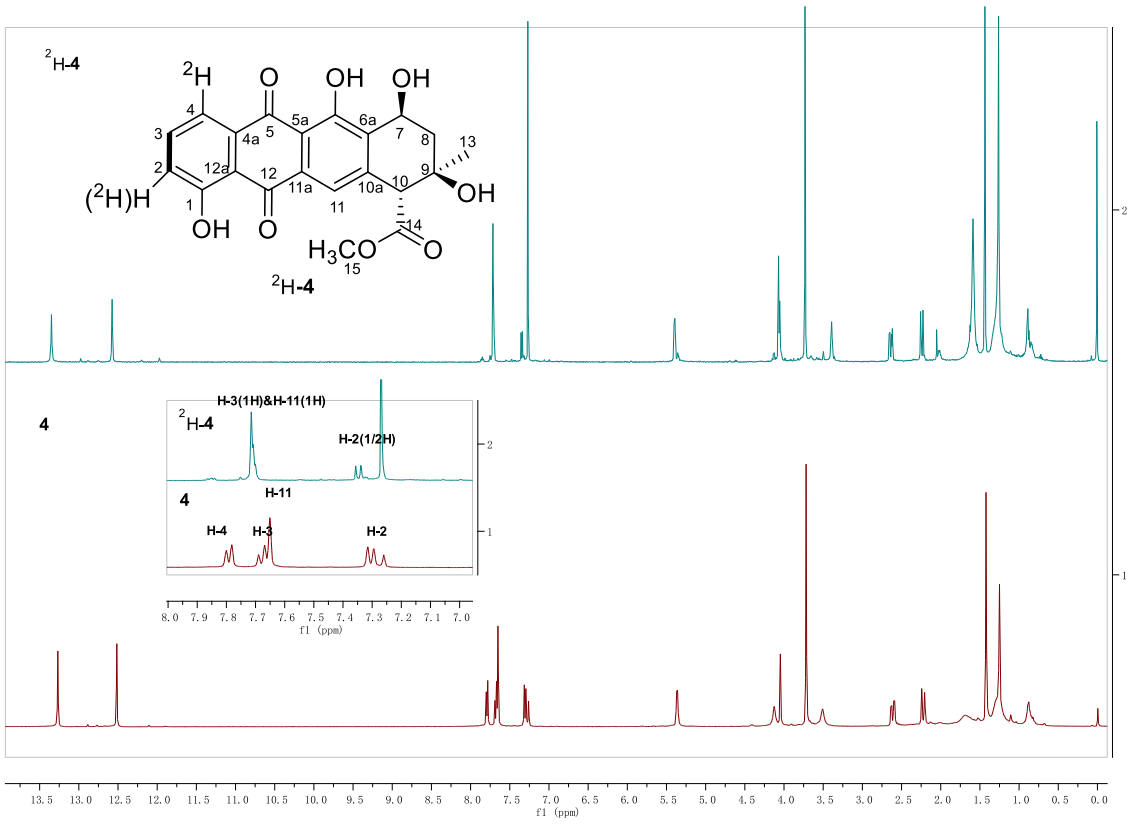

Comparison of the ^{13}C NMR spectra of ^{2}H-4 and 4